

Amphiphilic Block Copolymers as Agents for Solubilisation and Modification of Vesicle Phases

vorgelegt von
Diplom Chemikerin
HSIN-YI LIU
aus Chia-yi, Taiwan

von der Fakultät II- Mathematik und Naturwissenschaften
der Technischen Universität Berlin
zur Erlangung des akademischen Grades
Doktor der Naturwissenschaften
- Dr.rer.nat. -
genehmigte Dissertation

Promotionsausschuss:

Vorsitzender: Prof. Dr. Thorsten Ressler
Berichter : Prof. Dr. Michael Gradzielski
Berichter : Prof. Dr. Joachim Koetz (Uni Postdam)

Tag der wissenschaftlichen Aussprache: 18. Dezember 2012

Berlin 2013
D83

Zusammenfassung

Das Thema dieser Dissertation war die Untersuchung der Solubilisierung von Ölen unterschiedlicher Polarität in wässrigen Lösungen amphiphiler Copolymere und deren Einfluss auf die Eigenschaften von Vesikeln und Vesikeln Gelen. Im ersten Teil wird der Effekt der Ölzugabe auf die Thermodynamik des Mizellierungsprozesses mit Hilfe von DSC und cmc Fluoreszenzmessungen speziell am Beispiel des Triblock Copolymers F108 diskutiert, einem PEO-PPO-PEO Blockcopolymers. Hier zeigt sich, dass generell die Anwesenheit eines Öls diesen Prozess befördert, der auf der Dehydratisierung der PPO Einheit mit steigender Temperatur basiert, wobei dies allerdings nur auf Öle ausreichender Polarität zutrifft, während z. B. Alkane gar nicht solubilisiert werden. Im Detail hängt aber die Absenkung der Mizellierungstemperatur und die Zunahme der Umwandlungsenthalpie stark von der Polarität des Öls ab und für den Zusatz des Homopolymers PPO beobachtet man sogar gar keine Veränderung der Mizellierungstemperatur, was darauf zurückgeführt werden kann, dass hier keine zusätzliche Hydrophobisierung des sich bildenden Mizellkerns erfolgen kann. Die vorliegenden mizellaren Strukturen wurden dann mit Hilfe von DLS und SANS charakterisiert wobei sich zeigte, dass die sich ausbildenden Copolymermizellen auch entsprechend größer werden bei Zusatz der polaren Öle.

Im zweiten Teil wurde der Einfluss unterschiedlicher amphiphiler Polymer auf Struktur und Stabilität unilamellarer Vesikel aus dem Phospholipid DMPC oder einem Diesterquat untersucht. Die durch Extrusion erhaltenen Vesikel wurden dann über einen längeren Zeitraum mit Hilfe von DLS beobachtet und diese Untersuchungen zeigten eine Reduktion der Stabilitätsdauer mit zunehmendem Polymergehalt, wobei dieser Effekt allerdings stark von der Art des Polymers abhing. Die Destabilisierung ist umso stärker, je stärker das Polymer in der Lage ist unterschiedliche Vesikel zu verbrücken. Schließlich wurde auch der Einfluss der Polymere auf die Permeabilität der Vesikelmembranen untersucht, was mit Hilfe der Stopped-Flow Methode und einer dabei ablaufenden Komplexbildungsreaktion erfolgte. Der Polymerzusatz kann dabei zu einer Verlangsamung oder Beschleunigung des Austausches führen. Schließlich wurde noch der Einfluss solcher Polymer auf die rheologischen Eigenschaften von Vesikeln Gelen aus dichtgepackten multilamellaren Vesikeln (MLVs) betrachtet. Hierbei zeigte sich, dass die verbrückenden Polymere eine deutlich stärkere Erhöhung der elastischen Eigenschaften als nichtverbrückendes F108 ergaben.

Abstract

The investigation of micelle, vesicle and gel phases are all covered in this doctor dissertation. The thermal appearance of micelle phases is the main point in the first part. The triblock copolymer F108 is selected as the parent solution to be analysed by the methods of calorimetric instrument, because its amphiphilic character is sensitive to the temperature. The presence of selecting mixtures influences the thermal appearance of fixed F108 solutions; furthermore, the size of micelle phases is analysed by the scattering methods DLS and SANS. The size of the particles depends on temperature; however, not affected by the presence of mixture.

In the second part discusses the stability of the small unilamellar vesicles (SUVs) in aqueous solution. The phospholipids DMPC and diesterquat CR3099 are selected as parent solution. They form large unilamellar vesicles (LUVs) as different range of radius especially for DMPC solution. The size is controlled by means of extrusion with 100 nm poly carbonate filter. The stability of the small vesicles is investigated by DLS. The results show that small vesicles of DMPC are not stable, while those of CR3099 are stable for a period of at least six month. Each of small vesicles for DMPC tends to aggregate to form large vesicles in solution. The times of extrusion, in the presence of copolymer could be the factors of reducing and extending the time of stable small vesicles. The permeability of DMPC vesicles is determined by the Stopped Flow Technique with help of FeSCN^{2+} and F^- ions. The relaxation time τ is reduced in the presence of copolymer 10R5 and extended in the presence of L35. The thickness of uniamellar vesicles is analysed by model of Krotky-Porod from the experimental SANS date.

The final part focuses on gel solutions. The vesicle gels of zwiter ionic TDMAO, ionic TTABr and 1-Hexanol at different ratios appear as different phases of gel. The various ratios of these chemicals form the multilamellar vesicles (MLVs), which were found by Freeze-fracture electron microscopy [1]. These gel solutions, which are already formed by multilamellar vesicles, include copolymers such as 10R5, Rewopal 6000 and F108. They are analysed by rheology instruments.

Content

1. Introduction.....	7
1-1 Packing Parameter.....	7
1-2 Hildebrandt Parameter.....	9
1-3 Thermodynamics of micellization.....	10
1-4 Cloud point.....	11
1-5 Kinetic stability of vesicles.....	12
1-6 Thermotropic phase behavior of Phospholipids.....	13
1-7 Permeability of phospholipids membrane.....	16
2. Technical Methods and Materials.....	20
2-1 Differential Scanning Calorimetry (DSC).....	20
2-2 Dynamics Light Scattering (DLS).....	23
2-3 Small Angle Neutrons Scattering (SANS).....	27
2-4 Rheology.....	36
2-5 Stopped Flow.....	40
2-6 Viscometer.....	41
2-7 Materials.....	42
3. 1 st Part: Admixtures of cosurfactants and copolymers – Effects on size distribution and thermodynamics.....	45
3-1 Pure F108 solution.....	47
3-2 Mixtures of apolar oil and F108 solution.....	49
3-2-1 1-Hexanol.....	49
3-2-2 Geraniol	60
3-2-3 Toluene.....	64
3-2-4 Influence of apolar oil in F108 solution.....	68
3-3 Primary alcohols (Ethanol, 1-Butanol, 1-Hexanol and 1-Octanol) and F108solution	71
3-4 Mixtures of polymer and F108 solution.....	84
3-4-1 Homo copolymer PPO and F108 solution.....	84
3-4-2 Kollicoat MAE 30 DP and F108 solution.....	91
4. 2 nd Part: Kinetic stability of Phospholipids and CR3099 vesicles.....	94

4-1 Phospholipids solution.....	94
4-1-1 Phase behaviour.....	94
4-1-2 Phase transition.....	95
4-1-3 Membrane thickness of the unilamellar vesicles.....	97
4-1-4 Stability of the unilamellar vesicles.....	99
4-1-5 Permeability.....	103
4-1-6 Conductivity.....	108
4-2 Diesterquat CR3099 solution.....	109
4-2-1 Phase behaviour.....	109
4-2-2 Stability of small vesicles for CR3099 solution.....	110
4-2-3 Membrane thickness of the unilamellar vesicles.....	111
4-2-4 Additive and CR3099 solution	113
 5. 3 rd Part: Gel Phases of multi lamellar vesicles (TDMAO, TTABr and 1-Hexanol).....	 118
5-1 Phase behaviour.....	118
5-2 Properties of gel phases.....	122
 6. Conclusion and outlook.....	 129
7. Appendix.....	133
8. Acknowledgement.....	136
9. Literatures.....	137
10. List of publication.....	141

1. Introduction

This doctoral dissertation is subdivided into three parts. The first part discusses that solubilizers are effective in the formation of block copolymer micelles. The second part is concerned with the investigation into the effect that amphiphilic copolymers have on vesicle structure and stability. Finally, the last part puts an emphasis on the vesicle gels.

1-1 Thermodynamics and Packing Parameters[1, 2]

Surfactants are composed of hydrophilic head group and hydrophobic chain length. They can self-assemble in aqueous solutions once a characteristic concentration has been surpassed. At low concentrations, the surfactants are dissolved as single molecules due to the large contribution to the free energy from the entropy of mixing, which overcomes the unfavourable contributions from the hydrocarbon-water contact. At higher concentrations, i.e. above the critical micellar concentration (cmc), the surfactants form aggregates in the form of micelles. Some surfactants are also quite thermo-sensitive, e.g. Pluronics and all surfactants containing ethylene oxide (EO) units in general. Their micelle formation does not only depend on the concentration, but also on the temperature. Here the temperature above which micelles are formed is called the critical micellar temperature (cmt).

The aggregations due to this dual character are self-assembly in water in a variety of morphologically different structures [3-7]. The driving force for this aggregation process is the tendency of the hydrophobic part to minimize its contact with water. An effect, called the hydrophobic effect, is mainly due to the entropic gain of the water structure by not being in contact with the hydrophobic part [8]. The shape and structure of surfactant micelles are determined by the structure and properties of the constituting molecules, their interactions, and the thermodynamics of the system [9]. A variety of effective shapes within the micelle are observed from spherical and rod-like micelles to amphiphilic bilayers. The shapes of micelles depend on the molecular constitution of the amphiphilics and can be explained by a simple geometric consideration, which is called the packing parameter model. The packing parameter p is calculated from the ratio of hydrophobic volume (v_s) to the optimum head group area (a_s) and chain length (l_s). The scheme of the packing parameter model is presented in Fig.1-1-1 and the equation is expressed as follows:

$$p = v_s / (a_s \cdot l_s) \quad (1-1-1)$$

The packing parameter is able to determine the preferred curvature of aggregates. If p is

less than $1/3$, the aggregates form spherical objects. In the first part of this dissertation, the pluronic F108 is selected to analyse the formation of micelle phases dependent on temperature. Cylindrical and rod-like micelles are formed for $1/3 < p < 1/2$. If the amounts of F108 are increased in a solution, then rod-like micelles and other Pluronics like F127 would be observed as well [10, 11]. Bilayer structures are expected for $p < 1/2$ and normally they form lamellar phases or vesicles particles in a solution. The DMPC phospholipids and CR3099 diesterquat surfactants are selected to investigate the vesicles in the second part. They form large unilamellar vesicles (LUVs) in a variety of sizes, especially phospholipids. The small unilamellar vesicles (SUVs), having only one single bilayer, are obtained from LUVs by means of extrusion. If the value p is larger than 2, the reverse structures should be formed. In general, this simple scheme works well for the explanation of experimentally observed amphiphilic structures.

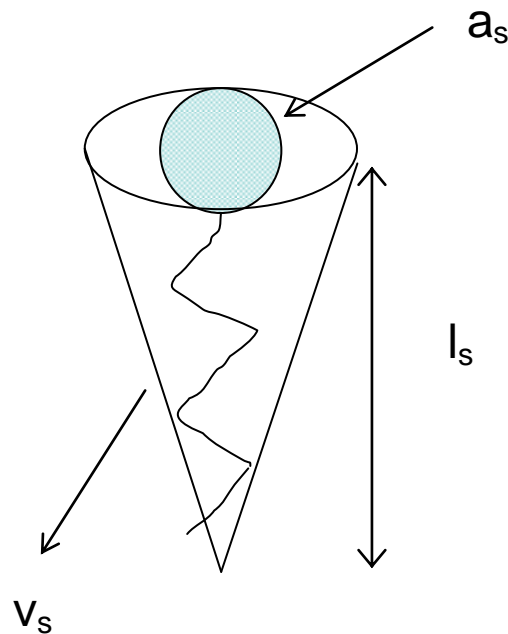


Fig. 1-1-1: Description of parameters of packing parameter from surfactants

1-2 Solubility capacity based on the Hildebrand parameter [12, 13]

The Hildebrand parameter, as well as the solubility parameter δ_H , based on a common solution theory, is proposed by Hildebrand [14]. Traditionally, this parameter δ_H has been expressed in $(\text{cal}/\text{cm}^3)^{1/2}$. It is obtained from the cohesive energy density ρ_U , which is the measure of the interactions among the molecules in the condensed phase [14]. The equation is as follows:

$$\delta_H = (\rho_U)^{1/2} \quad (1-2-1)$$

The Hildebrand parameter δ_H is often used to predict miscibility behaviour for medical and technological applications, such as the prevention of asphalt precipitation, the estimation of the shelf life of polymers and drug formulations [15-19], the development of synthetic membranes, and the formation of micelles self-assembly and gelation processes and nanocomposites [20-23]. Additionally, the correlate polymer properties, such as the glass transition temperature and the permeability of molecules, can be estimated accurately by means of the solubility parameter [24]. The Hildebrand parameters are determined by experiments via the heat of vaporization ΔH_v . The equation is, in general, presented as follows:

$$\delta_H = \left(\frac{\Delta E_v}{V} \right)^{1/2} = \left(\frac{\rho(\Delta H_v - RT)}{M_w} \right)^{1/2} \quad (1-2-2)$$

ρ is the density of the solvent, T is the absolute temperature and M_w is the molecule weight of the solvent. In this experiment, three apolar oils, which are 1-Hexanol, geraniol and Toluene, are selected as the mixtures at given concentrations of the F108 solution. Each of the Hildebrand parameters is calculated by equation (1-2-2).

Tab. 1-2-1

Oil	$\Delta H_v / \text{calmol}^{-1}$	M_w / gmol^{-1}	ρ / gcm^{-3}	$\delta_H / (\text{calcm}^{-3})^{1/2}$
1-Hexanol	12708.5	102.18	0.816	9.83
Geraniol	14060.7	154.25	0.882	8.77
Toluene	9368.5	92.14	0.862	9.06
PPO				9.34
PEO				10.5 ± 0.5
water				23.4

The Hildebrandt parameter of PPO, PEO and water molecules are found from the publications [25, 26]. If δ_H values of solvents are closed to each other, they can easily be homogenous.

1-3 Thermodynamics of micellization [27]

There is an interpretation for the micellization process that is viewed as an energy barrier-triggered phenomenon [28]. The micelle formation happens as the free enthalpy of the micelle is lower than that of the unimer's. The PEO–PPO–PEO copolymers are dissolved in water as unimers dispersed below their critical micelle temperature (cmt) or concentration (cmc). Micellization of Pluronics in aqueous solutions is mainly entropy-driven and can be initiated by increasing the temperature at a fixed concentration. It is reasonable to assume that the transport phenomena do not play a role in their formation. The blocks copolymer is sensitive to the concentration alone and temperature of the solution. The dehydrated process transitions very fast from unimer to micelle phases. Therefore, the kinetics of the micellization is of no practical interest.

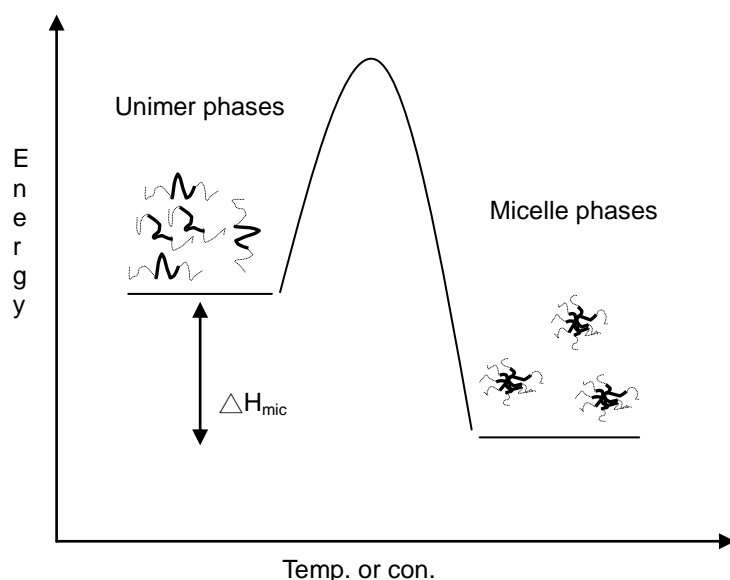


Fig. 1-3-1: Phase transition model of triblocks copolymer from unimers to micelles

Fig. 1-3-1 presents the thermodynamic process of blocks polymer. When the unimers translate into micelles, the energy is adsorbed. Forming the micelle phase is the endothermic reaction. The entropy of micelles is caused by the hydrophobic part of the copolymer. By adding oil at fixed solution of the copolymer results in an entropy increase

1-4 Cloud point

The cloud point is defined as when the additive in solution is no longer soluble at critical conditions, such as temperature or concentration. The phase behaviour of the solution will not be homogenous. When the solution is not homogenous, it starts to perform a turbid or diphasic solution. For a triblock copolymer solution, the cloud point, also known as the phase separate temperature, is the temperature at which the solution starts to be heterogeneous. Two phases appear, thus the solution becomes cloudy. The thermal cloud point for triblock copolymers is an interesting topic to investigate because they dehydrate depending on the temperature. Some research on the subject has been published in recent years [10, 29, 30]. Triblock copolymers contain amphiphilic character and are sensitive to temperature changes. PO block molecules start to dehydrate with increasing temperature. EO block molecules present more hydrophilic than PO blocks, but EO blocks can still start to dehydrate at high temperatures. For example, the dehydration process of F108 happens at 30°C at a weight concentration of 5%. It is caused by PO blocks. The dehydration process of EO blocks happens at 110°C and can be analysed by DSC. The entropy for dehydration of EO blocks is lower than the dehydration of PO blocks [10]. If the EO and PO blocks of F108 are all dehydrated, the solution becomes heterogeneous.

The cloud points of other triblock copolymers, such as F88, F68, P65 and L62, are all at higher temperatures in comparison with F108. The low molecule weight of EO blocks leads to increase the temperature of cloud points [10].

1-5 Kinetic stability of vesicles

This experiment puts emphasis on producing small unilamellar vesicles (SUVs) and investigating the stability of small unilamellar vesicles over a long period of time. The observation time usually takes at least one month, even if the sample appears to be an instable phenomenon, such as precipitation. It will stop being analysed. The phenomenon of precipitation is caused by the fusion effect. Each of the individual small vesicles fuses together in the solution. The large vesicle is formed by small ones. Fig.1-5-1 shows the mechanism of the fusion process. First, the unfused vesicles have to approach each other. The grey rhombus is the contact area between the two individual vesicles. Each of the unfused vesicles tries to approach then adhere to one another. In the adhesive part of two vesicles, the phospholipids will rearrange by themselves. Two adhesive lipid bilayers will disappear and the lipids are shifted nearby. After the fully-fused process is completely finished, two vesicles become one large vesicle. However the fully-fused process is hardly reversed.

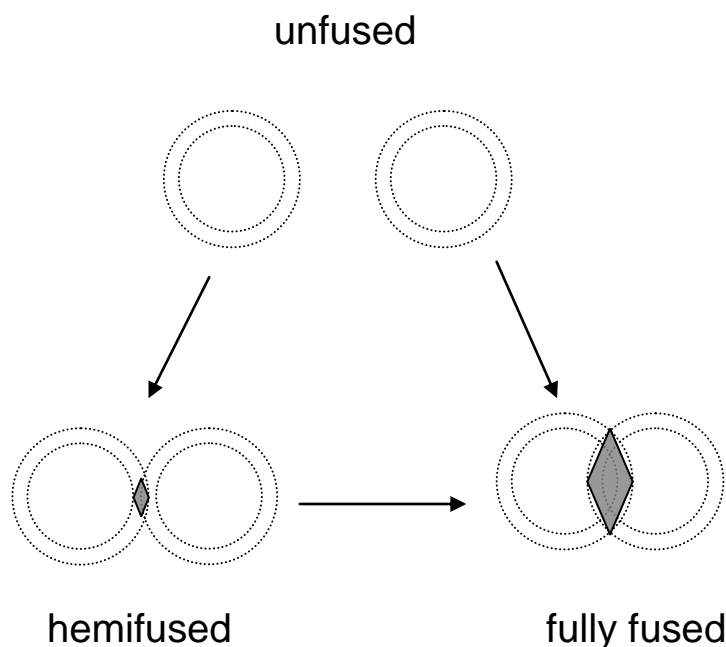


Fig. 1-5-1: Scheme of fusion process

The difference between hemifused and fully-fused vesicles is that fully-fused ones contact with the inner part of a membrane. Small vesicles combine only with bilayer parts of membranes when they are in a hemifused process. There are some forces between vesicles and solvents when they are in the fusion process.

Hydration repulsion

Hydration repulsion is caused by the solvent. The strong repulsion appears between bilayers, which are defined as hydration repulsion. These repulsion forces can be analysed by means of a surface forces apparatus (SFA). Normally this instrument is used for measuring forces between surfaces [31, 32]. Hydration repulsion can be explained as the work required for removing the water molecules around hydrophilic molecules in the bilayer system [33]. Precisely, the result is that the free energy between hydrophilic surfaces requires the modification of the H-bonding network of liquid water in the vicinity of polar and H-bonding surface groups.

Hydrophobic attraction

When small unilamellar vesicles approach each other successfully in the fusion process, the attraction of hydrophobic is enhanced. This phenomenon, known as the hydrophobic effect, is the driving force for the self-assembling of lipids into aggregates, such as bilayer membranes and other structures [34].

Van der waals forces[34, 35]

These forces are attractive due to the dipole-dipole interaction between bilayers. The dipole-dipole interaction includes permanent and induced dipoles. While vesicles are closed, a separable hydration interaction between them reduces with an exponential decay.

1-6 Thermotropic phase behavior of Phospholipids [36]

Phospholipids as well as triblock copolymers are sensitive to temperature. The sequence of thermotropic transitions of hydrated phospholipids can be generally represented by the following scheme:

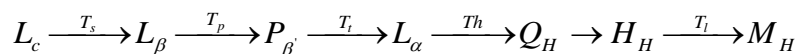


Fig. 1-6-1: Phase transition of phospholipid

The symbol L_c is called the crystalline phase, in which the phospholipids are not hydrated. When L_c turns to L_β at temperature T_s . L_β is the hydrated lamellar gel phase and L_α is the fluid lamellar phase. With increasing temperatures, the main phase transition process observed by Nano DSC occurs from L_β to L_α . The main phase transition happens at T_t . Below T_t , the pretransition from a low-temperature gel phase to an intermediate ripple

phase ($P_{\beta'}$) occurs at T_p . When the temperature keeps increasing, the fluid phase undergoes further transitions, first transforming into an inverted cubic phase (Q_H) and then an inverted hexagonal phase (H_H). The final stage is the transition into the inverted micellar phase (M_H) that occurs at temperature T_i . This phase is characterized as immiscible oil in excess water. Not all the phases and transitions mentioned above appear for a single phospholipids [112].

Phase L_{α} is characterized by disordered lipid chains. The main phase transition from L_{β} to L_{α} is explained as Trans-Gauche Isomerization. Microscopic chain melting is connected with rotation around the carbon bonds of phospholipid hydrocarbon chains. The lowest energy holds for *trans* and highest for *cis* conformations of the chains. In the gel state, the rotation is restricted and the saturated chains are in the all-*trans* conformation. When the temperature approaches the phase transition region, it increases the probability of rotation. Rotation by 120° relative to *trans* conformation results in the formation of *gauche* (+) or *gauche* (-) conformations.

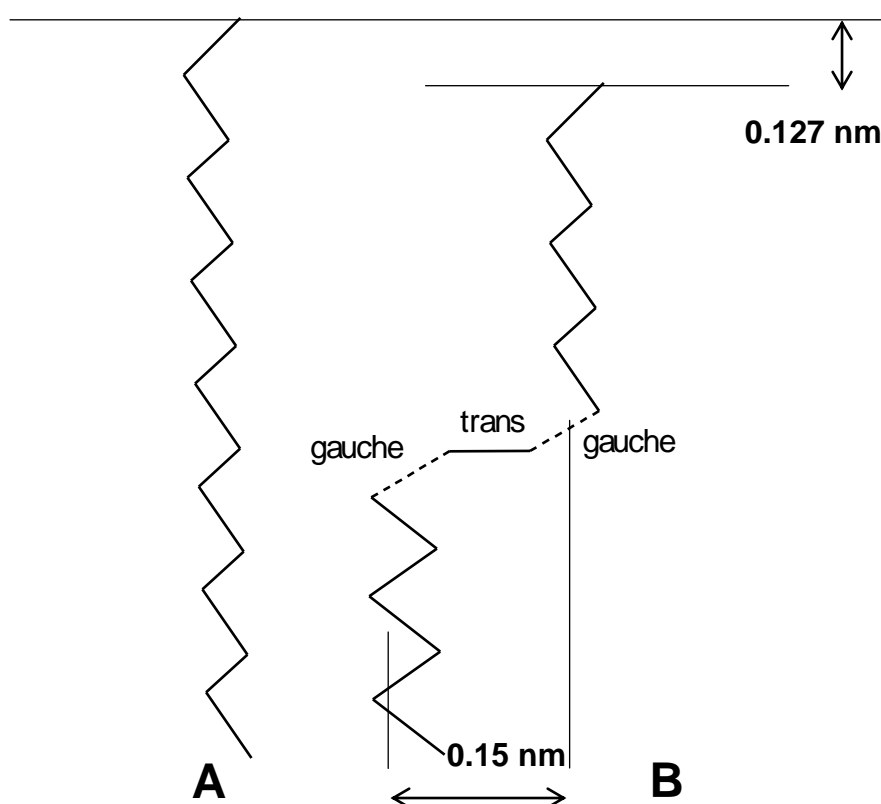


Fig. 1-6-2: Conformation of the hydrocarbon chain of a DMPC. A – trans configuration, B – gauche-trans-gauche conformation

Energetically, the gauche conformation does not differ substantially from the trans conformation ($2\text{--}3 \text{ kJ mol}^{-1}$). However, these two conformations are separated by a relatively high energetic barrier ($12\text{--}17 \text{ kJ mol}^{-1}$). The appearance of the gauche (+)

conformation causes stereo-dimensional difficulties in a bilayer. However, the subsequent gauche (-) rotation results in a diminishing sterical repulsion. As a result of the gauche (+)-gauche (-) rotation, a kink conformation appears in the lipid chain (see Fig. 1-6-2). In this case, the spatial configuration of the chain is preserved, but the chain is 0.127 nm shorter and the cross-sectional area increases. The phase transition in a lipid bilayer from a gel to a liquid state is therefore accompanied by a decrease in the thickness and an increase in the area per molecule. The energetic barrier, ΔE equal to ΔH , can be determined by Nano DSC. With the following equation:

$$\nu = \left(\frac{kT}{h} \right) \exp \left(- \frac{\Delta E}{RT} \right) \quad (1-6-1)$$

ν is the frequency of torsional oscillations as the unit of s^{-1} .

The gauche conformation appears with a high frequency due to torsional oscillations. ν is obtained from eq. 1-6-1 when the energetic barrier is found.

1-7 Permeability of phospholipids membrane [36, 37]

The biological membrane is one of the most important cell structures. It represents a city gate for the cell with a barrier function that provides directional transport of species into the cell, and waste and toxic compounds are pushed out of the cell. In addition, the low permeability of the membrane for charged particles, e.g. ions, allows a non-equilibrium ion distribution between the extracellular and cytoplasmic sides of the cell, which is crucial for cell function. Phospholipids are the most common lipids in cell membranes. A phospholipid bilayer membrane represents a self-assembled structure in an aqueous solution. This is the result of the hydrophobic effect, whereby the non-polar acyl chains of lipids (which form the interior of the bilayer) and the non-polar amino acid residues in proteins tend to be squeezed out from the aqueous phase. In this dissertation, determining the permeability of small unilamellar is presented. The kinetic reaction through the membrane takes place with the help of FeSCN^{2+} and F^- ions analysed by Stopped Flow.

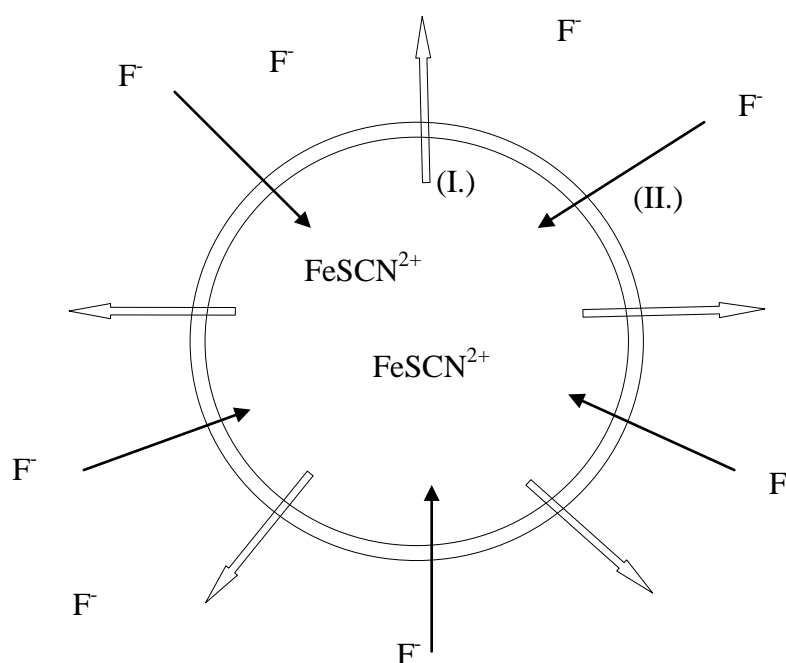


Fig. 1-7-1: Model for the diffusion of ions for 0.1% DMPC extruded solution: (I.) Diffusion of FeSCN^{2+} to outside of the vesicles, (II.) Diffusion of F^- to the inside of the vesicles

The reaction between FeSCN^{2+} and F^- leads to colourless, stable fluoride complexes, and is used to measure the permeability of vesicles:



While the rate constants for the formation of the red complexes between ferric and thiocyanate ions, mainly $FeSCN^{2+}$ and $Fe(SCN)_2^+$ [38], and the reactions between Fe^{3+} and F^- ions [39] [40] have been determined by kinetic measurements, no results seem to be available in the research that has been done on the reaction between $FeSCN^{2+}$ and F^- . The known rate and equilibrium constants in the reaction scheme are given in Tab.1-7-1.



The constants in Tab.1-7-1 show that the stability of the fluoride complexes is 100 to 1000 times larger than the stability of iron thiocyanate complexes.

Tab. 1-7-1: Constants of the fluoride complexe [38],[4]and [5]

Contants/ $L \cdot mol^{-1}$	SCN^-	F^-
K_1	150	105
K_2	20	104
K_3	-	103

This simple geometric model gives a calculated aggregation number for large unilamellar vesicles of the measured size. The membrane volumen of one unilamellar vesicle is approximately given by

$$V \approx 4\pi R^2 d \quad (1-7-7)$$

And

$$V = \frac{n_{agg} M_w}{\rho N_A} \quad (1-7-8)$$

Equation (1-7-7) and (1-7-8) giving the aggregation number

$$n_{agg} = \frac{4\pi R^2 d \rho N_A}{M_w} \quad (1-7-9)$$

where R is the radius of unillamellar vesicles, d is the thickness of membrane, ρ is the density of phospholipids, N_A is Avogadro's number, and M_w is the molecular weight of the phospholipids.

Fick's first law of diffusion

The diffusion of the FeSCN^{2+} complex and the F^- ion can also be discussed by Fick's first law of diffusion; the equation is given as follow:

$$\frac{dn}{dt} = -S \cdot D \cdot K \cdot \frac{dc}{dx} \quad (1-7-10)$$

From the inside membrane of FeSCN^{2+} , the rate diffusion of FeSCN^{2+} is driven out of the vesicles

$$\frac{dc_{\text{Fe}(\text{SCN})^{2+}}}{dt} = -\frac{S}{V} \cdot \frac{D \cdot K}{\delta} \cdot \Delta c_{\text{Fe}(\text{SCN})^{2+}}, \quad (1-7-11)$$

where n is the number of $\text{Fe}(\text{SCN})^{2+}$ complexes per vesicle, S is the membrane surface of one vesicle as the unit of m^2 , V is the volume of one vesicle as the unit of m^3 , δ is the thickness of membrane as the unit of m, D is the diffusion coefficient for the diffusion in the membrane as the unit of m^2s^{-1} , K is the partition coefficient of ions between water and hydrocarbon phases, as well as lipids bilayer phase, and Δc is the difference of concentrations outside and inside the vesicles.

In the model Fig. 1-7-1, the ferric complex should decay as a first-order process with the rate constant k_{exp} given by

$$k_{\text{exp}} = \frac{S}{V} \cdot \frac{D \cdot K}{\delta} \quad (1-7-12)$$

The above expression could be further simplified if a permeability coefficient P is defined:

$$P = \frac{D \cdot K}{\delta} \quad (1-7-13)$$

Combined with equation (1-7-12) the rate constant k_{exp} is then given by

$$K_{\text{exp}} = \frac{S}{V} \cdot P = \frac{4\pi R^2 \cdot 3}{4\pi R^3} \cdot P = \frac{3P}{R}, \quad (1-7-14)$$

where R is the vesicle radius as unit of cm, P is the permeability coefficient as unit of $\text{cm} \cdot \text{s}^{-1}$ and k_{exp} is the first-order rate constant as unit of s^{-1}

$$k_{\text{exp}} = \frac{1}{\tau}, \quad (1-7-15)$$

where τ is the relaxation time as unit of s.

2 Technical Method and Materials

In the following, techniques used to characterize micellization, vesicles and gel phases are discussed. These include methods for analysing thermodynamical properties and permeabilities, as well as classical methods for studying hydrodynamic radius R_h of unimers, micelles and vesicles. Characterization methods for rheology and viscosity are also introduced. Moreover the preparation of samples is put into this part.

2-1 Differential Scanning Calorimetry(DSC)[41]

Differential scanning calorimetry is a useful tool for analysing the thermal properties of materials. The phase transition of Pluronics and phospholipids are sensitive to temperature, so that they are suitable to be investigated by this instrument. The thermodynamical reaction is observed when DSC scans as a function of temperature. The basic theory of DSC relates to heat capacity C_p . The heat capacity C_p is measurable in physical quantity and defines the amount of heat required to increase the temperature of the sample by 1 degree Kelvin or Celsius. Thus,

$$C_p = \frac{Q}{\Delta T} \quad (2-1-1)$$

ΔT is the change in temperature and Q is the amount of Heat required to achieve ΔT . The heat capacity relates to the energy, which accompany endothermic and exothermic reaction. So the equation can be written as

$$C_p = \left(\frac{\partial H}{\partial T} \right)_p = \frac{\Delta H}{\Delta T} \quad (2-1-2)$$

Under the constant pressure condition, the required Heat Q is equal to the enthalpy ΔH .

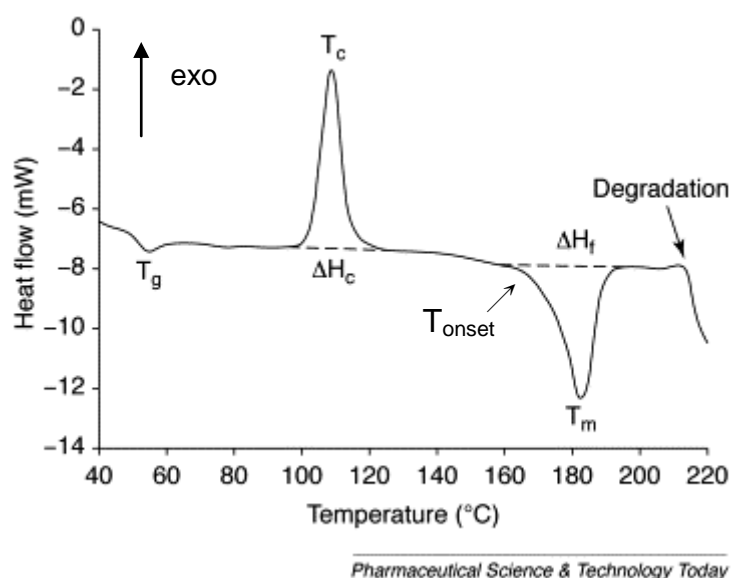


Fig. 2-1-1: DSC scan as function of temperature [41]

Fig. 2-1-1 provides the information to analyse the phase transition of samples, such as T_m , ΔH_f , T_c , ΔH_c and T_g . The parameter T_m is defined as the melting point of temperature and is read at the top of the endothermic peak. ΔH_f is the amount of energy that the sample absorbs while melting. The term T_c is called the crystallisation point and is read at the top of the exothermic peak. The enthalpy of ΔH_c is the amount of energy which the sample releases while crystallizing. In the part of the amphiphilic triblock copolymer the transition peak is marked as T_{peak} instead of T_m and T_c . The entropy of Pluronics is written as $\Delta H_{(PO)}$ for both process instead of ΔH_f and ΔH_c , because the phase transition happens as a result of the dehydration of each PO block. The parameter T_g is called the glass-transition temperature. It happens when an amorphous polymer or an amorphous part of a crystalline polymer goes from a hard, brittle state to a soft, rubbery state. This experiment puts no emphasis on discussing the T_g point of triblock copolymers and phospholipids. The Fig. 2-1-1 shows an arrow that points to the occurrence of thermal degradation of the polymer and the maximal temperature of thermal stability is determined. There is another arrow, which is called T_{onset} . It is read at the beginning of the thermal peaks. After measuring the samples, they were analysed by Nano Analyze software to determine the temperature and enthalpy. The Nano Analyze software and Nano DSC instrument were developed by the company TA Instrument.

The triblock copolymer F108 is sensitive about temperature and concentration. At a fixed concentration of F108, the critical micelle temperature (cmt) is analysed by means of DSC. The endothermic peak occurs when the PO blocks that are part of F108 become hydrophobic. The PO blocks acquire more hydrophobic features when temperature increases, accompanied by energy absorption. Normally, the PO blocks with hydrophobic

properties are hard to dissolve in aqueous solutions. Because they bond covalently with long chains of EO blocks, the phase behaviour appears homogeneously still in water, even if the sample is already over the cmt. Conversely, in the cooling process, PO blocks regain their hydrophilic character and the exothermic peak is caused by energy release. The phase transition of Phospholipids is observed by the Nano DSC instrument as well. The arrangement structure of phospholipids is sensitive to temperature. It turns from crystalline phases L_c to the fluid lamellar phase L_α when the temperature increases.

Set-up of instrument

In general, the set-up of the DSC instrument consists of pans and sources of heating and cooling. The Fig. 2-1-1 shows a simply sketched set-up of DSC. The measuring sample is put in pan S only. Pan R keeps empty usually. The furnace provides a stable continuous heat flux to both pans. Furnace system provides uninterrupted heats and leads temperature increasing. Heats are accepted by both pans. The accepted heats cause changes in the differential power supplied to the sample if the energy is adsorbed or released.

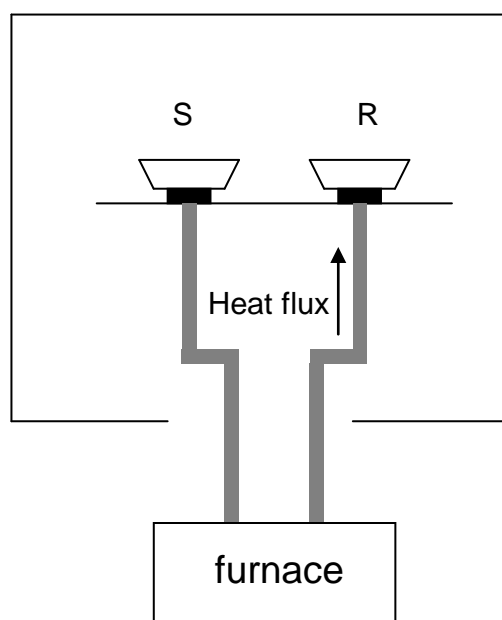


Fig. 2-1-1: Sketch set-up of the DSC instrument

There are two kinds of furnaces for DSC instruments. One is like the one shown in Fig. 2-1-1 and is called Heat flux DSC. The sample and reference materials utilize a single furnace and heat flows into both samples via an electronically heated constantan thermoelectric disk [42]. There is another type of DSC, which is called power-compensated DSC. It has two individual furnaces for samples and references respectively. The Nano DSC instrument is used in this experiment and it is of the Heat flux DSC type.

The shape of cell container has a special design, made as capillary cells for sample and reference materials (see Fig. 2-1-2).



Fig. 2-1-2: Picture of capillary cells

The Nano DSC instrument was designed by the TA instrument company. This instrument has a very high sensitivity and is suitable for analysing the diluted solution of bio molecules like phospholipids liposomes molecules. Capillary cells are one of the advantages. The contact area of capillary cells is larger than pan cells. It creates a stable post-transition baseline and it enables complete and accurate determinations of transition temperatures (T_m) and enthalpy (ΔH).

2-2 Dynamic Light Scattering (DLS) [43]

The size and the distribution of micelle phases and vesicles in the aqueous solution is analysed by the dynamics light scattering method. The basic theory of light scattering is that the light from a laser passes through a polarizer to define the polarization of the incident beam and then impinges on the scattering medium. The scattered light then passes through an analyser which selects a given polarization and finally enters a detector. The position of the detector defines the scattering angle θ . The intersection between the incident beam and the scattered beam is defined as a volume V , called the scattering volume or the illuminated volume.

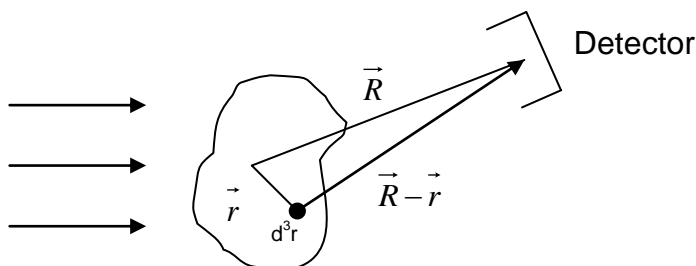


Fig. 2-2-1: Simple sketch of scattering geometry

The big blank is the illuminated volume V and the total radiated field at the detector is the superposition of the fields radiated from all infinitesimal volumes d^3r at positions r , with

respect to the center of V. The detector is at position R with respect to the center of the illuminated volume.

The molecules in the illuminated region are perpetually translating, rotating and vibrating by virtue of thermal interactions. Because of this motion, the positions of the charges are constantly changing so that the total scattered electric field at the detector will fluctuate in time. Thermal molecular motion is erratic, so that the total scattered field varies randomly at the detector. The vector q is defined in terms of the scattering geometry as

$$q = k_i - k_f \quad (2-2-1)$$

where k_i and k_f point respectively, in the directions of propagation of the incident wave and the wave that reaches the detector. The angle between k_i and k_f is called the scattering angle θ . The magnitudes of k_i and k_f are, respectively, $2\pi n/\lambda_i$ and $2\pi n/\lambda_f$, where λ_i and λ_f are the wavelengths in vacuo of the incident and scattered radiation, and n is the refractive index of the scattering medium. It is usually the case that the wavelength of the incident light is changed very little in the scattering process so that

$$|k_i| \cong |k_f| \quad (2-2-2)$$

Thus the triangle in Fig. 2-2-2 is an isosceles triangle and the extent q can be found from the law of cosines,

$$q^2 = |k_f - k_i|^2 = k_f^2 + k_i^2 - 2k_i \cdot k_f = 2k_i^2 - 2k_i^2 \cos \theta = 4k_i^2 \sin^2 \frac{\theta}{2} \quad (2-2-3)$$

$$q = 2k_i \sin \frac{\theta}{2} = \frac{4\pi n}{\lambda_i} \sin \frac{\theta}{2} \quad (2-2-4)$$

This is the Bragg condition. It specifies the wave vector component of the dielectric constant fluctuation that will give rise to scattering at an angle θ .

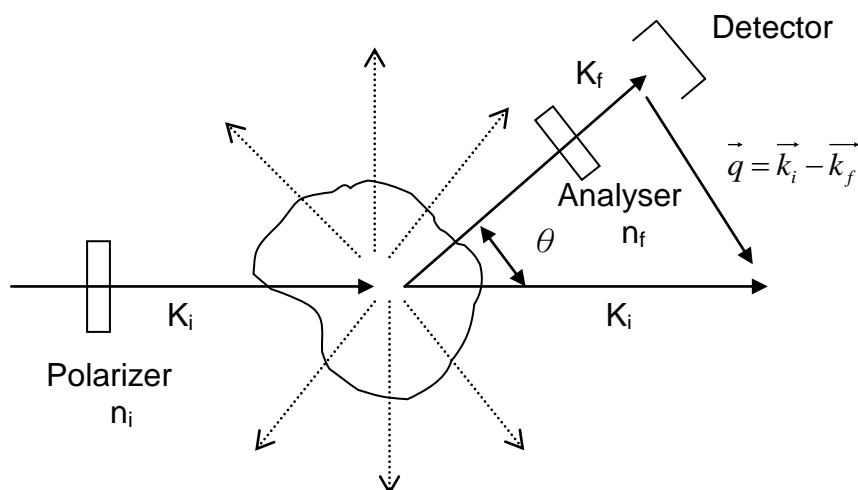


Fig. 2-2-2: Description of the scattering vector q

All samples were measured by this type of ALV/CGS-3 Compact Goniometer System with a He-Ne-laser at wavelength of 632.8 nm. The detecting angle was always at 90° , so the values of the scattering vector are the same in this experiment. The temperature of the medium is controlled normally at 25°C , while some pluronis samples are measured from 15 to 40°C . The measured samples were analysed with the software of ALV – 7004 version 3.0.

Analysis of DLS measurements

The scattered intensity is measured in Hz as a function of time and it fluctuates up and down dynamically with time. The particles moves as Brownian motion in a solution and it results in unstable scattering intensity. Those irregular fluctuations can be interpreted by autocorrelation functions. It is a mathematical tool used to describe the random process in statistics. In general, the function is written as

$$C(\delta t) = \int_0^T dt \cdot I(t)I(t + \delta t) \quad (2-2-5)$$

It describes the status of particles at the moment when $t=0$ second and the next moment at δt seconds. Deciding the measuring time of the sample is dependent on the particle size and the viscosity of the solvent, and it can be set from seconds to hours. The scattering intensity results in the relative distance of the position between particle and detector. It relates to the diffusion movements of particles in solutions. The particle diffuses dependent on time. When t is from 0 to 1 sec., the volume of the particle including diffusion area increases; it results in a high-intensity correlation function. If the particle is observed from 0 sec to a period of time, it still diffuses with time. However, the volume of

diffusion is limited because movements of the particle are similar and repeated with high probability. The correlation function intensity decreases when time is lengthening. Therefore, the autocorrelation function of DLS is time-dependent.

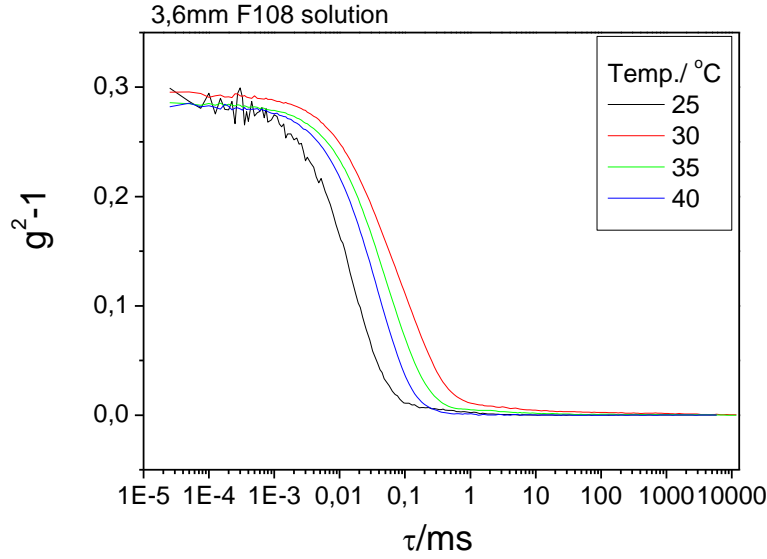


Fig.2-2-3: Autocorrelation function of 3.6 mm F108 measured with different temperatures

The analysis of the cumulant expansion of the correlation function is performed by fitting a polynomial up to third order to the function $\ln(g^2(t)-1)$. The polynomial coefficients are converted into the coefficients of the cumulant expansion of the field correlation function

$$\ln(g^1(t)) = \ln(A) - \bar{\Gamma}t + \frac{u_2}{2}t^2 - \frac{u_3}{6}t^3 \quad (2-2-6)$$

Amplitude (A), $\bar{\Gamma}$ (1/Gamma), u_2 , u_3 , are the parameters of this correlation function. The unit is in milliseconds (ms) and the unit of u_2 and u_3 are therefore $1/\text{ms}^2$ and $1/\text{ms}^3$. In this part takes the first order of parameter $\bar{\Gamma}$ to determine the hydrodynamic radius R_h .

$$R_h = \frac{kT}{6\pi\eta\bar{\Gamma}}q^2 \quad (2-2-7)$$

The value η is the viscosity of the measuring medium and in this case is water. It decreases with increasing temperature and q is scattering vector dependent on scattering angle and wavelength (see eq 2-2-4). When the ALV-7004 is used for analysing DLS measurements, step of simple fit will be selected. Simple fit is a model of cumulant fit to calculate the correlation function. After calculation of simple fit the width and polydispersity index (PD.I) of the sample is obtained. The equations of width and PD.I are as follows:

$$Width = \frac{\sqrt{u_2}}{\Gamma} R_h \quad (2-2-8)$$

$$PD.I = \frac{u_2}{\Gamma^2} \quad (2-2-9)$$

The other method for analysing the autocorrelation function, called the ALV-Regularized fit step. The decay time is taken from 0.001 to 100 ms into consideration. DLS-Exponential $g^2-1(t)$ is used as a nonlinear fit model (see eq. 2-2-10) and the size distribution is displayed as a function of the radius as a unit of nm and unweighted log.

$$g^2(t) - 1 = \left(\int_{\Gamma_{min}}^{\Gamma_{max}} e^{-\Gamma t} G(\Gamma) d\Gamma \right)^2 \quad (2-2-10)$$

In this experiment, the results of PD.I (Eq. 2-2-9) are calculated from a second and parameter of u_2 at eq. 2-2-6. It is a standard to determine the size distribution of particles in solutions. The low value of PD.I appears in the size distribution of particles more homogenously in solutions.

2-3 Small angle neutron scattering (SANS)[2, 44, 45]

One of the most suitable methods for obtaining information on the structure and interactions of micelles is by means of neutron scattering. This technique is called small angle neutron scattering, which is similar to other scattering methods, like DLS and SAXS. They are complementary to investigate the shape, size, distribution for colloid systems and soft matter. Neutrons are used for the technique SANS as scattering radiation. The specialty of neutrons has no charge and neutrons interact with atoms via nuclear rather than electrical forces, and nuclear forces are very short-range of the order of a few fermis (1 fermi = 10⁻¹⁵ meter). Furthermore, the wavelength of neutrons is in the range of 0.1 to 1 nm and the energy is approximately 1 to 100 eV. An important feature of neutron scattering is the high incoherent scattering cross-section of hydrogen. However hydrogen molecules appear low incoherent scattering cross section by measuring of X-ray scattering like SAXS because of the electron density.

Samples preparation and instrument set-up

Neutron scattering is the difference in the scattering length between hydrogen and deuterium, which is important for the variation of the contrast between the particles and

the matrix. So the samples are prepared normally in D_2O additionally. Considering that the density of D_2O is 1.1 times heavier than H_2O , the samples would be weighted 1.1 times heavier in order to equal the molar concentration of aqueous samples. The SANS measurements are usually prepared in D_2O solvents in order to enhance the contrast and reduces the incoherent background from scattering from hydrogen in the sample. Block copolymer micelles and microemulsions are analysed with the solvents D_2O and H_2O . The contrast and scattering length density is varied by changing the D_2O/H_2O concentration of the solvent. Those aggregates with various parts from each sample in solution can be highlighted in different mixtures of deuterated and hydrogenated solvents.

The software SASfit is used to analyse the measuring SANS curves. It is developed at the Paul Scherrer institute (PSI) in Switzerland and is written for analysing and plotting small angle scattering data [45]. Other important information, like gyration radius, scattering invariant and porod constants, can be obtained by SASfit. There are lots of models of form factors and structure factors to be selected to fit size distribution together.

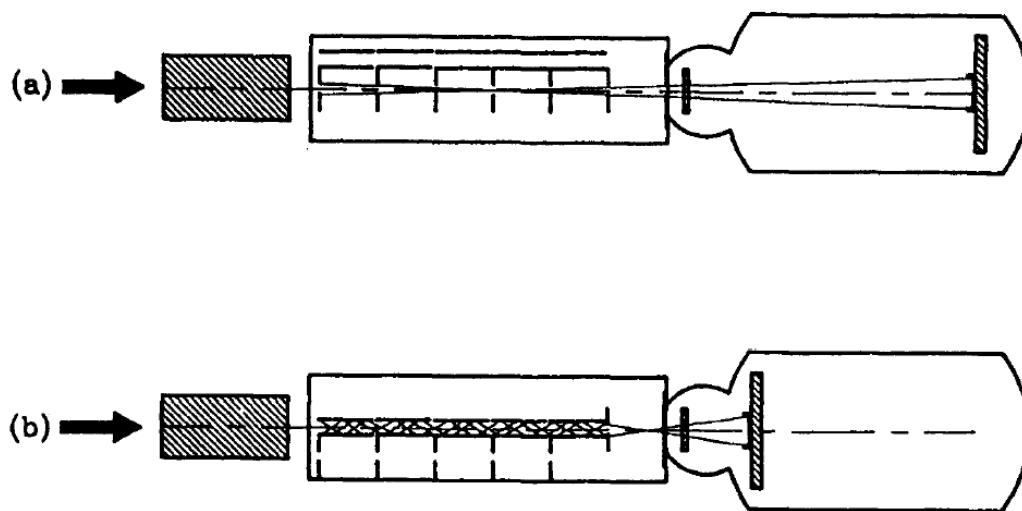


Fig. 2-3-1: The principle of a flexible steady-state SANS setup pictured by J.S. Pederson [2]

The most of the samples under the group of Prof. M. Gradzielski were measured at the ILL in Grenoble, France. There were same samples measured at the HZB in Berlin, Germany. The Fig. 2-3-1 shows the primary principle SANS setup for the steady-state type. It is one type of neutron source for SANS instruments. The steady-state means that the reactor is continuously produced by the fission processes. The other type, called a spallation source, provides a pulsed neutron beam. The range of available scattering vectors is typically from about $1 \cdot 10^{-3}$ to 0.5 \AA^{-1} , which typically requires the use of three different sample-detector distances and neutron wavelengths. A particularly broad range

of scattering vectors, from 10^{-3} to 1.5 \AA^{-1} , is covered by the D22 instrument at ILL in Grenoble, France. The principle of the set-ups is shown in Fig. 2-3-1. Part (a): The smallest q values are reached with the longest sample-detector distance, with a long collimation and neutron wavelength. Part (b): The largest q values are reached with the detector as closely to the sample as possible and a short neutron wavelength. The sample-detector distance can be varied and the divergence of the incident beam can be chosen to match the angular range covered by the detector. This is done by varying the distance from the source pinhole to the sample. Neutron guides are inserted in front of the source pinhole in order to prevent a loss of intensity. For all these instruments, a mechanical velocity selector is used for monochromatizing the neutrons. The smallest q values are reached with the longest sample-detector distance for which the collimation is chosen. The wavelength is as long as practically possible. The largest q values are reached with the detector as close to the sample as possible and with the shortest possible wavelength. The flux at the sample position depends strongly on the wavelength and the collimation. The flux is typically about 10^7 neutrons per second at the sample position for short wavelengths around 3 \AA . For longer wavelengths around 15 to 20 \AA and long collimation distances ($> 5 \text{ m}$), the flux is several orders of magnitude lower. Useful measurements can be done with a flux as low as 10^3 neutrons per second, but with long acquisition times from 4 to 12 hours. For example with the D11 instrument at ILL (Ibel, 1976), the length of the collimator can be varied from 2.5 to 40.5 m , and the sample-to-detector distance can be varied in the same range. The velocity selector provides a wavelength resolution of 9% and wavelength in the range from 2 to 20 \AA . For D22 at the ILL, the source, the neutron guide and the geometry have been optimized to provide a very intense incident flux. The length of instruments collimation and flight path is 7.6 and 18 m , respectively. With a large area-sensitive detector ($1.0 \times 1.0 \text{ m}^2$) which can be offset, a very broad range of scattering vectors can be covered in a single setting.

The primary theory of small angle neutron scattering

The scattering intensity, $I(q)$, from a solution composed of particles, can be expressed in terms of a form factor, $P(q)$, and a structure factor, $S(q)$, where q is the scattering vector (q), which is defined as the difference between the vectors of the scattered and incoming neutrons. The equation is given by

$$q = \frac{4\pi}{\lambda} \sin\left(\frac{\theta}{2}\right) \quad (2-3-1)$$

The form factor $P(q)$ reveals the geometric characteristics of the single aggregate in

solution, and the structure factor $S(q)$ accounts for correlations due to inter-particle interactions. The form factor and the structure factor are assumed to be independent, and the scattering intensity for spherical, monodisperse particles in the differential cross section, which is from the articles by Grillo, Narayanan and Das and Doniach [46-48] can be expressed as

$$I(q) = \frac{d\sigma}{d\Omega}(q) = N \cdot P(q) \cdot S(q) \quad (2-3-2)$$

N is the number density of the scattering particle and q is the scattering vector. $P(q)$ is the particle form factor related to the structure of the particles and is the scattering amplitude.

$$P(q) = A(q)^2 \quad \text{and} \quad A(q) = \Delta\rho \cdot V \cdot \Phi(q \cdot R) \quad (2-3-3)$$

In this expression

$$\Phi(x) = \frac{3[\sin(x) - x \cos(x)]}{x^3} \quad (2-3-4)$$

and $\Delta\rho$ is the difference in scattering length between the surfactant and solvent, V is the particle volume and R is the particle radius. $\Delta\rho$ can be determined by the equation as follows:

$$\Delta\rho = \rho_{surf} - \rho_{solv} \quad (2-3-5)$$

Where ρ_{surf} is the scattering length density (SLD) of the surfactant and ρ_{solv} is that of the solvent. These can be calculated from the apparent specific density, which means the effective density of the molecule in the solution, when the changes in the water in the vicinity of the molecules are also ascribed to the molecule, of the surfactant and the density of the solvent. They are calculated as the sum of all scattering lengths of the molecule, divided by the effective volume of the molecule calculated from the density. Since the densities and apparent specific densities can be determined accurately [49-51], it is also possible to obtain accurate values for the scattering length densities. The equations in eq. 2-3-2 to 2-3-4 can be reduced by relating V to the radius as $V = (4\pi/3)R^3$, and the number density N to the concentration of the solution c (mass per volume) corrected for the inter-micellar concentration c_0 as $N = (c - c_0)/(N_{agg} M_{surf})$, where M_{surf} is the mass of a surfactant molecule, and N_{agg} is the aggregation number calculated as $N_{agg} = V/V_{surf}$, where V_{surf} is the volume of a surfactant molecule calculated from the apparent specific density. With this, the only fit parameter of the model is the radius R of the micelles. The inter-micellar concentration c_0 is in a practice set equal to the cmc, which can be estimated independently, for example, by surface tension measurements. The

above considerations show, to give a very simple example, the strength of including molecular constraints in the analysis [52].

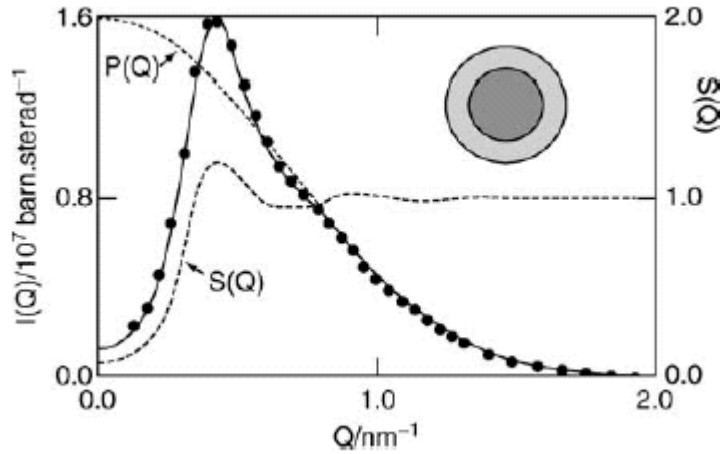


Fig. 2-3-2: SANS data of hexadecyltrimethylammonium chloride (HTAC or CTAC) micelles in D₂O without added salt [53]

This dissertation presents most of the SANS measurements as being from the triblock copolymer F108 with an addition of 1-Hexanol. The block copolymer model for aggregation process can be organized into three groups for analysing the behavior of micelles phases in solutions with suitable form factors. The model of background Gauss and Spherical shell in the experiment is selected for the form factor $P(q)$ to analyse the pluronic samples by SASfit program. Analysis of scattering data is expressed as a sum of two contributions.

$$I(q) = I_{coh}(q) + I_{inc} \quad (2-3-6)$$

I_{coh} is the coherent scattering dependent on the shape, size and repartition of domains in the sample. I_{inc} is a background because sometimes incoherent scattering is caused by atoms in particular hydrogen. The value of I_{inc} keeps normally constant. For a single population of monodisperse the coherent part of I_{coh} can be expressed as follows:

$$I_{coh}(q) = N \cdot V^2 \Delta SLD^2 \cdot P(q) \cdot S(q) \quad (2-3-7)$$

with the volumen fraction $\psi = N \cdot V$. The formfactor $P(q)$ is normalized. V is the average volumen and N is the number density. ΔSLD is the average contrast.

The model of Gauss is an interpretation of a polymer chain to explain the phenomenon of an isotropic random walk in solution. Considering a flexible copolymer coils and each

unimer locates at a distance R_m , its scattering field amplitude is given by

$$F(q, t) = \sum_{m=1}^N e^{-iqR_m(t)} \quad (2-3-8)$$

The scattering intensity averaged over all molecule configurations reads

$$\langle |F(q)|^2 \rangle = \sum_{m,n} \langle e^{-iq(R_m - R_n)} \rangle \quad (2-3-9)$$

The unimer copolymers $R_m - R_n$ are Gaussian-distributed if the micelle phases are not formed completely. The averages $\langle \dots \rangle$ can be written as

$$\langle e^{-iq(R_m - R_n)} \rangle = e^{\frac{q^2}{6} \langle (R_m - R_n)^2 \rangle} \quad (2-3-10a)$$

$$= e^{-\frac{q^2 b^2}{6} |m - n|^{2\nu}} \quad (2-3-10b)$$

Here b is the statistical segment length and L is the contour length, which equals $L = Nb$. The average of the segment inter-distances squares is kept in general for

$$\langle (R_m - R_n)^2 \rangle = b^2 |m - n|^{2\nu} \quad (2-3-11)$$

Symbol ν is the excluded volume parameter from the Flory mean field theory of polymer solutions [54, 55]. The radius of gyration R_g is given by

$$R_g^2 = \frac{1}{2N^2} \sum_{m,n} \langle (R_m - R_n)^2 \rangle \quad (2-3-12a)$$

$$= \frac{1}{2N^2} \sum_{m,n} b^2 |m - n|^{2\nu} \quad (2-3-12b)$$

$$= \frac{b^2}{N} \sum_k \left(1 - \frac{k}{N}\right) k^{2\nu} \quad (2-3-12c)$$

$$= \frac{b^2}{(2\nu + 1)(2\nu + 2)} N^{2\nu} \quad (2-3-12d)$$

Using the general identity

$$\sum_{i,j} y(|i - j|) = N + 2 \sum_{k=1}^N (N - k) y(k) \quad (2-3-13)$$

The form factor reads

$$P(q) = \frac{1}{N^2} |F(q)|^2 = \frac{1}{N^2} \left\{ N + 2 \sum_{k=1}^N (N - k) \cdot e^{-\frac{q^2 b^2}{6} k^{2\nu}} \right\} \quad (2-3-14)$$

Going to the continuous limit ($N \gg 1$), one obtains:

$$P(q) = 2 \int_0^1 dx (1-x) \cdot e^{-\frac{q^2 b^2}{6} N^{2\nu} x^{2\nu}} \quad (2-3-15a)$$

$$= \frac{U^{\frac{1}{2\nu}} \Gamma\left(\frac{1}{2\nu}\right) - \Gamma\left(\frac{1}{\nu}\right) - U^{\frac{1}{2\nu}} \Gamma\left(\frac{1}{2\nu}, U\right) + \Gamma\left(\frac{1}{\nu}, U\right)}{\nu U^{\frac{1}{\nu}}} \quad (2-3-15b)$$

With the modified variable

$$U = \frac{q^2 b^2 N^{2\nu}}{6} = (2\nu + 1)(2\nu + 2) \frac{q^2 R_g^2}{6} \quad (2-3-16)$$

SASfit has implemented the generalized Gaussian coil and the standard Debye formula Gauss. In both cases three versions are implemented which only differ in their parametrization of the scattering intensity. Flexible copolymer chains are not self-avoiding and obey Gaussian statistics. Debye (1947) has calculated the form factor of such chains:

$$I_{Gauss} = I_0 \cdot 2 \cdot \frac{\exp(-u) + u - 1}{u^2} \quad (2-3-17)$$

$$u = q^2 \cdot R_g^2 \quad (2-3-18)$$

R_g is gyration radius and I_0 is the scattering intensity when $q=0$.

The other form factor for Spherical Shell describes when the micelle phases have been formed. It is obtained by

$$I_{Shell}(q, R_1, R_2, \Delta\eta, mu) = [K(q, R_1, \Delta\eta) - K(q, R_2, \Delta\eta(1 - mu))]^2 \quad (2-3-19)$$

$$K(q, R, \Delta\eta) = \frac{4}{3} \pi R^3 \Delta\eta \cdot 3 \cdot \frac{\sin qR - qR \cos qR}{(qR)^3} \quad (2-3-20)$$

If scattering intensity for $q = 0$, the equation is given by

$$\lim_{q=0} I_{Shell}(q, R_1, R_2, \Delta\eta, mu) = \left(\frac{4}{3} \pi \Delta\eta [R_1^3 - R_2^3(1 - mu)] \right)^2 \quad (2-3-21)$$

R_1 is the overall radius of spherical shell and R_2 the core radius. The input parameter $\Delta\eta$ is the difference of scattering length density between shell and solvent, which is $\Delta\eta = \text{SLD}_{\text{shell}} - \text{SLD}_{\text{solvent}}$. The other input parameter mu is the difference of scattering length density between core and solvent, relative to the shell contrast, $mu = \text{SLD}_{\text{core}} - \text{SLD}_{\text{solvent}}$. Fig. 2-3-3 presents a simple sketch.

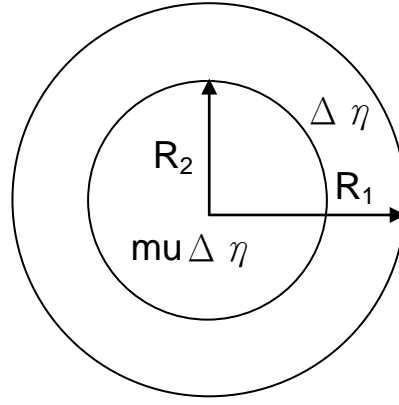


Fig. 2-3-3: Schematic diagram of spherical shell i

For each scattering object i next to a size distribution $N_i(x; \underline{l}_i)$, a structure factor $S_i(q; \underline{s}_i)$ can also be included. When a structure factor is included, there are several theoretical ways to account for it. The structure factor $S(q)$ can be calculated in various approximations, like the monodisperse approximation, decoupling approach, local monodisperse approximation, partial structure factor and scaling approximation of partial structure factors [45]. At the moment, it is assumed that there are no interactions between different species of scatterers so that the total scattering is given by the sum of the scattering of the individual species

$$\frac{d\sigma}{d\Omega}(q) = \sum_{i=1}^N \frac{d\sigma_i}{d\Omega}(q) \quad (2-3-22)$$

whereby $\frac{d\sigma_i}{d\Omega}(q)$ is the species of the differential scattering cross sections. The structure factor $S(q)$ with hard sphere interaction potential $U(r)$ is limited in the range when

$$U(r) = \infty \text{ for } 0 < r < \sigma \quad (2-3-23a)$$

$$U(r) = 0 \text{ for } r > \sigma \quad (2-3-23b)$$

The symbol σ is LogNormal distribution which is defined with reference to the normal distribution. A random variable is Log normally distributed if the logarithm of the random variable is normally distributed. The structure factor with hard sphere is obtained by

$$S_{HS}(q, R_{HS}, f_p) = \frac{1}{1 + 24f_p \frac{G(f_p, R_{HS}q)}{R_{HS}q}} \quad (2-3-24)$$

Where

$$G(q) = \alpha \frac{\sin A - A \cos A}{A^2} + \beta \frac{2A \sin A + (2 - A^2) \cos A - 2}{A^3} + \gamma \frac{-A^4 \cos A + 4[(3A^2 - 6) \cos A + (A^3 - 6A) \sin A + 6]}{A^5} \quad (2-3-25)$$

The symbol α , β , γ and A is the equations as follows:

$$\alpha = \frac{(1 + 2f_p)^2}{(1 - f_p)^4} \quad (2-3-26a)$$

$$\beta = -6f_p \frac{\left(1 + \frac{f_p}{2}\right)^2}{(1 - f_p)^4} \quad (2-3-26b)$$

$$\gamma = \frac{f_p \cdot \alpha}{2} \quad (2-3-26c)$$

$$A = 2R_{HS}q \quad (2-3-26d)$$

The symbol R_{HS} is a hard sphere radius and f_p is the different volumen fraction for a hard sphere interaction potential.

2-4 Rheology [56]

The word “Rheology” comes from Greek originally. The meaning of rheo is the river, flowing and streaming. Scientifically speaking, rheology is the deformation and flow and can also be called flow science. There has been some information obtained by means of rheology experiments, such as the flow behaviour of liquids and the deformation behaviour of solids. Both connect a large deformation, which is produced by shear forces and it occurs the materials to flow. The two plates model is used in this experiment to analyse the gel phases of multilamellar vesicles. The upper plate with the shear area A is set by the motion of shear force F and the result of the velocity v can be measured. The lower plate is stationary and it means $v=0$. The symbol h is the distance between upper and lower plates and the measured sample is sheared in this shear gap. In order to make the calculation of rheometer parameters accurate, there are shear conditions to follow:

- 1 the sample adheres to both plates and does not slide and slip along them
 - 2 it obeys lamellar flow conditions, in other words, it flows in the form of layers.
- Therefore, neither turbulent flow nor vortices occurs.

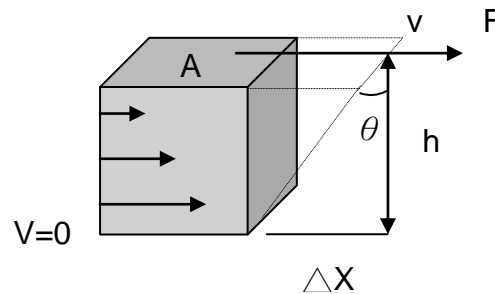


Fig. 2-4-1: The model of shear test

The shear stress τ defined a

$$\tau = \frac{F}{A} \quad (2-4-1)$$

F is the shear force as the unit of N, $1\text{N} = 1 \text{ kgm/s}^2$ and A is the shear area as the unit of m^2 . The unit of shear stress τ is Pa. $1\text{Pa} = 1 \text{ N/m}^2 = 1 \text{ kg/ms}^2$ and the symbol σ is used for yield stress[57]. The shear strain γ is defined as

$$\gamma = \tan \theta = \frac{\Delta X}{h} \quad (2-4-2)$$

, the ΔX is a movement of route of sample. The definition of shear rate $\dot{\gamma}$

$$\dot{\gamma} = \frac{v}{h} \quad (2-4-3)$$

The velocity is v as unit of m/s and h is the distance as unit of m between two gaps. Therefore the unit of shear rate is s^{-1} , which can be called reciprocal seconds. The term of viscosity here means shear viscosity. There is another term of complex viscosity determined by oscillation test. Sometimes they use the same symbol η . The definition of shear viscosity is at the equation as follows:

$$\eta = \frac{\tau}{\dot{\gamma}} \quad (2-4-4)$$

The value is the ratio of shear stress τ to the corresponding of shear rate $\dot{\gamma}$ as the unit of Pas.

Experimental set-up

There are two different set-ups of rheometers, either equipped with a single head or with separated heads. The type of separated heads means the motor and transducer are separated. They are mounted on a different side of measuring geometry. It leads to motor and torque sensor being decoupled. The other type of single head means the motor and transducer are mounted in a combined system on the same side. It is used in this experiment and the sketch is presented in figure.

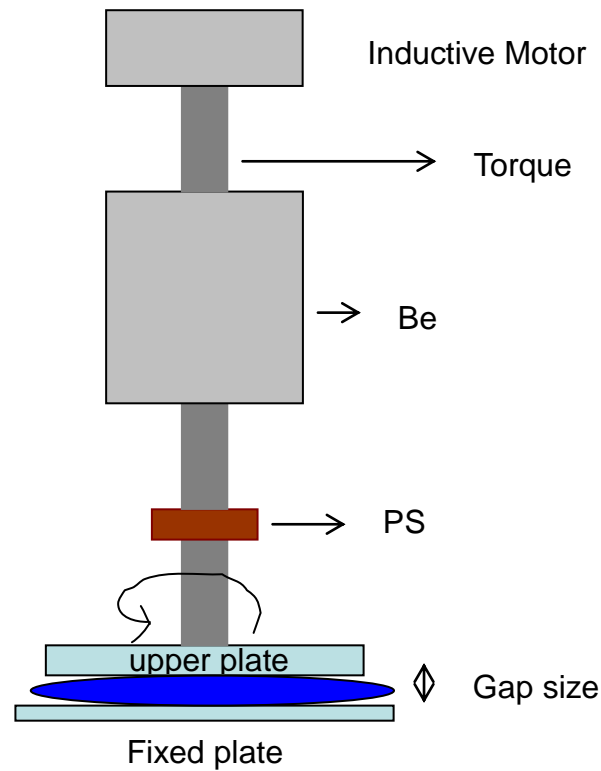


Fig. 2-4-2: Set-up of rehometer for single head type

The Fig. 2-4-2 shows the usual set-up of an oscillatory rheometer. The part torque relates to shear stress τ . When using the controlled shear stress, the electronic controller sends the appropriate operating current I to the motor which produces the corresponding torque. A breaking or restoring torque caused by the sample is acting against the motor torque. A breaking or restoring torque caused by the sample is acting against the motor torque. Be is the bearing, controlling and verifying the distance of gap size. PS is the position sensor and relates to the shear rate and deformation. It controls the rotational speed with angular displacement. The upper plate is selective and dependent on the characteristic measuring materials.

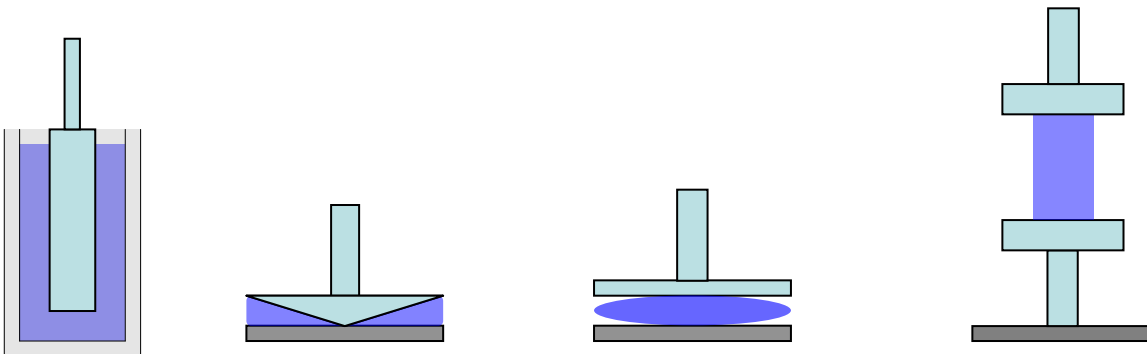


Fig. 2-4-3: The sketch of four measuring systems commonly using rheometers

Some different measurements systems are shown above: From left to right there is a coaxial cylinder in coquette flow, coaxial cone and plate, coaxial parallel plate, and a rectangular torsion (see Fig. 2-4-3). It depends how viscose the sample is, normally the

type of the coaxial cylinder in a coquette flow are very low-viscose solvent mediums, such as decane, whose viscosity is 920 uPas at 20°C. The coaxial cone and plate are used for very low to high viscose liquid and parallel plate is for low viscose liquid to soft viscose solids. The geometry of rectangular torsion is suitable for soft to rigid solids, like steel. Each of them overlaps partially. There are some important terms, like G' , G'' and η^* , when the amplitude sweep and oscillator sweep are measured. G' is the elastic modulus as the unit in [Pa] and G'' calls viscous modulus in [Pa], which relate to complex modulus G^* . In general

$$G^* = \frac{\text{stress}}{\text{strain}} \quad (2-4-5)$$

G^* is the overall resistance to deformation for measuring materials. However the symbol change to G_0 and is called a shear modulus in some publications [1]. The relationship of G^* , G' and G'' can be written as

$$G^* = G' + iG'' \quad (2-4-6)$$

The elastic modulus G' means measuring the elastic properties of materials and investigating how materials store energy so it can be called as storage modulus. The viscous modulus G'' denotes the ability of materials to dissipate energy. It analyses the lost energy as heat and can be called a lost modulus. The parameter η^* is the complex viscosity in [Pas].

2-5 Stopped Flow

Stopped Flow is the most frequently used technique to investigate the chemical kinetic reaction and movement in solutions. The precision of kinetic measuring time reaches microsecond (μs).

Experimental set-up

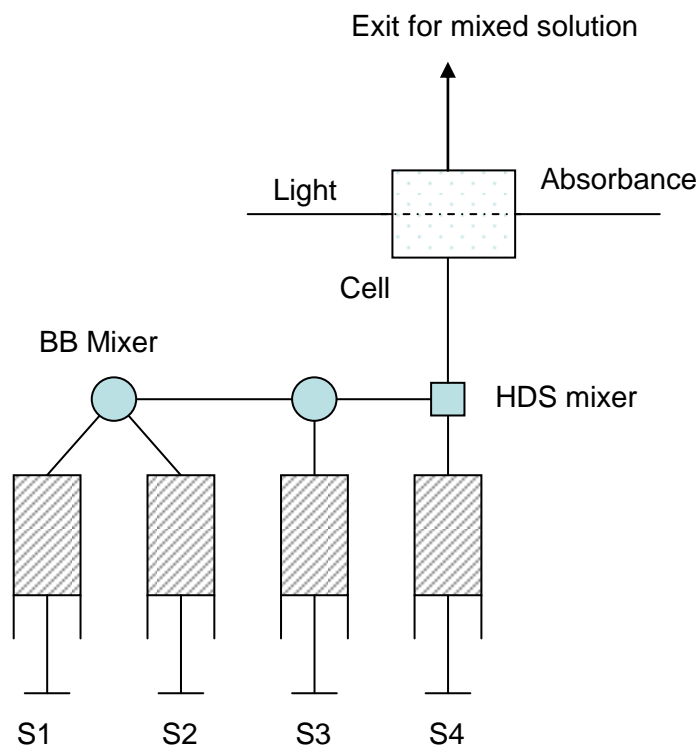


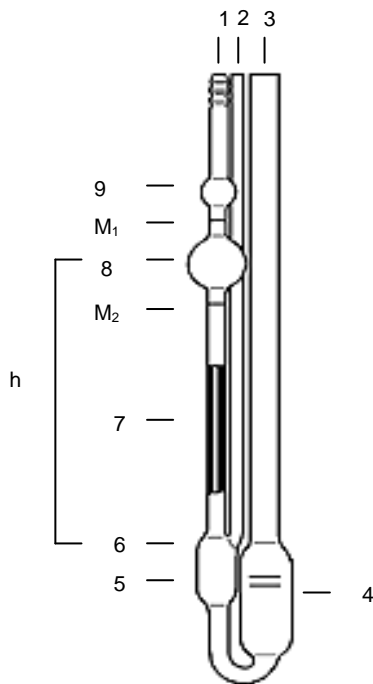
Fig.2-5-1: Schematic diagram of Stopped Flow instrument

The instrument employed was a Bio-Logic SFM400/S. The main part of the Stopped Flow contains four syringes (S1-S4), a BB Mixer and an HDS mixer. The light can be selected at suitable wavelengths; in this experiment it is at 450 nm. The BB mixer is the standard Berger ball mixer; the HDS mixer is a high density mixer. The Syringes S1 and S2 share the one mixer and S3 and S4 are with their mixer on their own, so the measuring sample, like FeSCN^{2+} with DMPC vesicle solution, was put into S4 and the NaF solution in S3.

2-6 Viscosity

The ubbelohde viscometer, a product made by the SCHOTT SCHOTT GERÄTE Company, is used to determine the viscosities of CR3099 and F108 solutions. Different types of capillaries are used for different adhesive level of samples. Capillary I_c , whose range of viscosity is from 3 to 30 mm^2s^{-1} , is used for the F108 solution compatibly. Another capillary O_a is selected for CR3099 solution that the viscosity range is from 0.8 to 9 mm^2s^{-1} .

Description of ubbelohde viscometer



The ubbelohde viscometer is basically consists of the three tube sections (1, 2 and 3), the working capillary (7) with the timing bulb (8) and the upper (9) and lower (5) reservoir. M_1 and M_2 are timing marks. They are defined as the flow-through volumen of the sample and the mean hydrostatic head is h .

Fig. 2-6-1: Schematic diagram of the basic ubbelohde viscometer

After measuring the efflux time of samples from M_1 to M_2 , the viscosity is obtained through the calculation. The equation is given as follows

$$v = K(t - \vartheta) \quad (2-6-1)$$

It is called kinematic viscosity in $\text{cSt} (\text{mm}^2/\text{s})$, because it takes the ratio of the inertial force to the viscous force into consideration. The symbol t is the average flow time in sec and for absolute measurements, the corrected efflux time multiplied by the constant K printed on each viscometer. The symbol ϑ is correction seconds dependent of flow time and the type number of capillary for viscometer.

2-7 Preparations of Materials

1st part: Pluronic F108

Triblock copolymer F108 is used without any purification to be dissolved directly in water. In this experiment, two kinds of fixed solution (3.6 mm and 7.0 mm) are prepared for the parent solution. Tab. 2-7-1 summarizes the structural formula and molecular weight for triblock copolymers.

Tab. 2-7-1: Pluronic

Name	Structural formula	M _w [g · mol ⁻¹]	Company
F108	$[\text{CH}_2\text{CH}_2\text{O}]_{132}[\text{CH}_3\text{CHCH}_2\text{O}]_{50}[\text{CH}_2\text{CH}_2\text{O}]_{132}$	14600	BASF
L35	$[\text{CH}_2\text{CH}_2\text{O}]_{11}[\text{CH}_3\text{CHCH}_2\text{O}]_{16}[\text{CH}_2\text{CH}_2\text{O}]_{11}$	1900	BASF
10R5	$[\text{CH}_3\text{CHCH}_2\text{O}]_{16}[\text{CH}_2\text{CH}_2\text{O}]_{11}[\text{CH}_3\text{CHCH}_2\text{O}]_{16}$	1950	BASF

The additive selected to be dissolved in fixed F108 solution is presented in Tab. 2-7-2 and Tab. 2-7-4.

Tab.2-7-2: Apolar oils and alcohols

Oils	Formula	M _w [g · mol ⁻¹]	Company
1-Hexanol	C ₆ H ₁₄ O	102.18	Merck
Toluene	C ₆ H ₅ CH ₃	92.14	Merck
Geraniol	C ₁₀ H ₁₈ O	154.25	ALDRICH
Ethanol	C ₂ H ₅ OH	46.07	Merck
1-Butanol	C ₄ H ₉ OH	74.12	Merck
1-Octanol	C ₈ H ₁₇ OH	130.23	Merck

2nd Part: Phospholipids DMPC and diesterquat CR3099

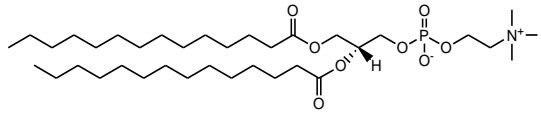
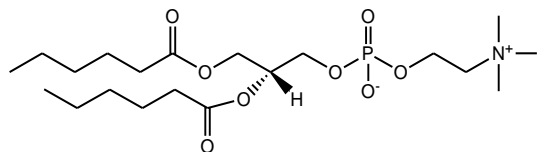
Part of DLS

Phospholipids DMPC are reserved in the refrigerator under -30°C as white powder. When DMPC is hydrated, there are large unilamellar vesicles at different sizes in the solution. Forming the small unilamellar vesicles of DMPC is controlled by means of extrusion.

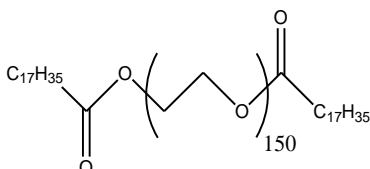
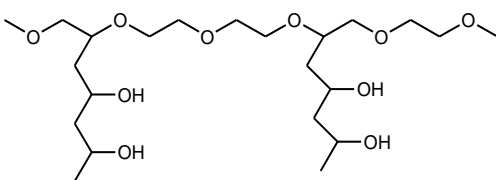
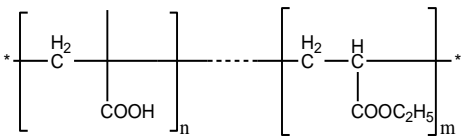
Diesterquat CR3099 appears as a yellow, viscous liquid and is reserved in a cool place without sunlight and at room temperature. Pure CR3099 dissolves in water and appears turbid and homogeneous solutions. It forms large vesicles homogeneously in the solution. Forming the small unilamellar vesicles of CR3099 is controlled by means of extrusion. Filters for 100 nm in diameter are chosen for the formation of the small vesicles. The numbers of extrusion times are at least 5 times; the number of 10 times shows the best efficiency for keeping the long time of the stable small vesicles in the solution. For the case

of CR3099, the samples of CR3099 are extruded only five times. Additives are added into the DMPC and CR3099 solutions respectively before extrusion.

Tab. 2-7-3: Phospholipids

Name	Structural formula	$M_w[\text{g} \cdot \text{mol}^{-1}]$	Company
1,2Dimyristoyl sn-Glycero-3- Phosphocholine (DMPC)		677.94	Avati® polar Lipids, Inc.
1,2Dihexanoyl- sn-Glycero-3- Phosphocholine (DHPC)		453.51	Avati® polar Lipids, Inc.

Tab. 2-7-4: Copolymers

	Structural formula	$M_w[\text{g} \cdot \text{mol}^{-1}]$	Company
PPO	$\text{HO}[\text{CH}_3\text{CHCH}_2\text{O}]\text{H}$	1000.0	ALDRICH
Rewopal 6000		7160	Evonik
Kollicoat® IR (Polyvinyl alcohol- polyethylen e glycol)		470.60	BASF
Kollicoat® MAE 30 DP		250000	BASF

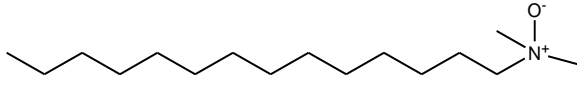
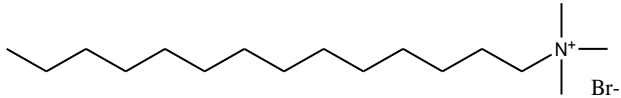
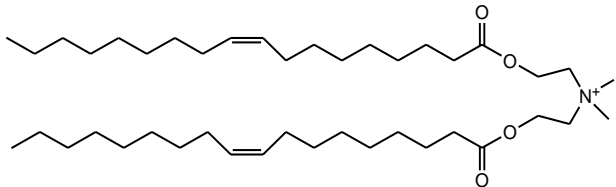
Part of Stopped Flow

The DMPC solution, which has already been extruded, is prepared with ions. There are FeCl_3 at 2 mM, NH_4SCN at 6 mM and NaNO_3 at 200 mM in the DMPC solution. Making the sonication for one hour, it lets the small vesicles and ions homogenous completely in solution. The presence of 200 mM NaNO_3 is because of 200 mM NaF solution in order to prevent the osmotic effect, when they are mixed.

3rd Part: Gel solution of TDMAO, TTABr and 1-Hexanol

The zwitterionic surfactant TDMAO was a noble and worthy gift as a liquid phase from the company of STEPAN. The TDMAO was processed before use with the following process: First, the liquid TDMAO was frozen in the round flask by liquid nitrogen. After that, it was put in the lyophilisation instrument for one week. As a result, it turned into powder. The final solution was prepared by proceeded TDMAO together with TTABr and 1-Hexanol, which were used as received. They are soluble together in water as the gel phases. In this experiment, three parent solutions were prepared at different ratios of TDMAO, TTABr and 1-Hexanol. The presence of an additive is dissolved directly in the parent solution.

Tab. 2-7-5: Surfactants

Name	Structural formula	M _w [g · mol ⁻¹]	Company
Tetradecyldimethylammonium oxide (TDMAO)		246.75	Stepan
Tetradecyltrimethylammonium bromide (TTABr)		336.41	ALDRICH
Di-Oleic Acidyl Isopropylester Dimethylammonium Methosulfate (Diesterquat_CR3099)		662	Evonik

3. Solubilization of oils of different polarity in PEO-PPO-PEO copolymers – Effects on the aggregation behaviour

Investigating the thermal characteristics of Pluronic triblock copolymers has been proceeding for over twenty years. The chemical structure is of the type $EO_n-PO_m-EO_n$ or $PO_m-EO_n-PO_m$ in general; it is one of the most useful amphiphilic surfactants in a variety of applications, such as stabilizers, gene therapy, drug delivery, vesicles, gel materials [58-61], etc. The temperature sensitivity is mainly because of the PPO blocks. The PPO blocks are soluble in water at low temperatures and start to dehydrate if the temperature is reached over the deciding point, which named as the critical micelles temperature (cmt). They are dependent on the concentration as well, and at a constant temperature they will turn hydrophobic once the critical micelles concentration (cmc) is reached. At low temperatures, the blocks of PPO are more hydrophilic than the blocks of PEO. They exist as individual unimers and if the temperature increases, the PPO blocks become more hydrophobic and the hydrophobic PO prefers to aggregate. With the hydrophilic blocks of PEO surrounding the aggregated PPO blocks, they form micelles in the solution, provided the solution is already over cmt and cmc. The micellar phases in water are homogeneous and transparent. There is no macroscopic difference between the unimer and the micelle phases.

There are lots of methods to determine the values of cmc and cmt such as NMR spectroscopy, fluorescence spectroscopy, surface tension meter and calorimeter methods, like isothermal titration calorimetry (ITC) and Differential scattering calorimeters (DSC), which have been published [62-67]. In this work, DSC is used to determine cmt values of fixed pluronic solutions in the presence of polar oils and other kinds of copolymers, respectively, and to characterize the aggregation process correspondingly. The pluronic F108 was selected as a rather hydrophilic copolymer surfactant and mainly concentrations of 3.6 mm and 7.0 mm were employed. The polar oils of 1-Hexanol, Toluene, and geraniol were selected as representative solubilizates of different polarities. In this system, cmt values were previously determined by means of fluorescence spectroscopy (diploma thesis and these values are given in the appendix). In this work the calorimetric aspects of such solubilization are studied and compared to structural investigation by means light scattering and neutron scattering.

1-Hexanol can be solubilized at the highest amounts of all the apolar oils. Its solubility capacity has been tested to be homogenous, at least 150 mm in 3.6 mm F108 solution; by the way, the 200 mm 1-Hexanol appears turbid. For a comparison other primary alcohols

were also studied, such as ethanol, 1-Butanol and 1-Octanol. For F108 solutions of 7.0 mm, correspondingly higher solubilization capacities are expected. In addition to the oils/alcohols, the pure homopolymer PPO at ca. $1000 \text{ g} \cdot \text{mol}^{-1}$ was selected to analyse its effect on phase behaviour and thermal properties at first, thereby comparing to a polymeric oil.

Let us now think back to the topic of my diploma dissertation, which focused on the solubilisation of polar oils in fixed solutions of the triblock copolymer F108. It tried to determine the solubility capacity of each selecting apolar oils in the F108 solution respectively by the macroscopic and microscopic methods. Analysing the modification of fluorescence absorbance is measured dependent on temperature in order to determine the cmc values. The force between the F108 solution and each of the oils was also discussed in the dissertation and they were analysed from 15°C to 40°C by means of interfacial force of spinning drop. Continuing this work, my doctoral dissertation investigates the thermal characteristics of triblock copolymers. Selecting the same triblock copolymer F108 solubilized with the reduplicate oils, like 1-Hexanol, Toluene, geraniol and homo copolymer PPO. The polymer Kollicoat MAE 30 DP, which has been used in pharmaceutical applications, is selected as an additive in the F108 solution; it is more hydrophilic in comparison to other additives. There are other additives in the group of primary alcohol, such as Ethanol, 1-Butanol and 1-Octanol, which is used for investigating thermal properties of F108. The analysis methods are differential scanning calorimeters (DSC), dynamic light scattering (DLS), small angle neutrons scattering (SANS) and viscosity. All the samples are measured by the DSC method and the cmc values and enthalpy of $\Delta H_{(\text{PO})}$ are determined for each of samples. In the presence of oils, normally the cmc decreases, this has been proved in my master's dissertation by the method of fluorescence spectroscopy. However, some additives, like PPO and Kollicoat MAE 30 DP, result in another appearance. The size of micelle phases was analysed by DLS. They were measured dependent on temperature in order to observe the dehydration process of the hydrophobic blocks. The hydrodynamic radius R_h is determined by the ALV 7004 Correlator software with methods of Simple Fit and Regularized Fit. The results of SANS give us additional information to reconfirm the existence of 1-Hexanol most in F108 not in D_2O solutions. The intensity $I(q)$ is increased markedly in the presence of 1-Hexanol at a fixed q position.

3-1 F108 solution

As the PPO blocks of F108 are sensitive to temperature, the unimer F108 phases can turn to micelle phases in the aqueous solution with increasing temperature. While the macroscopic appearance of the F108 solution is little affected by this transition (unimer and micelle phases are both homogeneous and transparent), it can be detected by the DSC method.

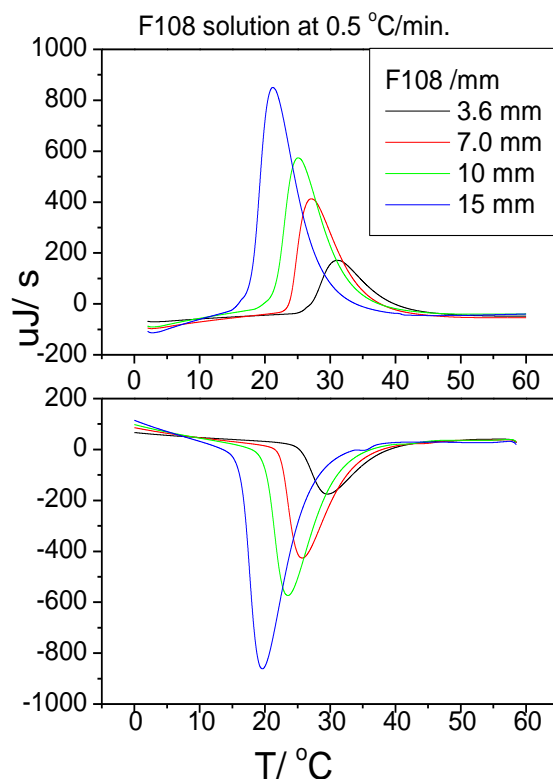


Fig. 3-1-1a and 1b : Thermal peaks of 3.6 mm, 7.0 mm, 10 mm and 15 mm F108 solution in heating (1a) and cooling (1b) processes as function of temperature.

The concentration of F108 solution is increased from 3.6 mm to 15 mm and signals appear in the heating and cooling process by means of the DSC instrument. The signals are an endothermic and an exothermic peak for both processes, respectively. With increasing temperature, the PPO blocks become dehydrated and more hydrophobic. The dehydration of PPO blocks is an endothermic reaction. In other words, if the temperature decreases, the PPO blocks start to be hydrated and release the energy again. With higher concentrations of F108, the endothermic and exothermic peaks are shifted to higher temperatures.

Tab.3-1-1: T_{onset} and T_{peak} of F108 in thermal process

F108 solution at scan rate of 0.5 °C/min				
	Heating process		Cooling process	
F108/ mm	T_{onset}	T_{peak}	T_{onset}	T_{peak}
3.6	26.6	31.1	39.1	29.6
7.0	23.6	27.1	37.5	25.6
10	21.4	25.1	34.3	23.5
15	17.3	21.2	29.2	19.5

The endothermic and exothermic peaks of increasing concentrations of F108 from 3.6 mm to 15 mm as a function of temperature are presented in Fig.3-1-1 and 3-1-2. Two positions of temperature are taken into consideration. They are called T_{onset} and T_{peak} . T_{onset} is at the point at which thermal reaction begins [68] and T_{peak} at the highest point of the thermal peaks. Both temperatures are used commonly as a cmt point to determine the micelle phases in the solution [11, 69-71]. There is another method for cmt determination, which is called the inflection point temperature (T_{inf}) by Hecht and Hoffmann [72]. The temperature T_{inf} is not discussed in this dissertation. With increasing amounts of F108, lower values of T_{onset} and T_{peak} are observed.

Tab.3-1-2: Intergration Q and $\Delta H_{(PO)}$ of F108 solution in thermal process

Integration Q and $\Delta H_{(PO)}$ of variable F108 solution / mm at 0.5 °C/ min				
	Integration Q/mJ		$\Delta H_{(PO)}$ / kJmol ⁻¹	
F108/ mm	Heating	Cooling	Heating	Cooling
3.6 mm	194.2	189.1	3.79	3.70
7.0 mm	386.3	372.1	4.10	3.95
10 mm	510.2	498.6	3.96	3.87
15 mm	735.7	711.8	4.08	3.95

Tab. 3-1-2 summarizes the integration area and the enthalpy of each PO unit for F108 solutions with the concentration from 3.6 mm to 15 mm. The integration area is proportional to the amounts of F108 copolymer. The 15 mm F108 solution results the highest endothermic and exothermic peak and the maximal values of the integration. After calculation, the enthalpy of each PO unit is on average around 4.0 and 3.9 kJmol⁻¹. Another publication results enthalpy $\Delta H_{(PO)50}$ of F108 copolymer 220 kJmol⁻¹ equally when the concentration is from 2% to 10%. The enthalpy is influenced by the measuring scanning rate. The scanning rate of 0.5°C/min. results in an enthalpy higher than 0.2°C/min. The enthalpy of dehydration from this experiment and publication shows the same results that the values become constant when the concentration of F108 is increasing [10].

3-2 Mixtures of apolar oil and F108 solution

The polar oils, like 1-Hexanol, geraniol and Toluene, were studied in mixtures with different concentrations of F108 solutions. The high amounts of F108 could be hard dissolve in water at room temperature. The phase behaviour of F108 solution at high concentrations, like 10 mm and 15 mm, is still transparent and homogenous, but it turns into a gel and becomes more viscous upon adding the solubilisate. The phase behaviour of F108 copolymers form unimer phases, micelle phases and lamellar phases in aqueous solutions dependent on concentration. However, they are all transparent and homogeneous under macroscopic observation. The admixture of 1-Hexanol, geraniol has been shown before by fluorescence spectroscopy to lower the critical micelle temperature, by analysing the ratio of I_1 and I_3 with Pyren in solution [73]. More comprehensive information was obtained here by the DSC method. The appearance of thermal peak position at given temperature allows to deduce precisely the cmt values and its integration gives the dehydration enthalpy of PO.

Phase Behaviour

Polar oils, PPO and 3.6 mm F108 solution

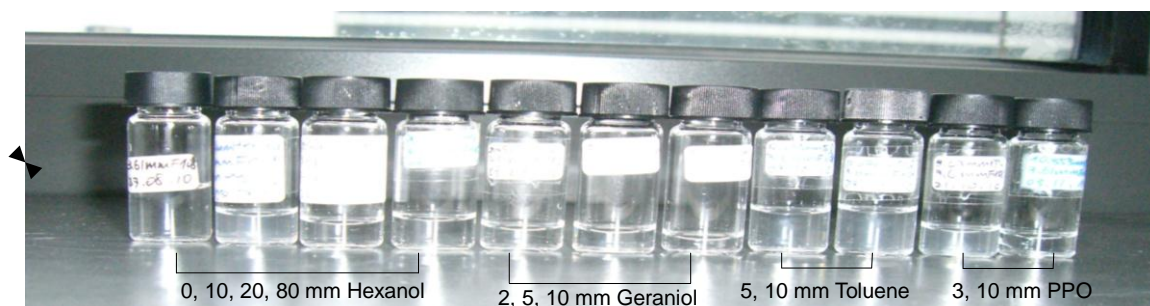


Fig. 3-2-1: Photo of samples containing various polar oils and PPO in a 3.6 mm F108 solution

The copolymer F108 was dissolved in water directly without any purification. They are used for parent solutions at the concentration of 3.6 mm and 7.0 mm. The selecting oils 1-Hexanol, geraniol, PPO, etc., were dissolved directly in the parent solution, respectively. Depending on their solubility, the highest amounts of them prepared are not the same. Fig. 3-2-1 shows the homogeneity and transparency of the samples.

3-2-1 1-Hexanol and F108 solution

This part presents the nano DSC measurements of 1-Hexanol, which is mixed with two different fixed parent solutions of 3.6 mm and 7.0 mm F108. The chemical structure of 1-Hexanol is similar to that of surfactants, with a hydrophobic and a hydrophilic part, but it can not form micelles itself. Such molecules can be classified as cosurfactant. 1-Hexanol

dissolves somewhat in aqueous solutions (5.9 g/L or 57 mm at 20 °C), but the F108 solution can dissolve much more 1-Hexanol than pure water. The reason can be due to it containing the hydrophobic and hydrophilic character of PEO-PPO-PEO blocks in the solution. The values of Hildebrandt parameters between 1-Hexanol and F108 are close each other, and relatively far from water. The F108 forms the extra hydrophilic and hydrophobic area in water that provides another environment for 1-Hexanol to coexist.

1-Hexanol and 3.6 mm F108

For the case of 3.6 mm F108, we studied 1-Hexanol concentrations of 0-100 m in the temperature range of -10 to 60°C by DSC heating and cooling cycles.

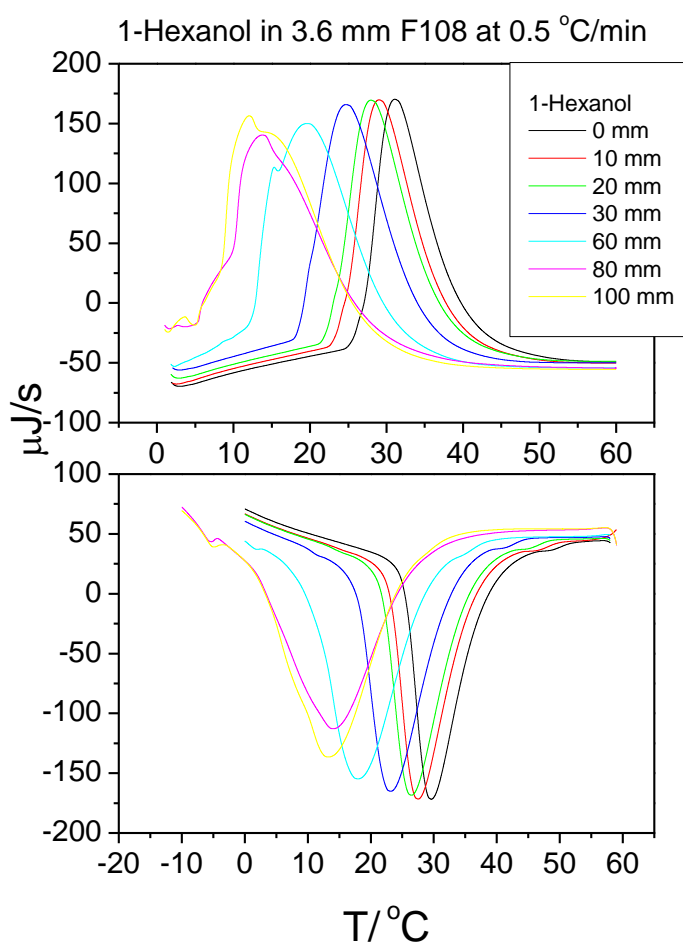


Fig. 3-2-1-1a and 1b: 1-Hexanol in 3.6 mm F108 as a function of temperature in heating(1a) and cooling(1b) processes.

In the heating and cooling process of 1-Hexanol and 3.6 mm F108 solution, the endothermic and exothermic peak appear in the range from 0°C to 60°C. The samples of 80 mm and 100 mm were measured in the heating process from 0°C to 60°C and cooling down from 60°C to -10°C (see Fig. 3-2-1-1a and 1b). The transformation of 1-Hexanol

containing the 3.6 mm F108 aqueous solution is a fully reversible process. The endothermic and exothermic peaks of 3.6 mm F108 shift to lower temperatures with increasing concentrations of 1-Hexanol. At low concentrations of 1-Hexanol, only the position of peaks is affected but not the shape. If the concentration of 1-Hexanol is increased above 60 mm, the peak shape becomes deformed. It could be the solubility of 1-Hexanol due to the low temperature decreasing. Limiting the set up of this instrument does not let the process start at subzero temperatures in the heating process, but in the cooling process can continue the measurements under 0 to -10°C. The samples of 80 mm and 100 mm begin to form micelle phases at a similar position of T_{onset} in the heating process and 100 mm results higher intensity than 80 mm 1-Hexanol.

Tab. 3-2-1-1: T_{onset} and T_{peak} of 1-Hexanol and 3.6 mm F108 in thermal process

1-Hexanol in 3.6 mm F108 solution at scan rate of 0.5 °C/min				
1-Hexanol/ mm	Heating process		Cooling process	
	T_{onset}	T_{peak}	T_{onset}	T_{peak}
0	26.6	31.1	39.1	29.6
10	24.2	29.0	38.3	27.4
20	22.8	27.9	36.2	26.4
30	18.3	24.6	33.7	23.1
60	12.5	19.5	30.4	17.9
80	4.20	13.8	26.8	12.5
100	4.50	12.3	24.5	4.70

Tab. 3-2-1-1 summarizes the temperatures of onset and peak with variable concentration of 1-Hexanol in 3.6 mm F108 solution. T_{onset} and T_{peak} values are both used to discuss the formation of micelle phases, i.e., by the critical micelle temperature. Both, T_{onset} and T_{peak} of 3.6 mm F108 solution decrease proportionally to the concentration of 1-Hexanol.

Tab.3-2-1-2: Integration Q and $\Delta H_{(\text{PO})}$ of 1-Hexanol and 3.6 mm F108 solution in thermal process

Integration Q and $\Delta H_{(\text{PO})}$ of 3.6 mm F108 with the variation of 1-Hexanol/ mm at 0.5 oC/ min				
1-Hexanol	Integration Q/mJ		$\Delta H_{(\text{PO})}$ / kJmol ⁻¹	
	Heating	Cooling	Heating	Cooling
0 mm	194.2	189.1	3.79	3.70
10 mm	204.2	199.8	4.00	3.90
20 mm	215.2	206.9	4.21	4.04
30 mm	237.9	226.1	4.65	4.42
60 mm	284.1	278.0	5.55	5.43
80 mm	--	305.3	--	5.97
100 mm	--	333.4	--	6.51

Tab. 3-2-1-2 summarizes the integration area and enthalpy of PO pro unit of the 3.6 mm F108 with the mixture of 1-Hexanol. The integrated heat Q increases with the addition of 1-Hexanol and is proportional to the 1-Hexanol concentration at the fixed F108 solution. The enthalpy of $\Delta H_{(\text{PO})}$ also increases in the presence of 1-Hexanol and indirectly proves that the PO blocks interact with the 1-Hexanol. In other words, 1-Hexanol as a cosurfactant enhances the efficiency of the dehydration of each PO block. Indirectly it is

proved that certain amounts of 1-Hexanol are dissolved in hydrophobic parts of PPO. The solubility of 1-Hexanol in water is low but is enhanced in the presence of F108. The thermal peaks for the sample of 80 and 100 mm are not complete in the heating process, so only the results are presented for the cooling process in the table.

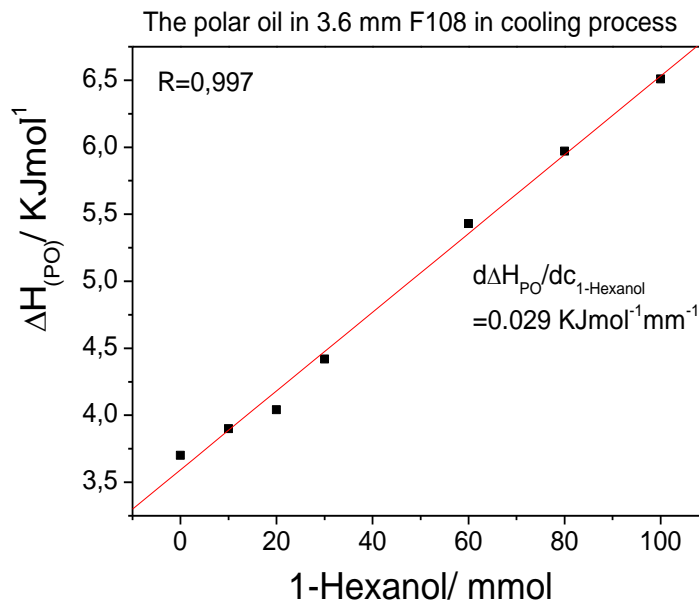


Fig. 3-2-1-2: Enthalpy $\Delta H_{(PO)}$ of 1-Hexanol in 3.6 mm F108 as function of concentration

Fig. 3-2-1-2 shows the enthalpy $\Delta H_{(PO)}$ of fixed 3.6 mm F108 in the presence of 1-Hexanol as a function of concentration. After linear fit calculation, the value R is 0.997. The result shows the optimal linear function. In the 3.6 mm F108, the solubility capacity of 1-Hexanol is not reached. The maximal of 1-Hexanol can be increased to 150 mm homogeneously in the F108 solution. In the presence of 1-Hexanol it is useful for the F108 solution to increase the energy of the dehydration and hydration processes.

1-Hexanol and 7.0 mm F108

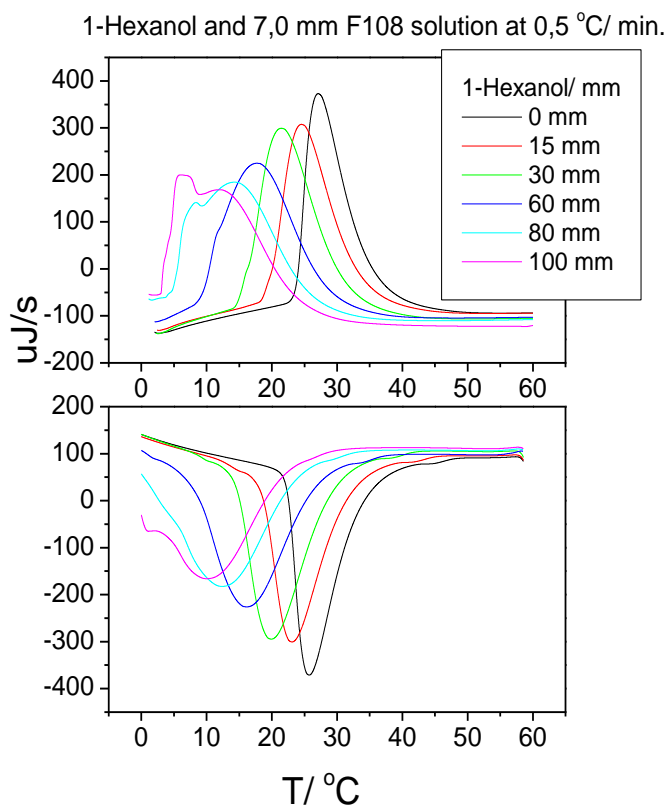


Fig. 3-2-1-3a and 3b: 1-Hexanol in 7.0 mm F108 as a function of temperature in heating (3a) and cooling(3b) processes

Also for admixtures of 1-Hexanol to 7.0 mm F108 solutions, the endothermic and exothermic peaks appear in the range from 0 to 60°C in the heating and cooling processes. Figures 3-2-1-3a and 3b indicate that the 7.0 mm F108 solution, which is mixed with 1-Hexanol, forms the micelle phases. The process of dehydration is reversible. Interestingly, the sample containing no 1-Hexanol shows the sharpest endothermic and exothermic peaks. Addition of the 1-Hexanol lowers the height of endothermic and exothermic peaks and the peaks shift to lower temperatures. The shapes of peaks become deformed if the concentration of 1-Hexanol is over 60 mm. It could be the low solubility of 1-Hexanol at low temperatures in the F108 solution. The result is similar to the 3.6 mm solution. The sample for 100, 80 mm could form complete endothermic and exothermic peaks under the experimental conditions of the Nano DSC measurements.

Tab.3-2-1-3: T_{onset} and T_{peak} of 1-Hexanol and 7.0 mm F108 in thermal process

1-Hexanol in 7.0 mm F108 solution at scan rate of 0.5 °C/min				
	Heating process		Cooling process	
1-Hexanol/ mm	T_{onset}	T_{peak}	T_{onset}	T_{peak}
0	23.6	27.1	37.5	25.6
15	19.4	24.5	32.4	23.0
30	15.7	21.4	30.5	19.9
60	9.1	17.6	28.2	16.2
80	4.8	14.6	25.0	12.3
100	3.0	6.4	23.5	9.9

Tab. 3-2-1-3 shows the reduction T_{onset} and T_{peak} in heating and cooling process for 7.0 mm F108 solution that is proportional to the amount of 1-Hexanol contained. In the presence of 1-Hexanol it is useful for 7.0 mm F108 solution to be successively decreased.

Tab.3-2-1-4: Integration Q and $\Delta H_{(PO)}$ of 1-Hexanol and 7.0 mm F108 solution in thermal process

Integration Q and $\Delta H_{(PO)}$ of 7.0 mm F108 with the variation of 1-Hexanol/ mm at 0.5 °C/ min				
	Integration Q/mJ		$\Delta H_{(PO)}/ \text{kJmol}^{-1}$	
1-Hexanol	Heating	Cooling	Heating	Cooling
0 mm	386.3	372.1	4.10	3.95
15 mm	391.2	382.8	4.16	4.07
30 mm	419.3	391.3	4.45	4.16
60 mm	452.5	397.8	4.81	4.23

The results of integration and enthalpy of $\Delta H_{(PO)}$ from the endothermic and exothermic peaks of the 7.0 mm F108 solution, composed of 1-Hexanol, are given in Tab. 3-2-1-4. The 7.0 mm F108 solution shows higher values of integration than 3.6 mm F108, because 7.0 mm F108 contains more hydrophobic blocks of PPO than 3.6 mm F108. However, the $\Delta H_{(PO)}$ results are almost the same, which demonstrates that this enthalpic process has to be associated with the PO. The presence of 1-Hexanol increases the enthalpy of PO dehydration appreciably and $\Delta H_{(PO)}$ is proportional to the concentration. The 7.0 mm F108 solution is more soluble with more than 100 mm 1-Hexanol. The amount of 1-Hexanol has been increased to 300 mm in 7.0 mm F108 homogeneously and was analysed by fluorescence spectroscopy (see appendix). The values of T_{onset} and T_{peak} will decrease close to 0°C. Tab. 3-2-1-4 summarized the results from 0 to 60 mm, because the thermal peaks for the samples of 80 and 100 mm are not complete in either process. After calculation both are not accurate in reality.

Results of SANS measurements

The 3.6 mm F108 is analysed intensively by means of the neutron scattering method. The SANS data provides us the details that the behaviour of 3.6 mm F108 induces in the presence of increased 1-Hexanol at a constant temperature. The data can be analysed by the program of SASfit [45]. The samples were prepared ready in Stranski-Laboratorium and measured at HzB by Dr. Sylvain Prévost.

1-Hexanol in the 3.6 mm F108 D₂O solution

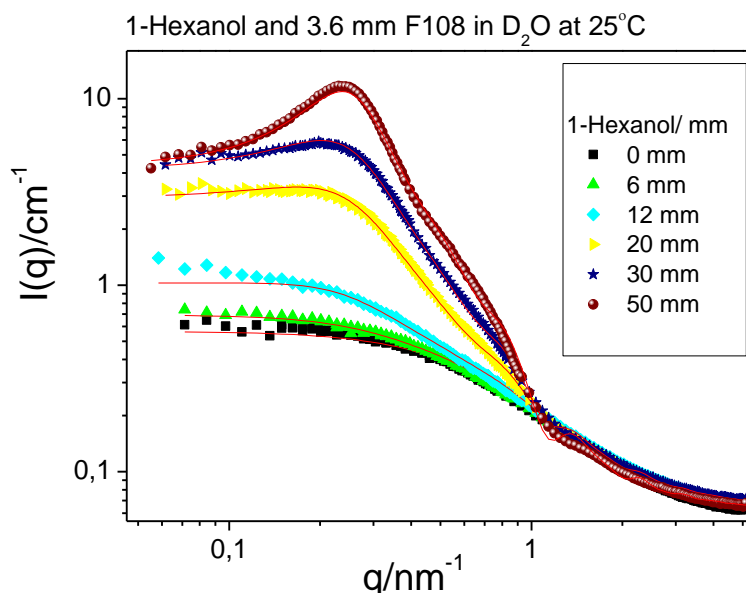


Fig. 3-2-1-4: SANS data of 1-Hexanol in the 3.6 mm F108 D₂O solution at 25°C (with fit data)

The models of background, Gauss and core shell i with hard sphere have been selected to fit the F108 SANS measurements in the presence of 1-Hexanol. The fitting equations are selected von the Gauss model with eq. 2-3-17 and Spherical shell i model with the structure factor Hard Sphere. The form factor von Spherical shell i model is the eq. 2-3-21 and the structure factor of Hard Sphere is followed by eq. 2-3-24.

Fig. 3-2-1-4 shows results of SANS for samples with 1-Hexanol from 0 to 50 mm in 3.6 mm F108 in D₂O, respectively. The presence of 1-Hexanol increases the intensity at low q and middle q position. The D₂O samples were all measured at room temperature around 25°C and are under of cmt of the pure 3.6 mm F108 solution. The presence of the 1-Hexanol leads to an increase of scattering intensity, where this increase is particularly pronounced in the range of 15-20 mm. Apparently for lower 1-Hexanol content, one has unimers present, which then become transformed to micelles for higher 1-Hexanol content.

For the unimer solutions of F108, the radius of gyration R_g , which means the size of the individual F108 copolymers, was determined by a coil model with the Debye equation [54, 74]. Small amounts of 1-Hexanol can be dissolved in the unimer phase of F108 and D₂O without altering the structure much. When 1-Hexanol increases to 50 mm, the intensity of $I(q)$ remains equal to the 30 mm 1-Hexanol at low q but a correlation peak is developing. The solubility capacity of unimer and D₂O is saturated and the extra 1-Hexanol still can be dissolved in the aggregates of F108. A Spherical shell i model (Fig. 2-3-3) was employed in the analysis of the SANS data and was fitted to the data using the software program SASfit. The best fit results are presented with the SANS data in Fig 3-2-1-4. Three models have been selected, which is background, Gauss and spherical shell i including of hard sphere, in order to do calculations of the SANS measurements by the SASfit software.

Tab. 3-2-1-5: Input parameters of form factors and the structure factor for the 3.6 mm F108 in the presence of 1-Hexanol

3.6mm F108	Background	Gauss		Spherical Shell i					Hard sphere	
1-Hexanol [mm]	I_{inc} [cm ⁻¹]	I_0 [cm ⁻¹]	R_g [nm]	N_{agg}	R_1 [nm]	R_2 [nm]	μ [nm ⁻²]	η [nm ⁻²]	R_{HS} [nm]	fp
0	0.055	0.51	2.31	-	-	-	-	-	-	-
6	0.059	0.51	2.31	0.36	9.6	3.9	15.18	8.7E-5	11.36	0.021
12	0.061	0.52	2.31	1.58	9.6	3.9	15.18	8.7E-5	11.36	0.047
20	0.060	0.51	2.31	10.62	9.6	3.9	15.18	8.7E-5	11.36	0.075
30	0.063	0.48	2.31	21.63	9.6	3.9	15.18	8.7E-5	11.36	0.113
50	0.061	0.36	2.31	42.27	9.6	3.9	15.18	8.7E-5	11.36	0.188

The results of the parameters are summarized in Tab. 3-2-1-5. The background I_{inc} is one of the parameters from the Porod approximation at the beginning of an integral structure. It is like the noise correction of scattering. The Gauss model describes the random walk for a polymer chain in a solution. The parameters of the Gauss model are I_0 and R_g . R_g is the gyration radius and I_0 is forward scattering at $q=0$. The form factor of Spherical shell i is parameterized with an inner radius R_2 and outer radius R_1 . The parameter of $\Delta\eta$ is the scattering length density difference between shell and solvent. μ is the scattering length density difference between the core and solvent, relative to the shell contrast (see. Fig. 2-3-3). R_{HS} is a hard sphere radius. The six samples in the presence of increasing 1-Hexanol respectively make a multiple fit calculation and the results are summarized in Tab. 3-2-1-5. In Fig. 3-2-1-4, the each of the fit dates corresponds to their measurements. Some parameters are in question, like the parameter I_0 from Gauss model. It leads to a decreasing value when the 1-Hexanol is increasing, but the curve presents the contrary. The gyration radius R_g has the same result at a radius of 2.31 nm with increasing amounts of 1-Hexanol because the unimer phases are only from F108 and at the fixed solution of 3.6 mm. Other radius parameters, like R_2 , R_1 and R_{HS} , remain constant result in the presence of 1-Hexanol. Those radiuses indicate indirectly the size of the triblock copolymer F108 after dehydration effects, in other words, the size of micelle phases. They indicate the size and distance of each micelle when the copolymers of F108 have been

aggregated. The presence of 1-Hexanol does not influence the size of particles; however, the parameter N is improved. N_{agg} are the numbers of aggregation and can be calculated by the characteristics of the components (molecular, volumenn and SLDs) and the total volume fraction of additives [75].

Normally the micelles are expected to have a high-density compact core, which is a hydrophobic part of PO blocks and a low-density compact corona, which is the hydrophilic part of EO blocks. These parameters are presented as a scheme in Fig. 3-2-1-4. In the absent of 1-Hexanol the 3.6 mm F108 is measured under critical micelle temperatures. In the presence of 1-Hexanol it leads the critical micelle temperature of 3.6 mm F108 to go down. At a constant temperature like 25°C the aggregation numbers of F108 copolymers grow with increasing amounts of 1-Hexanol. The model of Spherical shell i is concerned about Hard sphere, which contains two parameters R_{HS} and fp . R_{HS} is called the hard sphere radius, which is the distance between two particles, and fp is the volume fraction.

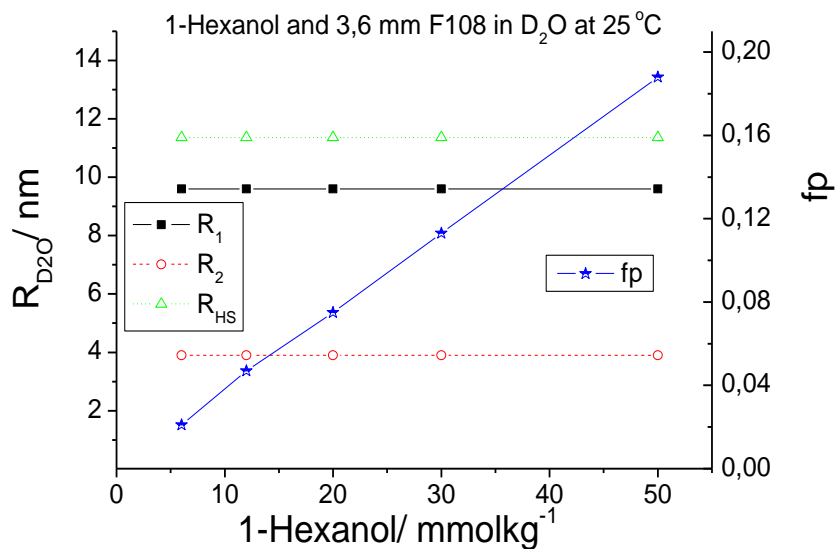


Fig.3-2-1-6: Results of R_1 , R_2 , R_{HS} and fp as a function of 1-Hexanol in mm

Fig. 3-2-1-6 summarizes the results of inner and outer radii R_2 and R_1 , Hard sphere radius R_{HS} and volume fraction fp as function of 1-Hexanol in mm. The outer R_1 and inner R_2 radius result in no changes with increasing amounts of 1-Hexanol. The radius R_1 can look on as the size of F108 after aggregation and R_2 is the hydrophobic part of PPO blocks from F108. Comparing with the DLS measurements the SANS present a similar size in the aggregation process. The presence of 1-Hexanol leads to no influences that modify the radius of F108 copolymer. The Hard sphere radius keeps constant with increasing amounts of 1-Hexanol. The aggregation of F108 distributes homogenously in

the solution. There are no attractive effects for 1-Hexanol as a bridge that packed each micelle or aggregation densely. However, the increasing of volume fraction ϕ_p indicates the existence of 1-Hexanol in the solution. The high scattering intensity $I(q)$ grows at the same q position in the middle, indicating that 1-Hexanol dissolved in the parts of F108 copolymers after aggregations have been already formed. The low q position appears with high intensity in the presence of 1-Hexanol. The fixed solution of 3.6 mm F108 at 25°C is under the cmt, which is determined by the DSC method. Some amounts of 1-Hexanol could be soluble the unimer phases of F108. There are some parameters, like μ eta and R_g that are not presented in Fig. 3-2-1-7. The gyration radius of R_g results in a constant radius after SASfit calculations with increasing amounts of 1-Hexanol. It appears to have no influence on modifying the unimer radius in the presence of 1-Hexanol.

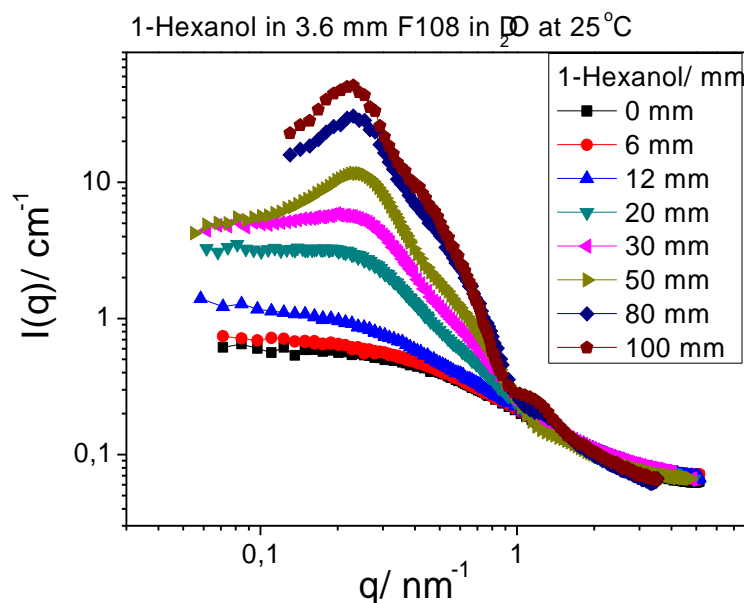


Fig.3-2-1-7: SANS data of the 1-Hexanol in 3.6 mm F108 D₂O solution (without fit data)

The samples of 80 and 100 mm 1-Hexanol in 3.6 mm F108 were measured recently by Mr. Raphael Michel at ILL in Grenoble after the samples from 0 to 50 mm. Compared with the old dates, the scattering intensity continues to increase at the middle q position when the concentration of 1-Hexanol increases to 100 mm. The phase behaviour of SANS samples for 80 mm and 100 mm is transparent and homogenous. They are dissolved mostly in the core – shell of F108 aggregations. The scattering intensity of 80 mm and 100 mm 1-Hexanol is not measured at the low q position, so it is hard to investigate the influence with the old data. SANS data of Fig. 3-2-1-7 have been fitted by Dr. Sylvain Prévost and published [76].

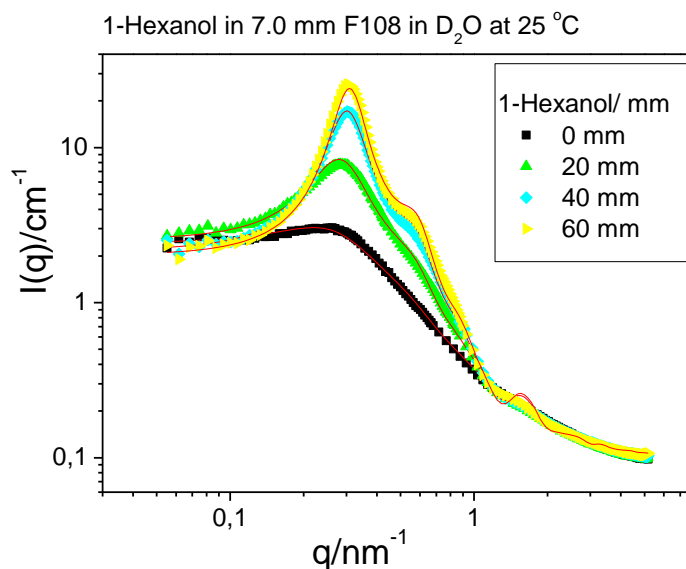


Fig.3-2-1-8: SANS data of the 1-Hexanol in 7.0 mm F108 D₂O solution (with fit data)

At a fixed concentration of 7.0 mm F108 in D₂O is measured by the SANS method in the presence of 1-Hexanol from 0 to 60 mm. The samples contain similar amounts of 1-Hexanol (see Fig. 3-2-1-4) and the F108 solution is increased to 7.0 mm. From the results of Nano DSC the 7.0 mm F108 has been already aggregated at 25°C. At the low q position there appears to be no increasing scattering intensity in the presence of 1-Hexanol. However, $I(q)$ increases at the middle q position with increasing amounts of 1-Hexanol. Most of the triblock copolymers have been dehydrated at 25°C at a concentration of 7.0 mm in the solution. 1-Hexanol prefers to stay in the aggregation of F108 than the aqueous solution, when micellization conditions of the F108 solution is comformed even if it can be soluble in at least 40 mm in water. Fig. 3-2-1-8 presents the best fit curve for each of the samples, which are analyzed by SASfit. The models of Background, Gauss and Spherical Shell i models including Hard sphere are selected. The results of fit parameters existed questionably, like 3.6 mm F108 in D₂O, so they will not be summarized in this dissertation.

3-2-2 Geraniol and F108 solution

The polar oil geraniol appears clear and the solubility in water is 686 mg/L, which is equal to 4.45 mm at 20°C [77]. The organic compounds of Geranial – an allyl alcohol with an acyclic monoterpene chain length, which is one kind of flavour chemical –, can be synthesized and extracted from plants, such as lavender, geranium, roses, orange leaves and lemon peels. Although geraniol is dissolved in water very low, the solubility is increased in the presence of F108. The solubility parameters of F108 and geraniol are similar. It can be predicted that they can be soluble to each other in aqueous solutions.

Geraniol and 3.6 mm F108

For the case of 3.6 mm F108, we studied geraniol concentrations of 0 to 13 m in the temperature range of 0 to 60 °C by DSC heating and cooling cycles.

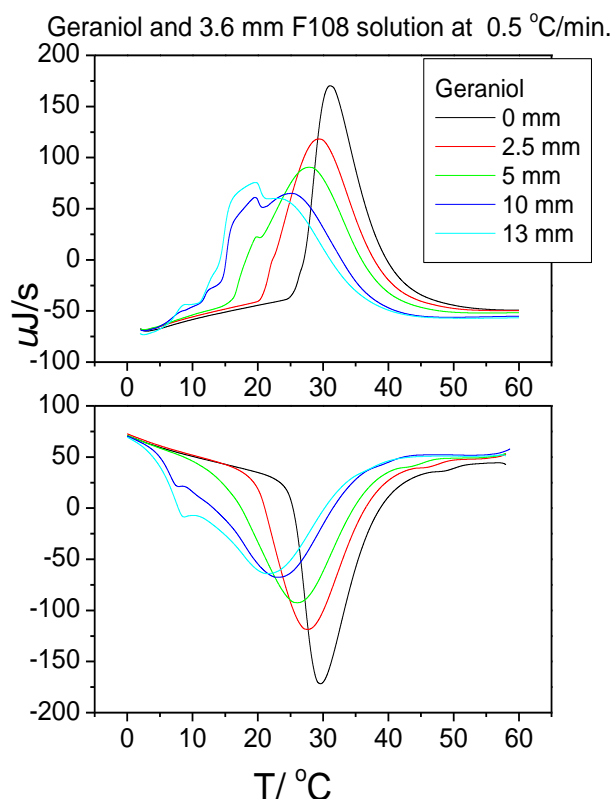


Fig. 3-2-2-1a and 1b: Geraniol in 3.6 mm F108 as a function of temperature in heating (1a) and cooling (1b) processes

3.6 mm F108 solutions in the presence of geraniol from 0 to 13 mm have shown, in Fig. 3-2-2-1a and 1b, the thermal peaks via the DSC measurements in the heating and cooling processes. The highest peak intensity is reduced in the presence of geraniol and the peak

width gets broader. The peak position shifts to the lower temperature when the concentration of geraniol is increased in the 3.6 mm F108 solution. At high concentrations of Geraniol, like 5 mm, a slightly deformed endothermic peak appears, although in the cooling process a broadening exothermic peak appears. If geraniol continues to increase to 10 and 13 mm in 3.6 F108 solutions, strongly deformed thermal peaks in both processes are present. When the amounts of Geraniol are increased, the scanning curves show unstable signals around the baseline especially at low temperature.

Tab. 3-2-2-1: T_{onset} and T_{peak} of Geraniol and 3.6 mm F108 in thermal process

Geraniol in 3.6 mm F108 solution at scan rate of 0.5 °C/min				
Geraniol/ mm	Heating process		Cooling process	
	T_{onset}	T_{peak}	T_{onset}	T_{peak}
0	26.6	31.1	39.1	29.6
2.5	20.4	29.3	38.5	27.5
5.0	16.2	27.8	37.4	25.9
10	14.4	25.0	36.5	23.2
13	11.6	22.8/19.5	35.2	21.4

Tab. 3-2-2-1 summarized the values of T_{onset} and T_{peak} for the samples of geraniol from 0 to 13 mm in the 3.6 mm F108 solution, respectively, in both thermal processes. In the presence of geraniol reduces 3.6 mm F108 solution the values of T_{onset} and T_{peak} . The decreasing temperature is proportional to the amounts of geraniol. The solubility capacity of geraniol in 3.6 mm F108 solution is lower than 1-Hexanol, so in this experiment the geraniol is prepared till 13 mm. The deformed peak appears at two high points for the 13 mm sample in the heating process. Therefore, there are two peak temperature values for the 13 mm sample geraniol.

Tab.3-2-2-2: Integration Q and $\Delta H_{(PO)}$ of Geraniol and 3.6 mm F108 solution in thermal process

Integration Q and $\Delta H_{(PO)}$ of 3.6 mm F108 with the variation of Geraniol/ mm at 0.5 °C/ min				
	Integration Q/mJ		$\Delta H_{(PO)}/ \text{kJmol}^{-1}$	
	Heating	Cooling	Heating	Cooling
0 mm	194.2	189.1	3.79	3.70
2.5 mm	206.1	195.0	4.03	3.81
5.0 mm	223.7	206.5	4.37	4.04
10 mm	253.2	222.2	4.95	4.34
13 mm	261.0	238.3	5.10	4.66

The results of integration Q and $\Delta H_{(PO)}$ enthalpy for the samples of geraniol in the 3.6 mm F108 solution is presented in Tab. 3-2-2-2. The integration of the thermal peak is increasing with the addition of geraniol and is dependent on the concentration. High amounts of geraniol lead to the area of both thermal peaks being improved. The enthalpy of $\Delta H_{(PO)}$ also increases in the presence of geraniol, which means directly that it is effective to improve the dehydration process of PO blocks.

Geraniol and 7.0 mm F108

For this case of 3.6 mm, F108 is increased to 7.0 mm and we studied geraniol concentrations of 0 to 10 m in the temperature range of 0 to 60°C at scanning rate of 0.5°C/min. by DSC heating and cooling cycles.

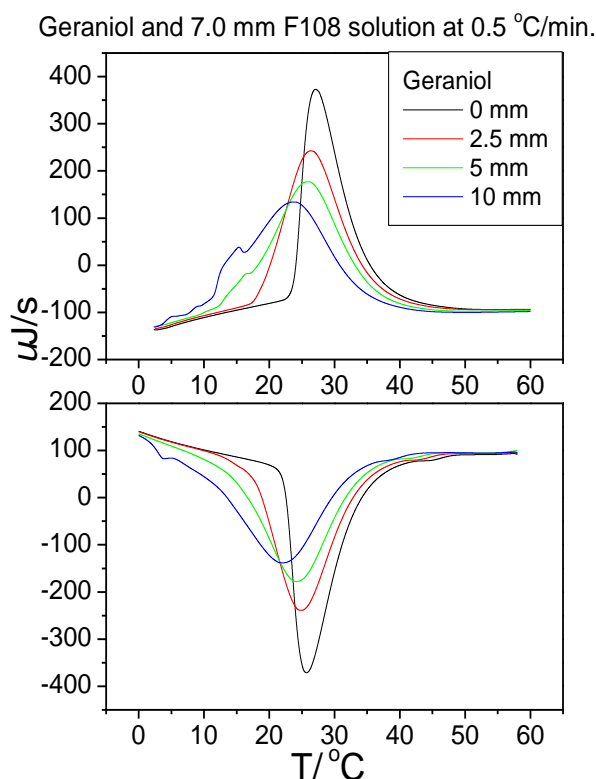


Fig. 3-2-2-2a and 2b: Geraniol in 7.0 mm F108 as a function of temperature in heating (2a) and cooling (2b) processes

As the diagrams 3-2-2-2a and 2b have shown, 7.0 mm F108 solutions in the presence of geraniol from 0 to 10 mm the endothermic and exothermic reaction appear by the method of the DSC in thermal cycles. The pure 7.0 mm F108 solution results in the intensity and width of thermal peaks being stronger and narrower than in the pure 3.6 mm F108 solution. In the presence of geraniol the thermal peaks of 7.0 mm F108 shifts to the low temperature and the intensity of peaks decreases, with the width of peaks broadening in both scanning processes. The appearance of deformed peaks exists for the increased concentration of 7.0 mm F108 in the presence of geraniol at low temperatures.

Tab. 3-2-2-3: T_{onset} and T_{peak} of Geraniol and 7.0 mm F108 in thermal process

Geraniol in 7.0 mm F108 solution at scan rate of 0.5 °C/min				
	Heating process		Cooling process	
Geraniol/ mm	T_{onset}	T_{peak}	T_{onset}	T_{peak}
0	23.6	27.1	37.5	25.6
2.5	18.2	26.4	34.8	24.8
5.0	15.1	25.8	34.1	24.1
10.0	11.2	23.6	32.5	21.9

Tab. 3-2-2-3 summarizes the values of T_{onset} and T_{peak} of the 7.0 mm F108 solution in the presence of Geraniol from 0 to 10 mm respectively in both thermal processes. The pure 7 mm F108 solution results in a lower T_{onset} and T_{peak} than 3.6 mm F108 solution. The high concentration of F108 leads to low temperatures of T_{onset} and T_{peak} . The presence of geraniol is able to decrease temperature values of the 7.0 mm F108; the decreasing temperatures of T_{onset} and T_{peak} are proportional to the quantity as well.

Tab.3-2-2-4: Integration Q and $\Delta H_{(\text{PO})}$ of Geraniol and 7.0 mm F108 solution in thermal process

Integration Q and $\Delta H_{(\text{PO})}$ of 7.0 mm F108 with the variation of Geraniol/ mm at 0.5 °C/ min				
	Integration Q/mJ		$\Delta H_{(\text{PO})}/ \text{kJmol}^{-1}$	
Geraniol	Heating	Cooling	Heating	Cooling
0 mm	386.3	372.1	4.10	3.95
2.5 mm	388.8	378.6	4.13	4.02
5.0 mm	425.0	393.3	4.51	4.18
10.0 mm	445.0	419.2	4.73	4.45

Table 3-2-2-4 summarizes the integration Q and enthalpy $\Delta H_{(\text{PO})}$ of Geraniol from 0 mm to 10 mm in 7.0 mm F108 solution. In the presence of Geraniol, the result is that the area of thermal peaks increases and is dependent on the concentration. The enthalpy $\Delta H_{(\text{PO})}$ is enhanced with increasing amounts of Geraniol in both thermal processes. Geraniol as a co-surfactant is effective in the dehydration process of the 7.0 mm F108 solution.

3-2-3 Toluene and the F108 solution

Toluene is a clear and redolent solution, because it is an aromate derivative with a benzene group. The solubility of toluene in aqueous solutions is 0.47g/L equal to 5.1 mm and is enhanced in the presence of F108.

Toluene and the 3.6 mm F108 solution

In the case of 3.6 mm F108, we studied toluene concentrations of 0 to 20 mm in the temperature range of 0 to 60°C at a scanning rate of 0.5°C/min. by DSC heating and cooling cycles.

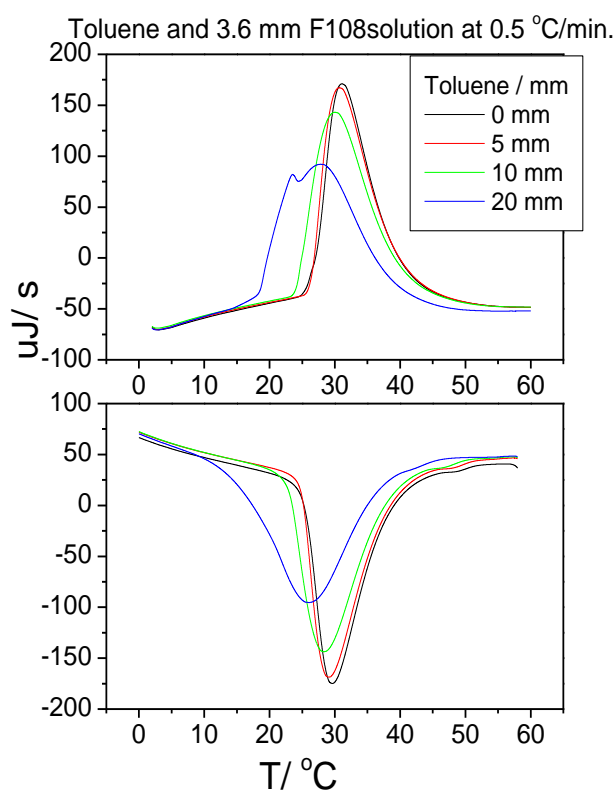


Fig.3-2-3-1a and 1b: Toluene in 3.6 mm F108 as a function of temperature in heating (1a) and cooling (1b) processes

The curves for toluene in 3.6 mm F108 solutions from 0 to 20 mm, respectively, are shown in Fig. 3-2-3-1a and 1b. In the presence of toluene shifts the thermal peaks to low temperatures in both processes. Besides, the heights of the thermal peaks tend to be reduced, but the width of the peaks becomes broader depending on the concentration of toluene. High amounts of toluene, like 20 mm, lead to the peaks being slightly deformed and are observable in the heating process.

Tab.3-2-3-1: T_{onset} and T_{peak} of Toluene and 3.6 mmF108 in thermal process

Toluene in 3.6 mm F108 solution at scan rate of 0.5 °C/min				
	Heating process		Cooling process	
Toluene/ mm	T_{onset}	T_{peak}	T_{onset}	T_{peak}
0	26.6	31.1	39.1	29.6
5.0	26.5	30.7	38.9	29.1
10	24.2	30.0	37.9	28.3
20	18.2	27.9	37.7	25.8

Tab. 3-2-3-1 summarizes the values of T_{onset} and T_{peak} in the presence of toluene from 0 to 20 mm in both processes. Both values result in a decrease with increasing amounts of toluene. It indicates that toluene induces the temperature of dehydration of 3.6 mm F108 decreasingly. Toluene is effective in lowering the critical micellar temperature at the fixed concentration of the F108 solution.

Tab.3-2-3-2: Integration Q and $\Delta H_{(PO)}$ of Toluene and 3.6 mm F108 solution in thermal process

Integration Q and $\Delta H_{(PO)}$ of 3.6 mm F108 with the variation of Toluene/ mm at 0.5 °C/ min				
	Integration Q/mJ		$\Delta H_{(PO)}/ \text{kJmol}^{-1}$	
Toluene/ mm	Heating	Cooling	Heating	Cooling
0	194.2	189.1	3.79	3.70
5.0	203.0	198.7	3.97	3.88
10	215.5	204.4	4.21	4.00
20	244.4	221.9	4.78	4.34

Tab. 3-2-3-2 presents the summary of integration and enthalpy of each PO block for the samples of toluene and the 3.6 mm F108 solution. Toluene enhances the integration of the 3.6 mm F108 solution, and the growing area of thermal peaks is proportional to the increasing toluene.

The solubility of toluene in water is lower than 1-Hexanol. If the functional group of Toluene from CH_3 - changes to OH -, the solubility will be increased. The solubility of Phenol in water is around 84 g/L equal to 975 mm [77]. In the presence of phenol shifts the thermal peaks of triblock copolymer solution to low temperature [78].

Toluene and the 7.0 mm F108 solution

In this case, 3.6 mm F108 is increased to 7.0 mm and we studied toluene concentrations of 0 to 40 mm in the temperature range of 0 to 60°C at scanning rate of 0.5°C/min. by DSC heating and cooling cycles.

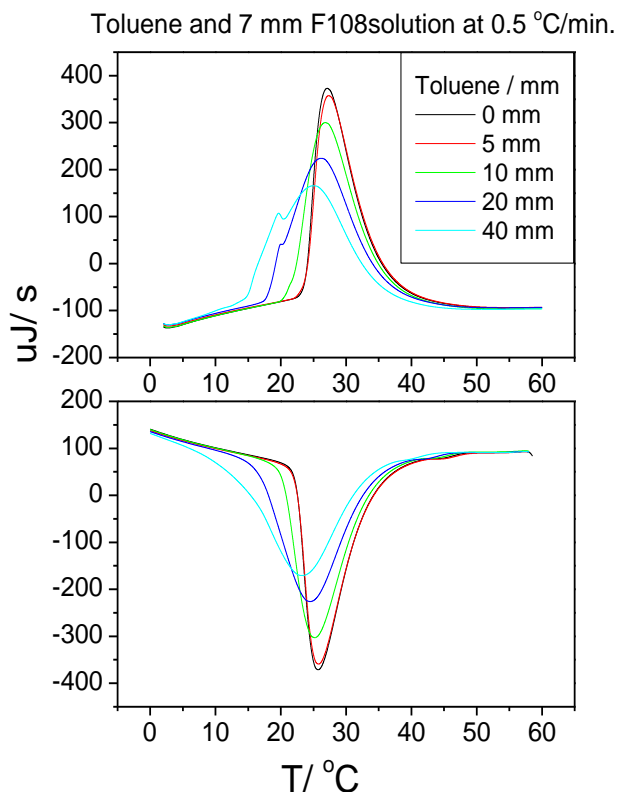


Fig. 3-2-3-2a and 2b: Toluene in 7.0 mm F108 as a function of temperature in heating (2a) and cooling (2b) processes

The thermal peaks of the 7.0 mm F108 solution shift to low temperatures in the presence of toluene, which are shown in Fig. 3-2-3-2a and 2b. The shifted peaks are proportional to the concentration of toluene. High amounts of Toluene, like 20 mm and 40 mm, enhanced not only the peaks' position, but also the deformed thermal peaks', especially in the heating process. Like other additives, e.g. Geraniol, the deformed peaks all occur under room temperature. For the most part, F108 copolymers form unimer phases at lower a temperature, which leads to reduced solubility capacity space for more additives.

Tab.3-2-3-3: T_{onset} and T_{peak} of Toluene and 7.0 mmF108 in thermal process

Toluene in 7.0 mm F108 solution at scan rate of 0.5 °C/min				
	Heating process		Cooling process	
1-Hexanol/ mm	T_{onset}	T_{peak}	T_{onset}	T_{peak}
0	23.6	27.1	37.5	25.6
5.0	23.7	27.3	34.5	25.7
10	21.6	26.8	34.3	25.1
20	18.1	26.2	33.6	24.5
40	14.6	25.0	33.3	23.2

Tab. 3-2-3-3 summarizes the values of T_{onset} and T_{peak} for samples of toluene in 7 mm F108 in both processes. Both temperatures are decreased in the presence of Toluene. The decreasing temperature is proportional to the concentration of Toluene. The 7mm F108 solution results lower T_{onset} and T_{peak} than the 3.6 mm F108 solution. Toluene is helpful to induce the decreasing values of T_{onset} and T_{peak} in both thermal processes.

Tab. 3-2-3-4: Integration Q and $\Delta H_{(\text{PO})}$ of Toluene and 7.0 mm F108 solution in thermal process

Integration Q and $\Delta H_{(\text{PO})}$ of 7.0 mm F108 with the variation of Toluene/ mm at 0.5 °C/ min				
	Integration Q/mJ		$\Delta H_{(\text{PO})}/ \text{kJmol}^{-1}$	
Toluene/ mm	Heating	Cooling	Heating	Cooling
0	386.3	372.1	4.10	3.95
5.0	384.1	370.0	4.08	3.93
10.0	381.7	371.4	4.05	3.94
20.0	400.6	378.0	4.25	4.01
40.0	429.6	416.4	4.56	4.42

The results of integration Q and enthalpy $\Delta H_{(\text{PO})}$ have been shown in Tab. 3-2-3-4. The results of integration increase in the presence of toluene and are dependent on concentration in both thermal processes. It means that the transition state of micellization has been influenced with the addition of Toluene. The enthalpy of each PO block results in increasing amounts of toluene in the 7.0 mm F108 solution.

3-2-4 Influence of apolar oil in F108 solution

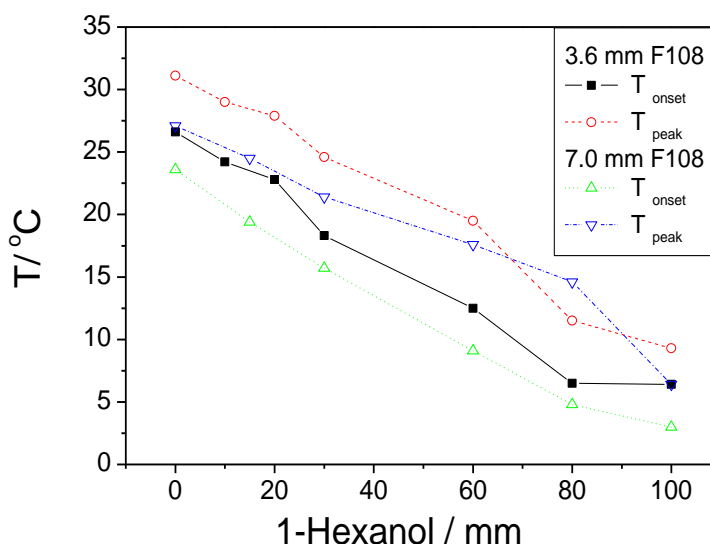


Fig. 3-2-4-1: Values of T_{peak} and T_{onset} of in 3.6 mm and 7.0 mm F108 solutions in the presence of 1-Hexanol

Fig. 3-2-4-1 summarizes the values of T_{peak} and T_{onset} for two fixed concentration of F108 solution as a function of 1-Hexanol. The results show that increasing amounts of 1-Hexanol lead to lower temperatures of T_{peak} and T_{onset} . Both T_{peak} and T_{onset} decrease nearly as linear functions with increased concentrations and T_{onset} is approximately parallel to T_{peak} . The results of T_{onset} and T_{peak} for 7.0 mm F108 are lower than 3.6 mm F108, but parallel to them, because the decreasing temperature is proportional to the concentration of F108. The cmt values of F108 were approximately a linear function of the polymer concentration below 10 wt.% [79]. T_{onset} and T_{peak} can be used as an index to anticipate the micelle phases and to determine the values of critical micelle temperature [78, 80-82]. Normally the T_{onset} is defined as cmt. When the temperature is below its cmt at a fixed concentration, polymer chains in water exist as unimers. The micellization begins at cmt and ends at T_{off} , which is the temperature at the end of the thermal peak. In the region between cmt and T_{off} , polymer chains exist as unimers, micelles, or both. Above T_{off} , all the micelles would have been formed, but this does not necessarily mean that there are no free F108 chains in the aqueous solution. However, no significant heat is detected above T_{off} [68].

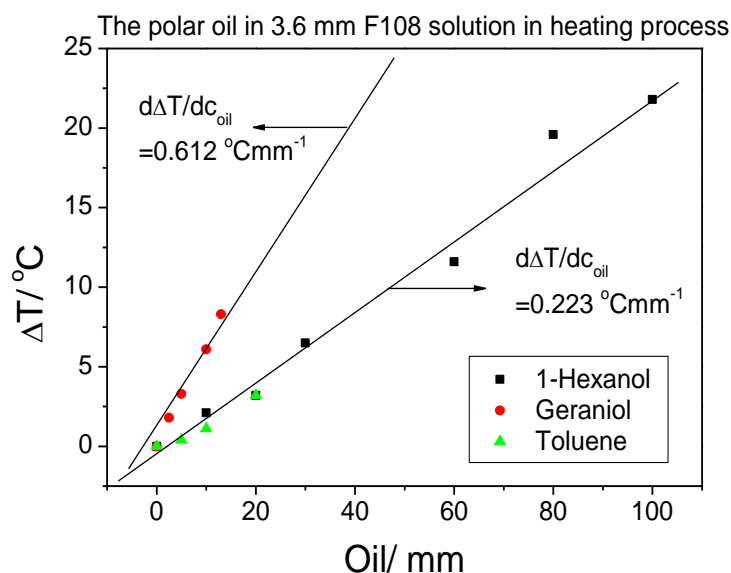


Fig. 3-2-4-2: Reduced T_{peak} of 1-Hexanol, Geraniol and Toluene as a function of concentration

The ΔT of 3.6 mm F108 is presented in Fig. 3-2-4-2 as a function of concentration for oil which is 1-Hexanol, Geraniol and Toluene. The value ΔT comes from the difference between T_{peak} of pure 3.6 mm F108 and T_{peak} of 3.6 mm F108 in the presence of oil. The curve shows that each of them induces the decreasing values of T_{peak} and is proportional to the amounts of oils. Forming micellization is mainly controlled by the length of the hydrophobic part of PO blocks because of dehydration. The oils selected in this experiment results effectively in lowering the peak temperature. Geraniol results reducing T_{peak} values with increasing concentration. The curve line of Geraniol grows as linear function and results highest slope $d(\Delta T/C_{oil}) = 0.612\text{ }^\circ\text{Cmm}^{-1}$ of other oils. Geraniol more effectively lowers the temperature of the dehydration process of F108 than do 1-Hexanol and toluene. This process characterizes an appearance of micellization formation. It reduced $0.612\text{ }^\circ\text{C}$ per mmol. The curves of 1-Hexanol and toluene appear nearly equal in slope $d(\Delta T/C_{oil}) = 0.223\text{ }^\circ\text{Cmm}^{-1}$; they are able to be effective to lower the critical micelle temperature as well. 1-Hexanol can be dissolved more than Geraniol and Toluene in F108 aqueous solution. Per mmol 1-Hexanol reduced only 0.223°C for 3.6 mm F108 solution, but high solubility capacity can overcome this disadvantage to reach the lowest reduced temperature purpose. Toluene has been shown to effectively lower peak temperature, but the solubility in the F108 solution is lower than 1-Hexanol.

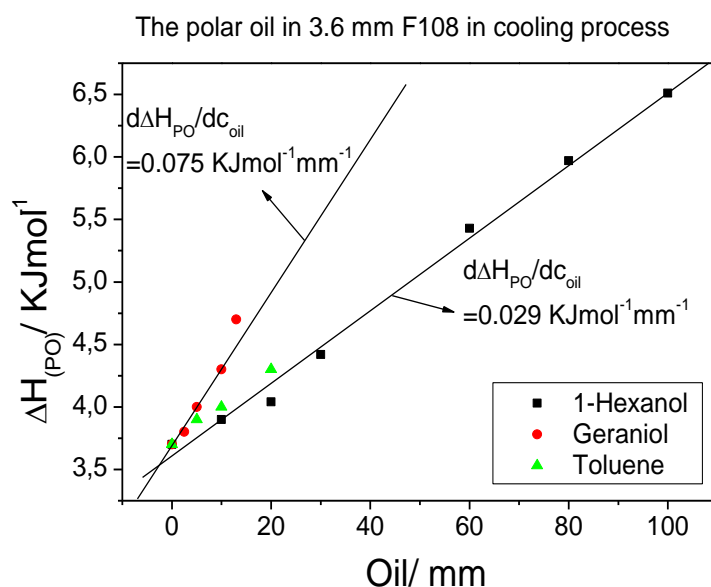


Fig. 3-2-4-3: Enthalpy $\Delta H_{(PO)}$ of 1-Hexanol, geraniol and toluene in 3.6 mm F108 as a function of concentration

The endothermic and exothermic reactions, which are due to the dehydration and hydration of PPO, are enhanced in the presence of polar oil. Fig. 3-2-4-3 summarizes the enthalpy $\Delta H_{(PO)}$ as a function of the concentration for the different oils for the cooling process. The enthalpy $\Delta H_{(PO)}$ is obtained from the thermal phase transition of the F108 solution. In the presence of oil, it is helpful to enhance the enthalpy of F108, although the oils perform no thermal reaction alone in solution. Enthalpy of each PO increases directly proportional to the amounts of oil added with a slope $d(\Delta H_{PO}/c_{oil}) = 0.029 \text{ kJmol}^{-1}\text{mm}^{-1}$. This linearity still works well for 1-Hexanol for the highest concentration of 100 mm, which indicates that the solubility capacity of 3.6 mm F108 for 1-Hexanol is still not reached. The other oils Geraniol and Toluene have a lower solubility capacity than 1-Hexanol. The enthalpy of $\Delta H_{(PO)}$ is increasing in the presence of Geraniol and Toluene in a similar fashion and the slope $d(\Delta H_{PO}/c_{oil}) = 0.075 \text{ kJmol}^{-1}\text{mm}^{-1}$. Geraniol results in highest efficiency for the thermal reaction of PPO. The additional enthalpy is increased proportional to the concentration. Other oils, like toluene and 1-Hexanol in the F108 solution, produce energy lower than geraniol. Because the highest solubility capacity of other oils, 1-Hexanol can help F108 produce more energy in solutions by an increase of at least more than 60 mm.

3-3 Primary alcohols (Ethanol, 1-Butanol, 1-Hexanol and 1-Octanol) and the F108 solution

In this part different primary alcohols were selected as co-surfactants in the 3.6 mm F108 solution. The solubility capacity of those four alcohols is found commonly on information platforms, like Google. At 20°C, ethanol is soluble arbitrarily in water and 1-Butanol is soluble around 7.9 g/L in water, 1-Hexanol is 5.9 g/L and 1-Octanol is 0.30 mg/L. Their solubility in water is decreased in relation to the chain length. The phase behaviour is all homogeneous at amounts of 30 mmol in the presence of 3.6 mm F108 solution.

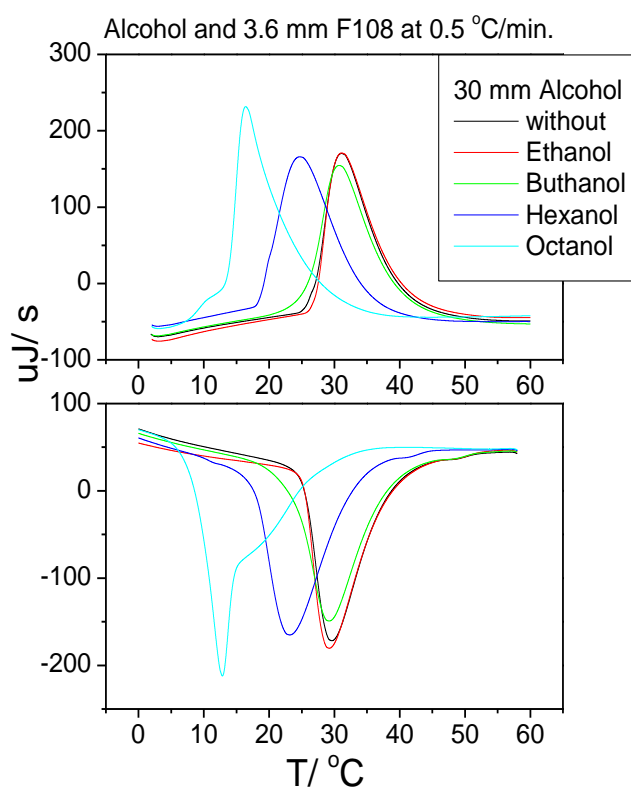


Fig. 3-3-1a and 1b: Alcohol in 3.6 mm F108 at scan rate of 0.5°C/min. in heating (1a) and cooling (1b) processes

Fig. 3-3-1a and 1b describe thermal processes for four different primary alcohols at the same chemical amounts of 30 mmol in the 3.6 mm F108 solution, respectively. The thermal peaks of 30 mmol ethanol are observed that no movements shift to low temperature. For the peaks of 30 mmol 1-Butanol increases indistinctly compare with the pure 3.6 mm F108 solution. Both are relatively polarer than 1-Hexanol and 1-Octanol. 30 mmol Ethanol and 1-Butanol are soluble in pure water, so they have no influence, or maybe unobviously, on the dehydration process of F108 solution. The 30 mmol 1-Hexanol is independently soluble in water in the absence of F108 as well. However, the thermal peaks shift to lower temperatures in the presence of 1-Hexanol. The 30 mmol 1-Octanol results in the lowest peak temperature in comparison to other 30 mmol alcohols. Deformed thermal peaks

appear in the presence of 1-Octanol at low temperatures in the thermal processes. The samples of 30 mm 1-Octanol have been measured R_h with decreasing temperature from 25 to 15°C. The phase behaviour becomes a turbid solution when the temperature goes down to 16°C. The solubility capacity of 30 mmole octanol is limited under 16°C in uncompleted micelle phases of 3.6 mm F108.

Tab.3-3-1: T_{onset} and T_{peak} of alcohols and 3.6 mmF108 in thermal process

30 mm alcohol in 3.6 mm F108 solution at scan rate of 0.5 °C/min				
	Heating process		Cooling process	
Alcohol	T_{onset}	T_{peak}	T_{onset}	T_{peak}
No	26.6	31.1	39.1	29.6
Ethanol	27.1	31.1	39.0	29.2
1-Butanol	25.5	30.7	38.4	29.2
1-Hexanol	18.3	24.6	33.7	23.1
1-Octanol	13.2	16.4	25.6	12.8

Tab. 3-3-1 summarizes the T_{onset} and T_{peak} of 30 mm primary alcohol in the 3.6 mm F108 solution in heating and cooling processes. The presence of Ethanol does not influence T_{peak} , but the T_{onset} is increased. In the presence of 1-Butanol, 1-Hexanol and 1-Octanol, it results in decreasing values of T_{onset} and T_{peak} for the 3.6 mm F108 solution and is proportional to the alkyl chain length. 1-Butanol, 1-Hexanol and 1-Octanol are effective for F108 in lowering the temperature of the dehydration process. 1-Octanol shows the most efficiency in lowering the critical micelle temperature of the 3.6 mm F108 solution.

Tab.3-3-2: Integration Q and $\Delta H_{(PO)}$ of alcohols and 3.6 mm F108 solution in thermal process

Integration Q and $\Delta H_{(PO)}$ of 3.6 mm F108 with the 30 mm alcohol at 0.5 °C/ min				
	Integration Q/mJ		$\Delta H_{(PO)}/ \text{kJmol}^{-1}$	
	Heating	Cooling	Heating	Cooling
No alcohol	194.2	189.1	3.79	3.70
Ethanol	189.9	183.9	3.71	3.59
1-Butanol	195.6	191.2	3.82	3.74
1-Hexanol	237.9	226.1	4.65	4.42
1-Octanol	277.5	253.5	5.42	4.95

Tab. 3-3-2 summarizes the results of integration Q and enthalpy $\Delta H_{(PO)}$ for the 3.6 mm F108 solution in the presence of primary alcohols, respectively. The integration Q and enthalpy $\Delta H_{(PO)}$ are decreased in the presence of Ethanol. This phenomenon is similar to the other publication. The presence of Ethanol decreases the thermal peaks of triblock copolymer solution and the presence of Methanol decreases as well [83]. In the presence of 1-Butanol, 1-Hexanol and 1-Octanol result integration Q and enthalpy $\Delta H_{(PO)}$ increasingly. At the same chemical amounts of alcohols, the increasing enthalpy is related to chain length. 1-Octanol shows the highest efficiency in lowering the cmt and increasing the entropy on each PO block in comparison to other primary alcohols.

Four different primary alcohols with the same chemical amounts are mixed in the 3.6 mm F108 solution respectively. The thermal peaks of 30 mm ethanol result in decreasing integration and the 30 mm 1-Butanol is increased a little bit. The length of the alkyl chain influences the polarity of alcohols. Short alkyl chains like Ethanol tend toward polar molecules and are soluble easily in water. Methanol and Ethanol perform the water-structure-breakers prevent the self-hydration of water, resulting in increased polymer solubility [83]. When the longer chain are selected such as 1-Butanol, 1-Hexanol and 1-Octanol, they could exist in the water environment, but to a limited extent. In the addition of longer chain alcohols is effective on decreasing cmt. They perform a water-structure-maker promoting the self-hydration of water by favourable interaction between longer chain alcohol and water resulting in the exclusion of copolymer in the solvent region [83]. The longer chain alcohols favour the aggregated form of the copolymer [84]. The solubility does not decrease as a linear function because ethanol dissolves at high solubility in water and 1-Octanol can almost not be dissolved in water. The phase behaviour of 30 mm 1-Octanol in the 3.6 mm F108 solution is clear, transparent and homogeneous, but they are all prepared at room temperature. There are some DSC thermal peaks, which appear deformed, at low temperatures. This tells us that the solubility is reduced and limited for oil and caused by the uncomplete micelle formation. In the cooling process the exothermic peak of 30 mm 1-Octanol becomes deformed and the reason is the solubility capacity of hydrophobic blocks being reduced dependent on temperature as well. 30 mm 1-Hexanol is observed no deformed thermal peaks, because it is still soluble in water at this quantity in the absence of F108. In the 3.6 mm F108 aqueous solution the solubility capacity of 1-Hexanol is tested personally at at least 150 mmol.

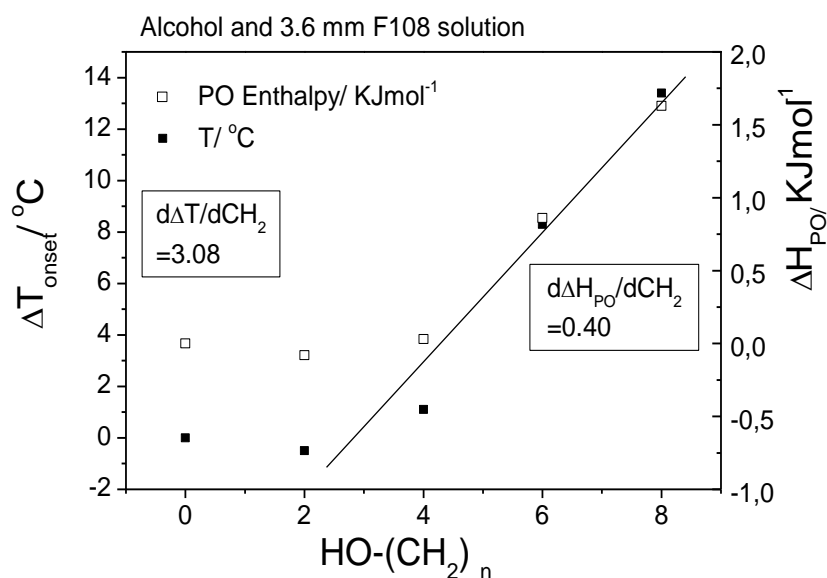


Fig.3-3-2: ΔT_{onset} and Enthalpy $\Delta H_{(PO)}$ of primay alcohol in 3.6 mm F108 as a function of carbon values

Fig. 3-3-2 summarizes ΔT_{onset} and Enthalpy $\Delta H_{(PO)}$ as a function of carbon chain value. In the presence of ethanol, where the carbon chain value is at 2, there appear to be no significant influences on the F108 solution. The influence is a little clear when the CH_2 is increased to 4. Then it is increased as a linear function when the CH_2 keeps increasing. If alcohols have to be chosen as co-surfactants, 1-Butanol is the bottom line for influencing the dehydration of F108, because ethanol is not effective. 1-Octanol is the most efficient alcohol as a co-surfactant for improving the dehydration process of F108. The slope $d(\Delta T/CH_2)=3.08^\circ C$ means that they are effective in lowering the temperature for each extra CH_2 on average and the slope $d(\Delta H_{PO}/CH_2)=0.40 \text{ KJmol}^{-1}$ indicates the enhancement. The enthalpy of PO is effective dependent of carbon chain length of alcohols as well.

Results of DLS measurements

Each of the 30 mm alcohols was measured by DLS from 20°C to 40°C to analyse the size modification of the dehydration process for the 3.6 mm F108 solution.

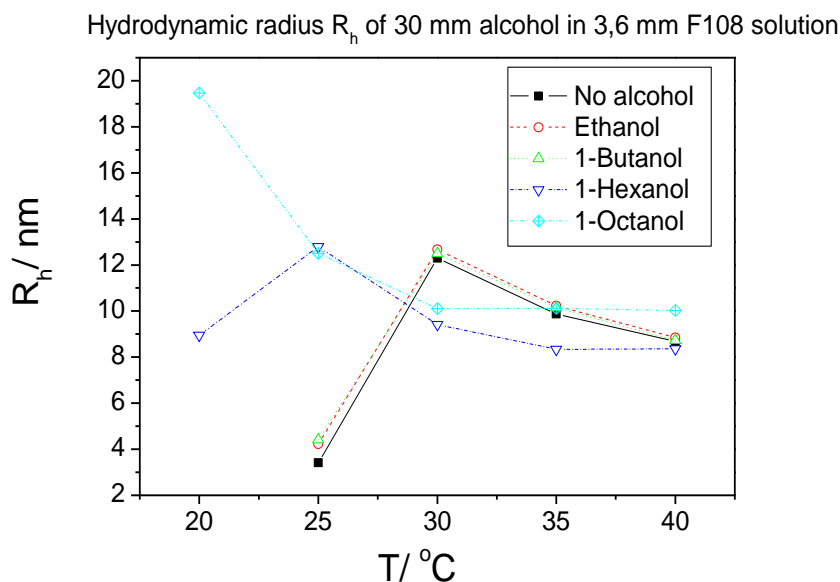


Fig. 3-3-3: Results of R_h for primary alcohols as a function of temperature

Fig. 3-3-3 shows the results of the hydrodynamic radius of primary alcohol in 3.6 mm F108 as a function of temperature. At 25 °C, it shows the radius of 1-Hexanol and 1-Octanol as being higher than the radius of ethanol and 1-Butanol. The results of DSC measurements (see Fig.3-3-1a and 1b) have been observed that the endothermic and exothermic peaks of 3.6 mm F108 shift obviously to lower temperatures in the presence of 1-Hexanol and 1-Octanol, respectively. In the presence of 30 mm 1-Hexanol, the 3.6 mm F108 holds the maximal hydrodynamic radius R_h at 25°C, it starts to reduce when the temperature increases. In this Fig. 3-3-3 the highest value of R_h for 3.6 mm F108 in the presence of 1-Octanol is at 20°C, because later this sample is measured at lower temperatures (see Fig. 3-3-8). The maximal R_h of 1-Hexanol and 1-Octanol for 3.6 mm F108, respectively, is close to their peak temperature. A high intensity of thermal peaks of F108 solution results in the maximum of R_h . In the presence of ethanol and 1-Butanol, the maximal R_h at 30°C appears and is close to the results of their peak temperature. Their thermal peaks of 3.6 mm F108 in the presence of ethanol have an influence on lowering the temperature and, in the presence of 1-Butanol, shift a little. If all the samples are measured continually at 35°C and 40°C, the R_h results decreasingly. They decrease until the constant stable state. There is short R_h around 3 to 4 nm detected at 25°C for the pure 3.6 mm F108 solution. In the presence of ethanol and 1-Butanol short R_h is observed as well. They are the size of

unimer phases. The R_h of unimer F108 is enhanced in the presence of Ethanol and 1-Butanol, although it does not increase much. Ethanol and 1-Butanol are at high solubility capacity in water, the 30 mmol amounts have an extremely low influence on lowering temperature of dehydration processes of F108. In the presence of both alcohols, the similar cmt value with no alcohol F108 solution results. Therefore, due to high solubility in water, the short chain length alcohol, like Ethanol and 1-Butanol, has almost no influence on the decreasing temperature of the dehydration effect for the F108 solution. If the R_h of F108 is measured at 30°C, the results appear only slightly increasingly in the presence of ethanol and 1-Butanol. The results are not demonstrative to prove the existence of ethanol and butanol in the micelle phases of F108. In other words, the long chain length alcohol like 1-Hexanol and 1-Octanol, compared with ethanol and 1-Butanol, have low solubility in water. Their solubility capacity is related to the length number of $(CH_2)_n$ and is proportionally inverse. 1-Hexanol at the amount of 30 mmol is still homogenous in water; the solubility capacity of 1-Hexanol is 5.9 g/L and is equal to 57 mm in water, so the sample of 30 mm 1-Hexanol is unnecessary to exist in the F108. However the maximal R_h of 3.6 mm F108 is detected at 25°C in the presence of 1-Hexanol. This maximum value occurs at the temperature lower than no alcohol F108 solution. 1-Hexanol induces the temperature of dehydration processes of the F108 solution. This phenomenon is more obvious in the presence of 1-Octanol, because the solubility capacity is extremely low – around 0.30 mg/ L in water. It is equal with the concentration in 2.3×10^{-3} mm. However the phase behaviour of 30 mm 1-Octanol is homogeneous in the 3.6 mm F108 solution at room temperature. The maximal R_h of F108 is found in Fig. 3-3-3 in the presence of 1-Octanol at 20°C. At fixed concentrations of F108 under their cmt, mostly unimer phases appear in the solution. The space of unimers for hydrophobic parts is smaller than in the micelle phase, even the hydrophobic part of PO blocks prefers to be less hydrophobic. Therefore the oil wants to be solubilized in the solution, especially at low temperatures. The oil, like 1-Hexanol or 1-Octanol, forces each F108 copolymer aggregate to let its critical micelle temperature be reached in advanced. At the same time the activation energy decreases in the presence of oil. For this reason, the large space of hydrophobic area is formed for the hardly soluble water of oil.

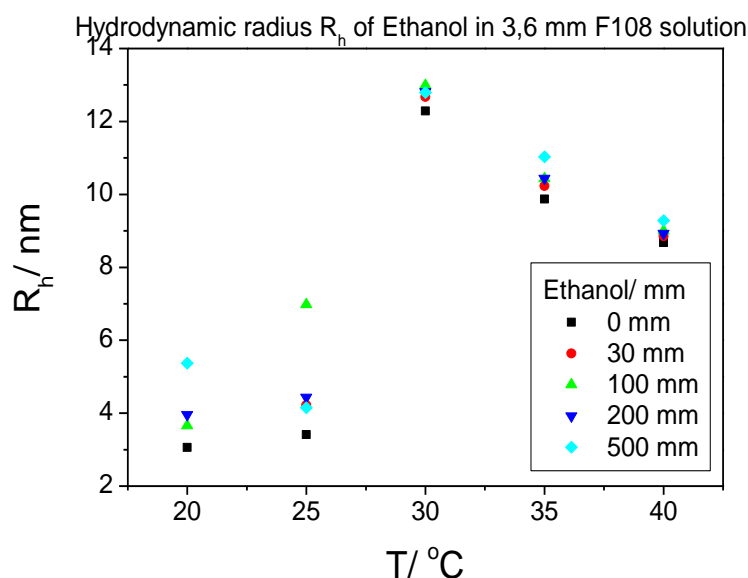


Fig. 3-3-4: Hydrodynamic radius R_h of the variable concentration of ethanol in the 3.6 mm F108 solution as a function of temperature

Fig. 3-3-4 summarizes the R_h of 3.6 mm F108 in the presence of Ethanol as function of temperature. Compared with the same chemical amounts of alcohols like 1-Hexanol and 1-Octanol (see Fig. 3-3-1 and 3), ethanol induces no surprising phenomenon at fixed concentrations of F108. The amounts of ethanol keeps increasing to 100 mm, 200 mm and 500 mm in order to analyse the influence on the micelle phases of F108 by means of DLS. They were measured dependent on temperature and there appears to be no significant hydrodynamic radius R_h under cmt. The R_h of 100 mm ethanol at 25°C is debatable because the R_h of 200 mm and 500 mm result relatively smaller. It is hard to make a conclusion that with increasing amounts of ethanol it would induce the aggregation of F108. The hydrodynamic radius R_h is dependent on temperature and solvent properties like viscosity (see part 2-2). The solvent is water; the viscosity of water is dependent on temperature. It is 1.002 cp at 20°C and decreases with increasing temperature. The amounts of ethanol are at high value in 3.6 mm F108, the 500 mmol Ethanol occupies around 2.5 % of total solution. Although the density of Ethanol, which is 0.79 g/cm³ at 20°C, is lower than water. The viscosity of pure Ethanol is 1.200 cp at 20°C, and decreases with high temperature as well. Ethanol with hydroxyl (-OH) group and water are polar molecules. Another possibility is that the hydrogen bond is formed between the hydrogen of the -OH group of ethanol and the oxygen of the water molecule. This could result in that mixtures of ethanol and water at different temperatures show a wide range of dielectric constants, viscosities, densities and a high degree of hydrogen bonding effects. The hydrophobic effect between ethanol, water and the F108 copolymer is considered also. If we want to take the viscosity mixture of water and ethanol for this experiment into consideration, the value can be calculated in accordance with the

equation as follows:

$$\eta = \eta_{\text{Water}} \frac{\rho \cdot t}{\rho_{\text{Water}} \cdot t} \quad (3-3-1)$$

The viscosity η of water and ethanol is related to the density ρ and flowing time t . The samples are directly measurable by the Ubbelohde viscosimeter. If the temperature is increased to 35°C, the R_h of the samples at the highest value decreases to 10 nm. When the temperature keeps increasing to 40°C, the R_h of them keeps decreasing. The high temperature leads the F108 copolymer to become more hydrophobic in solution, so water or ethanol partially would be dispelled from PO and even EO blocks, letting the hydrophobic blocks aggregate more condensable. In the presence of high amounts of ethanol, no significant influence has an effect on the increasing size of aggregation of the F108 solution.

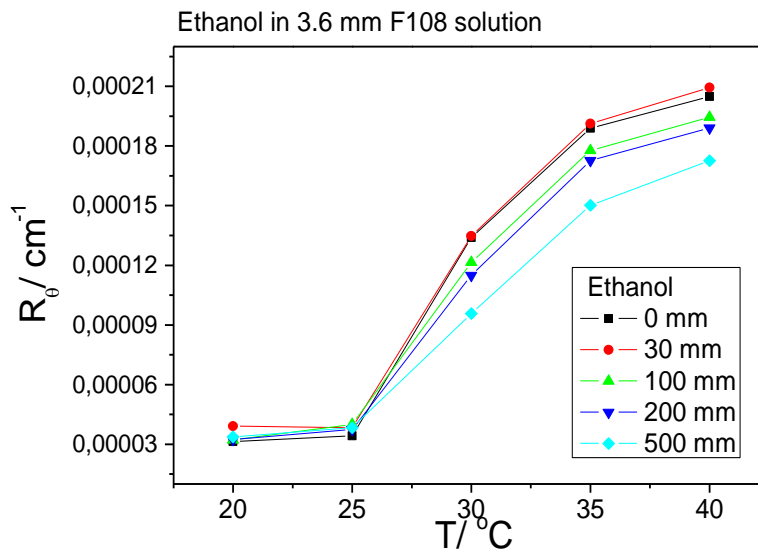


Fig. 3-3-5: Intensity of variable concentrations of ethanol in the 3.6 mm F108 solution as a function of temperature

The scattering intensity I in Hz fluctuates as a function of measuring time. It can be translated into the Rayleigh ratio R_θ in cm^{-1} with a mathematical equation. The values R_θ come from

$$\frac{I_{\text{Sample}}}{I_{\text{Toluene}}} = \frac{R_{\theta_{\text{Sample}}}}{R_{\theta_{\text{Toluene}}}} \quad (3-3-2)$$

The scattering intensity I_{sample} and I_{Toluene} is obtained by DLS measurements and R_θ from toluene is constant at the value $1.4 \times 10^{-5} \text{ cm}^{-1}$. It is also the reference to characterize the

scattering intensity at each scattering angle θ . The results of R_θ of ethanol for increasing amounts in 3.6 mm F108 respectively is presented as a function of temperature in Fig. 3-3-5. The fluctuation is sensitive to the size of particles in the solution. At 20°C the lowest intensity of ethanol results, which means they appear as mostly unimer phases in the solution. In the presence of ethanol, the R_θ of intensity enhances even though they are still as unimers in the solution. The Rayleigh ratio R_θ is obtained from theory of Static light scattering.

When temperature is on the increase, the F108 copolymer tends to dehydrate and translate with high probability to the micelle phases, which results high values of R_θ . To compare the Result in Fig. 3-3-4, the R_h of them appear the highest values at 30°C, because ethanol has nearly no influence on lowering the cmt values of F108. If the temperature keeps going up, the R_h remain decreasing. On the contrary, the intensity at 30°C is not the maximum, it keep increasing when the temperature warms to 35°C and 40°C. The intensity, due to the density of each dehydrated F108, leads to the size of aggregation reduced. However the intensity is not proportional with the concentration of ethanol. The sample of 30 mm of ethanol results the highest intensity than other samples. When the concentration of ethanol increases to 100 mm, 200 mm and 500 mm, they result in the decreasing values of R_θ proportionally over 30°C.

Analysis of regularized fit

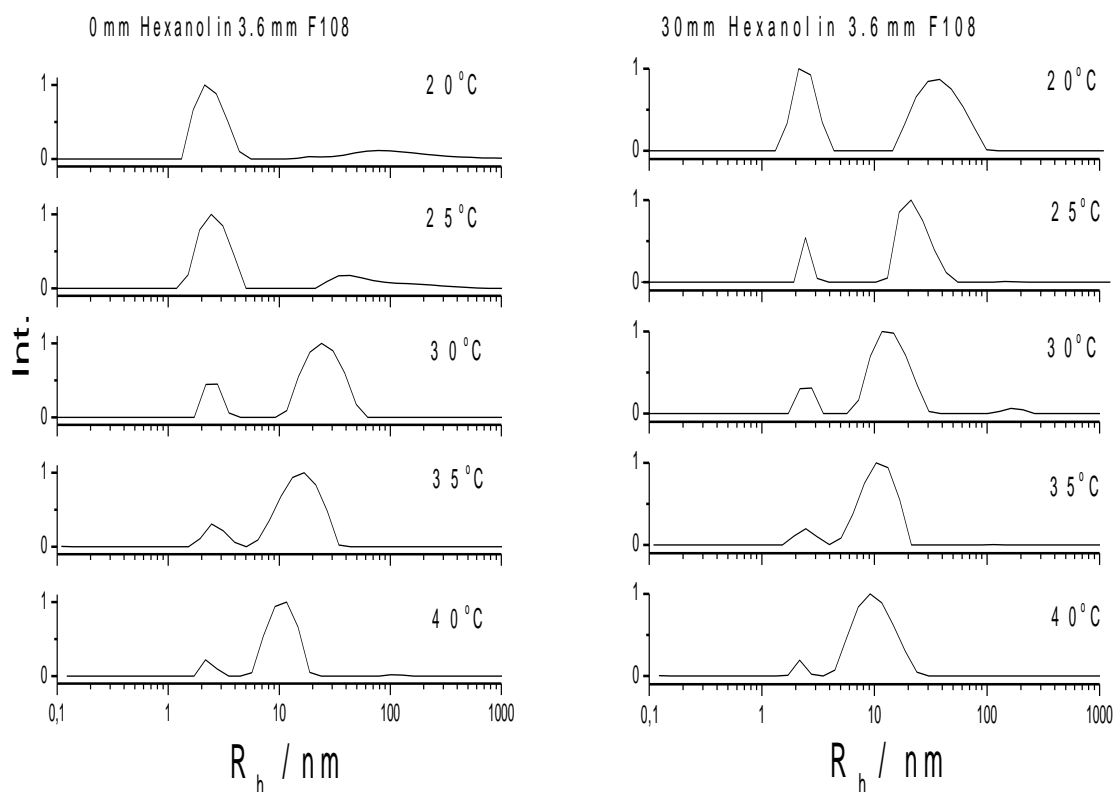


Fig. 3-3-6: Results of size distribution analysed by regularized fit for 30 mm 1-Hexanol in 3.6 mm F108 from 20°C to 40°C

Fig. 3-3-6 shows the results of size distributions by DLS measurements for samples of 0 mm and 30 mm Hexanol in fixed concentration of 3.6 mm F108 solution. Both samples were measured with for temperatures from 20°C to 40°C and analysed with the regularized fit model. Left curve from Fig. 3-3-6 is the F108 solution in the presence of 0 mm 1-Hexanol from 20 to 40°C. It appears as one peak at 20°C and peak position is at around 2.44 nm. The hydrodynamic radius R_h for 2.44 nm is close to the gyration radius R_g 2.31 nm that is analyzed by SANS. It implies that there are no micelle phases for the given concentration of 1-Hexanol in the F108 solution at this temperature. They exist as almost unimer phases in the solution. When the temperature keeps increasing, there is another peak that seems to appear and is located between 10 nm to 100 nm. At 30°C, this peak appears obviously to be seen. Meanwhile, the first peak at 2.44 nm becomes weak as the temperature goes up higher. Unimer phases could translate into micelle phases because of dehydration of PO blocks, so the second peak grows. Moreover it tends to shift to the short R_h position around 10 nm when the temperature increases to 40°C. Phase transition of the dehydration process of PPO influences the size of aggregation. PO blocks are dependent on temperature and they gain a hydrophobic appearance with increasing temperature.

Because hydrophilic appearance from PO blocks disappears gradually, it results as R_h reduces. As the temperature continues increasing, the hydrophobic character of PO is enhanced at the same as the hydrophilic character PO is reduced. The reduced hydrophilic phenomenon leads to the exclusion of hydrophilic solution from the hydrophobic parts of PPO.

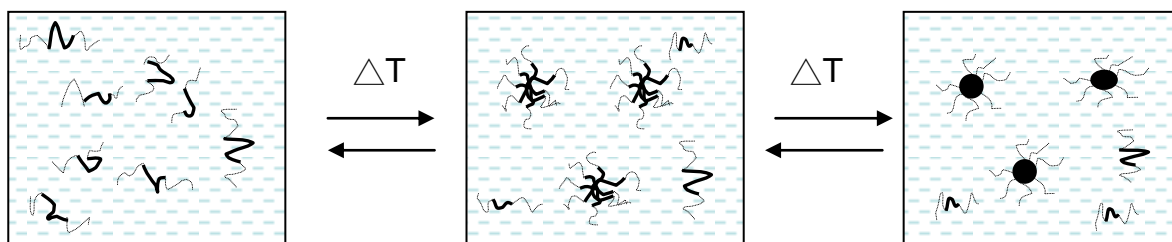


Fig. 3-3-7: Model of triblock copolymer F108 in aqueous solution as a function of temperature

Fig. 3-3-7 is an image model for F108 in the aqueous solution at different temperatures to interpret the process of phase transition from unimer to complete micelle phases in detail. The triblock copolymer F108 can be soluble in water as unimer phases at low temperatures, like the left curve. The increased temperature leads to the PO blocks of F108 being dehydrated and the dehydrated PO blocks form aggregates as irregular shapes in the solution at the beginning (middle curve). During the process of phase transition they contain hydrophilic appearance, so PO blocks and water are coexistent in the core and appear as huge swelling particles. The model in the middle presents the F108 form aggregation like micelle phases. At this moment they have already gone over their cmt, but the parts of PPO exist still with water. If the temperature keeps increasing, the hydrophilic character of PPO decreases and pushes the remaining water out of the hydrophobic part. Particles for the hydrophobic parts become more densely and result in a decreasing R_h .

Fig. 3-3-6 (at the right side) shows the results of size distribution as a function of temperature in the presence of 30 mmol 1-Hexanol. Compared with the pure F108 solution, the curve appears as two peaks at 20°C. One is for unimer phase of F108 and the other is micelle phase. The presence of 1-Hexanol is effective in lowering the temperature of the dehydration process for the F108 solution. This phenomenon corresponds with the results of the Nano DSC.

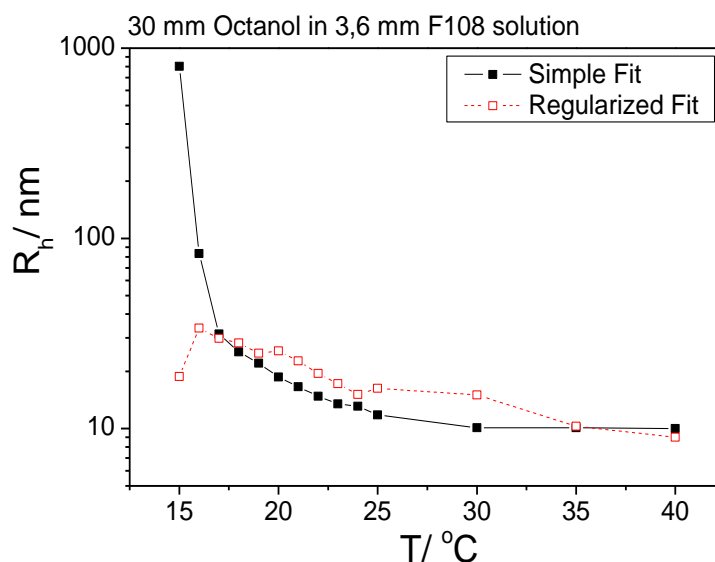


Fig. 3-3-8: Hydrodynamic radius R_h of 30 mm 1-Octanol in 3.6 mm F108 analysed by means of Simple Fit and Regularized Fit as a function of temperature

Fig. 3-3-8 summarizes the hydrodynamic radius R_h of samples containing 30 mm 1-Octanol in the 3.6 mm F108 solution as a function of temperature. The autocorrelation function is analysed by the ALV 7004 programme and two methods are used to determine the R_h . One is the Simple Fit. Only one R_h is obtained by calculation of the model, which are the size particles mainly in solution. The other calls ALV-Regularized Fit; it presents not only the R_h but also the percentage of unimer and micelle copolymers. The sample was measured from -25°C to 15°C because the DSC peak of 30 mm 1-Octanol is obtained at 16.4°C. The results of R_h lead to increases when the temperature goes down. At low temperature the PO blocks of F108 turn to be hydrophilic relatively and the aggregates swell because of water. The solubility capacity of 1-Octanol in water is only 0.30 mg/L at 20°C and it is almost insoluble in water [85]. In the presence of 3.6 mm F108, it lets the solubility of 1-Octanol increase to 3.9 g/L in water homogenous at the same temperature. Compared with other 30 mm alcohol samples (see Fig. 3-3-1), 30 mm 1-Octanol results in the lowest peak temperature of other samples. 1-Octanol accelerates the dehydration process for PO blocks of F108 in order to homogenize in the solution, so the endothermic and exothermic peaks shift to a low temperature position. 30 mm 1-Octanol starts to turn turbid slightly at 16°C below the perceptible observation. Emulsions could be formed in solution. The turbid solution is due to partial insoluble 1-Octanol and the solubility of octanol in the F108 solution is reduced when the temperature goes down. Therefore the turbid solution results to the R_h closed to 100 nm and 1000 nm at 16°C and 15°C, respectively. The interference from the turbid solution of 30 mm 1-Octanol leads to inaccuracy of R_h at 15°C and 16°C.

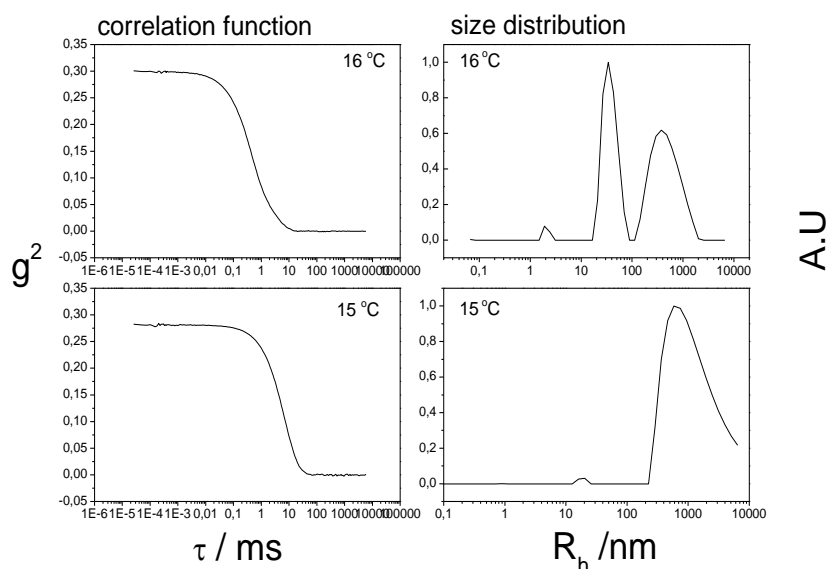


Fig. 3-3-9: Autocorrelations function and size distribution of 30 mm 1-Octanol in 3.6 mm F108 at 15°C and 16°C

Fig. 3-3-9 presents the curves of the autocorrelation functions and size distribution for the sample of the F108 solution in the presence of 30 mm 1-Octanol. The sample was measured at 15°C and 16°C, respectively. At 16°C, the autocorrelation function shows the first exponential decay at lag time position from 0.01 ms to 0.1 ms. Significant particles are detected and R_h is 31 nm after the calculation of simple fit. There are three peaks observed in the curve of size distribution. They are at 33.7 nm. Both of them are appropriate to micelle size. At 15°C the exponential decay shifts to late position from 0.1 to 0.01 ms.

However the sample is prepared with 220 nm filter 5 times before measurements. The samples which are measured below their cmt, result sometimes no significant particles in solution. The results of size distribution appear only one strong peak at huge size position and the other peaks disappeared. The observation of its phase behaviour is turbid because the solubility of 30 mmol octanol is over the limited in 3.6 mm F108 solution at 15°C.

3-4 Mixtures of polymer and F108 solution

In this part two kinds of different polymers were selected to be admixed to a fixed concentration of the F108 solution. One is the homo block polymer PPO, connected without any EO blocks. PO_{17} and M_w is around 1000 g mol^{-1} . The chain length of PO_{17} is shorter than the hydrophobic part of F108 (PO_{50}). It can be expected to be soluble in the core of micelle phases when micelles have been formed. Otherwise PPO becomes increasingly hydrophilic with decreasing temperature. The other polymer is Kollicoat MAE 30 DP. It is a copolymer of methacrylic acid/ethyl acrylate and used as a film-former in the pharmaceutical industry as well as in the production of enteric coatings or solid dosage forms. The solubility of Kollicoat MAE 30 DP is freely miscible in water and Kollicoat MAE retains its milky white appearance when mixed with water.

3-4-1 Homo copolymer PPO and the F108 solution

PPO and the 3.6 mm F108 solution

We studied PPO concentrations of 0 to 20 mm in the presence of the 3.6 mm F108 solution in the temperature range of 0 to 60°C by DSC heating and cooling cycles.

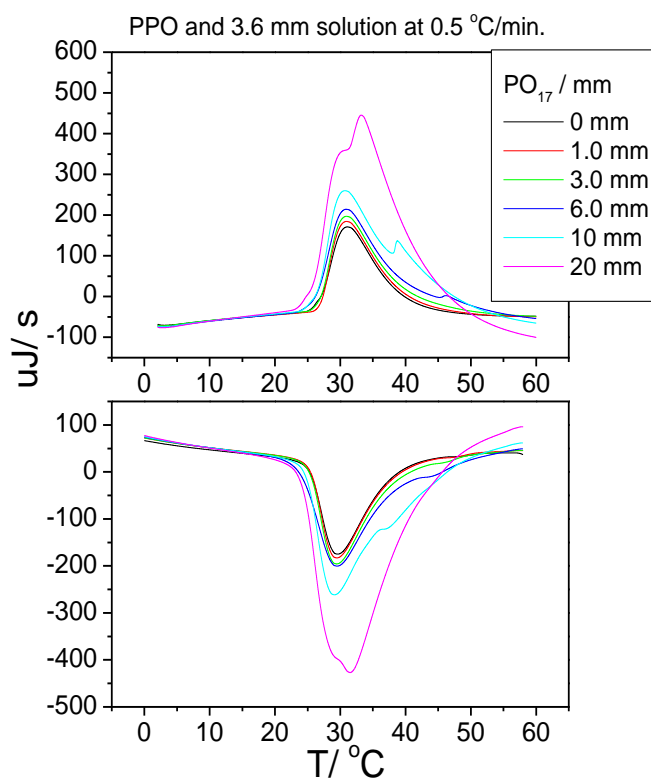


Fig.3-4-1-1a and 1b: DSC curve of PPO in 3.6 mm F108 as a function of temperature in heating (1a) and cooling (1b) processes

In the presence of homo copolymer PPO shifts no movements of thermal peaks to low temperatures. The peak intensity increases with the addition of PO blocks in both processes and is proportional to the concentration. In the heating process for the sample of 6 mm PPO, a small peak appears close to 47°C and so does the cooling process. If we increase the PPO to 10 mm, this small additional peak shifts to low temperatures around 40°C. Samples above 6 mm PPO (see Fig. 3-4-1-1) are observed an additional peak at right side. These additional peaks for the sample of 6, 10 and 20 mm is at 46.4°C, 38.7°C and 33.2°C respectively. The increasing amounts of PPO shift the additional peak to low temperature. The sample of 10 mm PPO was put into a constant temperature furnace to observe the phase behaviour. The temperature was set at 56°C and the sample turns turbid in the furnace (see Fig. 3-4-1-2). If we take it in the air, it turns clear in a few seconds. So these additional peaks for 6, 10 and 20 mm PPO should be associated with the cloud point. Normally the cloud point of a pure 3.6 mm F108 solution is at 107°C and it is due to the dehydration effect of EO blocks [10]. Apparently the presence of hydrophobic PPO makes the cloud point substantially lower.

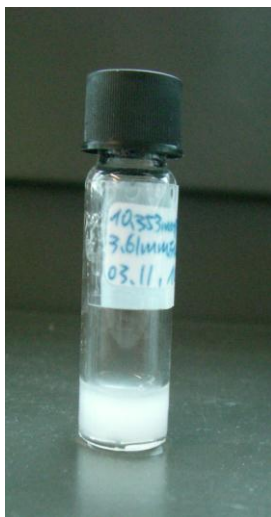


Fig. 3-4-1-2: 10 mm PPO in 3.6 mm F108 at 56°C. It turns clear very quickly at room temperature.

Compared with other mixtures, like 1-Hexanol, Toluene and Geraniol are in the same fixed concentration of the F108 solution. They appear transparent at the same high temperature. The homo copolymer PPO is like oils and hardly soluble in water. It is lipophilic and contains mostly hydrophobic character. The presence of F108 improves the solubility of PPO in the solution. The heterogenous phase is observed when the temperature is increased.

The triblock copolymer F38 contains similar values of hydrophobic blocks equal to PO₁₇. The chemical structure of F38 is EO₄₂PO₁₆EO₄₂ and the cmt is at around 70 °C at the amounts 40 mmolkg⁻¹. The ratio and value of EO blocks influence the cmt of triblock copolymers. For example, three Pluronics, F68, P65, and L62 contain similar numbers of propylene oxide units around 29 and the numbers of ethylene oxide units are 76, 19 and 8 for F68, P65 and L62, respectively. Under the same weight concentration, the Pluronic L62 results in the lowest value of the cmt of other pluronics [10]. The clouding point for other triblock copolymer solution has been influenced by adding of oil [78, 86].

Tab. 3-4-1-1: T_{onset} and T_{peak} of PPO and 3.6 mmF108 in thermal process

PPO in 3.6 mm F108 solution at scan rate of 0.5 °C/min				
PPO/ mm	Heating process		Cooling process	
	T _{onset}	T _{peak}	T _{onset}	T _{peak}
0	26.6	31.1	39.1	29.6
1.0	26.8	30.9	39.6	29.4
3.0	26.6	30.9	38.5	29.3
6.0	26.0	30.9	39.0	29.4
10.0	26.1	30.8	41.2	29.2
20.0	25.6	30.5	42.8	29.4

Tab. 3-4-1-1 summarizes the values of the T_{onset} and T_{peak} in the presence of PPO in both thermal processes. Both temperatures result in no significant modification when the amounts of PPO are increased.

Tab. 3-4-1-2: Integration Q and ΔH_(PO) of PPO and 3.6 mm F108 solution in thermal process

Integration Q and ΔH _(PO) of 3.6 mm F108 with the variation of PPO/ mm at 0.5 °C/ min						
PPO/ mm	Integration Q/mJ		ΔH _(PO) / kJmol ⁻¹		ΔH _(PO+PO) / kJmol ⁻¹	
	Heating	Cooling	Heating	Cooling	Heating	Cooling
0	194.2	189.1	3.79	3.70	3.79	3.70
1.0	204.5	202.8	4.00	3.96	2.98	2.96
3.0	241.3	226.5	4.72	4.43	3.52	3.30
6.0	289.7	268.6	5.66	5.25	4.22	3.92
10.0	434.7	419.8	8.49	8.20	5.42	5.24
20.0	676.3	660.3	13.22	12.90	6.19	6.05

Tab. 3-4-1-2 summarizes the integration and the enthalpy ΔH_(PO) in the presence of PPO in the 3.6 mm F108 solution. The integration of thermal peaks is increasing with increasing concentration of PPO in the 3.6 mm F108 solution. The homo copolymer PPO is different from other co-surfactants, like other oils. By adding PPO, it causes large enthalpy when they turn to dehydrate. Taking the adding PPO into consideration, this table summarizes another result for entropy ΔH_(PO+PO). The enthalpy ΔH_(PO+PO) is increases likewise with increasing amounts of PPO. Therefore in the presence of PPO, it is effective for the F108 solution to increase the entropy energy on each PO unit and to be proportional to the concentration. By adding a low concentration of PPO, like 1.0 or 3.0 mm, it does not seem

effective; indeed, the entropy decreases.

PPO and 7.0 mm F108

In this part we study the effect of PPO on a 7.0 mm F108 solution. The maximal amounts of PPO are increased to a 40 mm solution and they are measured by the DSC in thermal cycles.

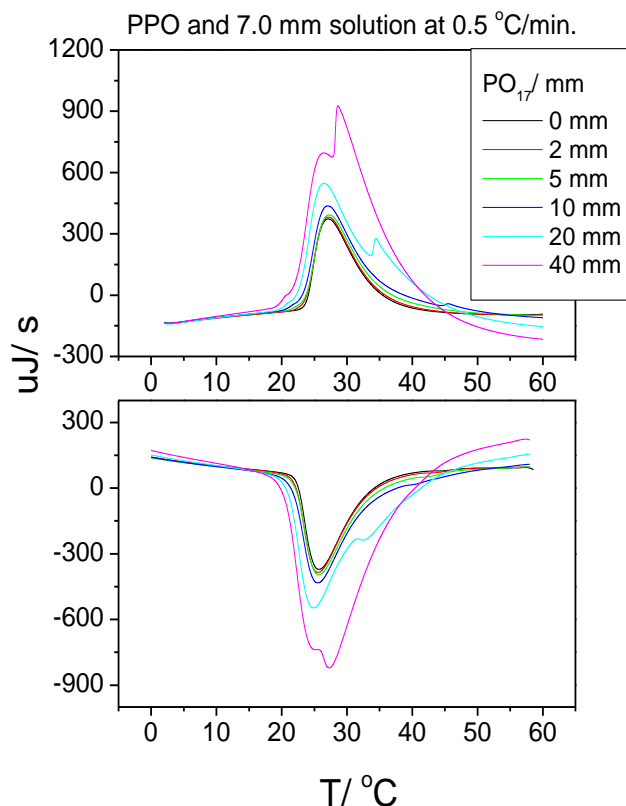


Fig. 3-4-1-3a and 3-4-1-3b: DSC curve of PPO in 7.0 mm F108 as a function of temperature in heating (3a) and cooling (3b) processes

Fig. 3-4-1-3a and 3-4-1-3b show DSC curves of the 7.0 mm F108 solution in the presence of homo polymer PPO in heating and cooling processes. By adding PPO, it increases the area of thermal peaks of F108 but the peaks remain fixed at same position. The shifts of thermal peaks for the 7.0 mm F108 solution result in almost no influence in the presence of PPO. The additional peak is found first for the sample of 10 mm. It appears around 45.5°C and is very weak in the heating process. The samples for 20 and 40 mm appear more apparently at 34.3 and 28.5°C. By adding higher concentrations of PPO, it shifts the additional peak to low temperature.

Tab. 3-4-1-3: T_{onset} and T_{peak} of PPO and 7.0 mm F108 in thermal process

PPO in 7.0 mm F108 solution at scan rate of 0.5 °C/min				
	Heating process		Cooling process	
PPO/ mm	T_{onset}	T_{peak}	T_{onset}	T_{peak}
0	23.6	27.1	34.0	25.6
2.0	23.4	27.1	34.5	25.4
5.0	23.3	27.2	35.1	25.6
10.0	22.8	27.0	35.3	25.5
20.0	22.0	26.5	37.7	25.1
40.0	21.5	26.3	39.7	24.6

Tab. 3-4-1-3 summarizes the T_{onset} and T_{peak} of the 7.0 mm F108 solution with addition of the PPO homo copolymer. The results of T_{onset} decrease slightly in the heating process with increasing amounts of PPO because of the growing area of the thermal peak. There is the same appearance for the results of T_{onset} in the cooling process. They increase slightly dependent of PPO. The results of T_{peak} shift the peaks extremely a bit of temperature with increasing of PPO.

Tab. 3-4-1-4: Integration Q and $\Delta H_{(\text{PO})}$ of PPO and 7.0 mm F108 solution in thermal process

Integration Q and $\Delta H_{(\text{PO})}$ of 7.0 mm F108 with the variation of PPO/ mm at 0.5 °C/ min						
	Integration Q/mJ		$\Delta H_{(\text{PO})}$ / kJmol ⁻¹		$\Delta H_{(\text{PO}+\text{PO})}$ / kJmol ⁻¹	
PPO/ mm	Heating	Cooling	Heating	Heating	Cooling	Heating
0	386.3	372.1	4.10	3.95	4.10	3.95
2.0	392.2	390.0	4.17	4.14	3.11	3.10
5.0	435.7	421.5	4.63	4.48	3.45	3.34
10.0	503.8	493.8	5.35	5.24	3.99	3.91
20.0	878.6	854.3	9.33	9.07	5.55	5.40
40.0	1345.6	1297.1	14.29	13.78	6.06	5.84

Tab. 3-4-1-4 presents the results of integration and enthalpy of 7 mm F108 in the presence of homo polymer PPO. The increasing amounts of PPO lead increasingly to the intensity of thermal peaks. Moreover, the results of integration Q and $\Delta H_{(\text{PO})}$ are increasing as they should be. Calculating the enthalpy for each PO unit take the units of homo copolymer PPO into consideration, written as $\Delta H_{(\text{PO}+\text{PO})}$, results growing enthalpy with the increasing of PPO.

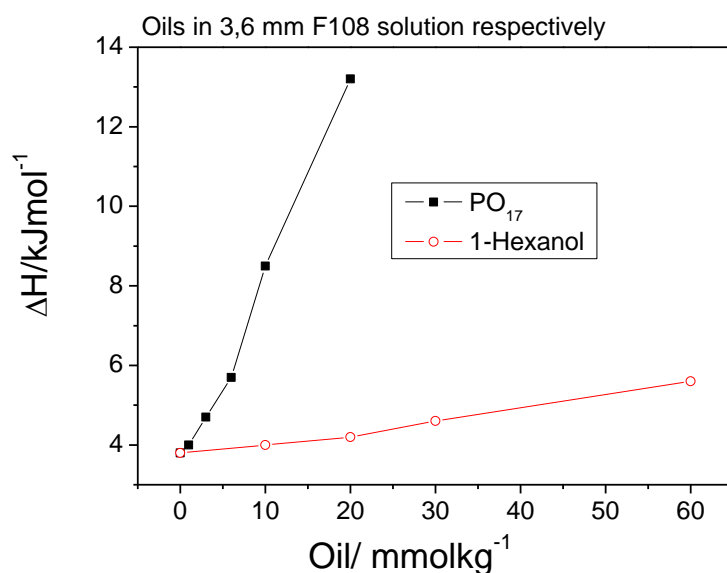


Fig. 3-4-1-4: Results of $\Delta H_{(PO)}$ as a function of oil concentration in the 3.6 mm F108 solution

Fig. 3-4-1-4 summarizes the results of enthalpy $\Delta H_{(PO)}$ as a function of oil concentration from PO₁₇ and 1-Hexanol in the 3.6 mm F108 solution, respectively. The homo copolymer PPO shows results of higher entropies than 1-Hexanol for the dehydration process of F108. If we take $\Delta H_{(PO)}$ including PO₁₇ into consideration, they remain increasing especially at high concentration of PPO (see Tab. 3-4-1-2). The homo polymer PPO, which is composed of PO blocks same as F108, is able to become dehydrated independently. 1-Hexanol, as optimal co-surfactant, has no effects on phase transition. However, it is helpful for increasing the enthalpy of dehydration of PO blocks.

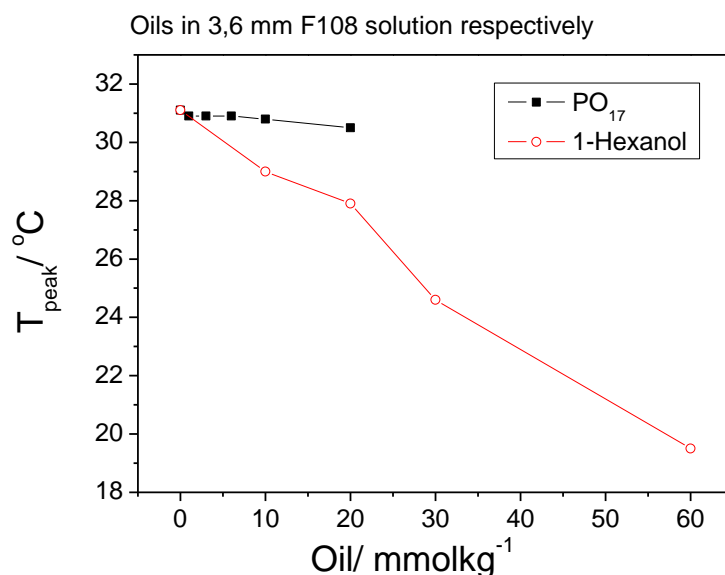


Fig. 3-4-1-5: Results of T_{peak} as a function of oil concentration in the 3.6 mm F108 solution

The peak temperatures of PPO and 1-Hexanol in the 3.6 mm F108 solution are presented in Fig. 3-4-1-5. The homo copolymer of PO₁₇ leads to no influence on lowering the temperature of the phase transition peak. By adding PPO it has no effect on decreasing the cmt values in the 3.6 mm F108 solution, while 1-Hexanol shows high efficiency in decreasing the peak temperature in the 3.6 mm F108 solution. The solubility capacity of them in water is limited and can be increased in the presence of the F108 in solution. PPO is generally not water-soluble at room temperature because of its apolar chemical structure [87]. Only polymers with low molecular weights have been reported to exhibit solubility below 18°C [88]. The solubility of 1-Hexanol in water is 5.9 g · L⁻¹ at 20°C is equal to 60 mm in water. In the presence of 3.6 mm F108, the solubility of 1-Hexanol is tested to above 150 mm homogeneous at room temperature, but the highest amounts of 1-Hexanol in this diessertation are increased only to 100 mm, which are investigated by the Nano DSC. The sample of 20 mm 1-Hexanol lowers the peak temperature of 3.6 mm F108 to 27.9°C in the heating process but the other peak temperature is at 30.8°C for the sample of 20 mm PPO. The presence of PPO shows low efficiency in lowering the cmt of the F108 solution.

3-4-2 Kollicoat MAE 30DP and the F108 solution

Kollicoat MAE 30 DP, abbreviated as Kollicoat MAE, is an aqueous dispersion with a solid content of 30%. It is a milky white and low-viscosity product manufactured by the BASF Company.

Kollicoat MAE and 3.6 mm F108 solution

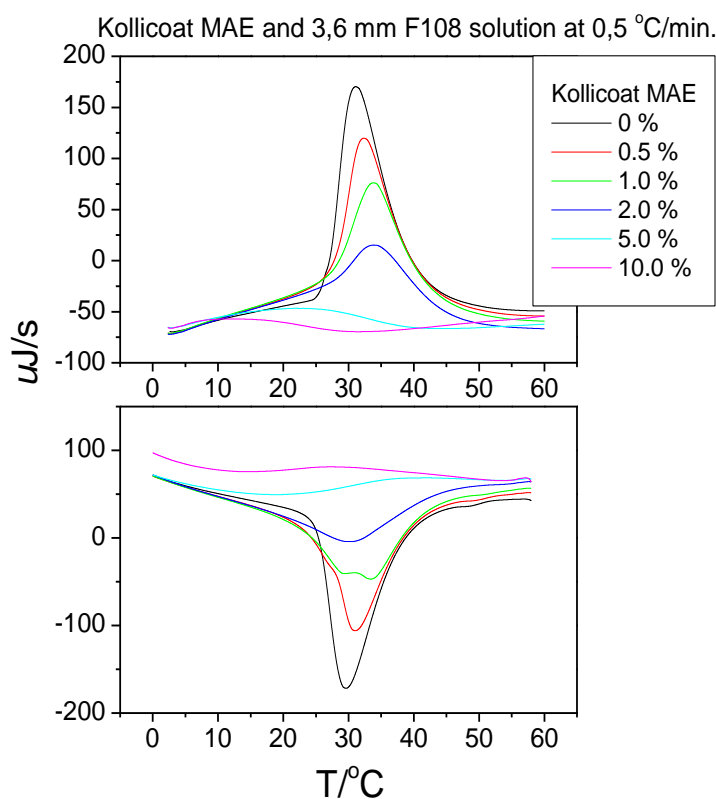


Fig. 3-4-2-1a and 3-4-2-1b: Kollicoat MAE in 3.6 mm F108 as a function of temperature in heating (1a) and cooling (1b) processes

Fig. 3-4-2-1a and 3-4-2-1b show the results of the thermal behaviour of 3.6 mm F108 in the presence of Kollicoat MAE in both processes. The maximal thermal peaks are observed for the pure F108 solution in the absence of Kollicoat MAE. The intensity of phase transition peaks of F108 decreases in the presence of Kollicoat MAE. This appearance is similar to the presence of Methanol and Ethanol.* In other words, the dehydration process of F108 disappears in the presence of Kollicoat MAE. The samples of 5% and 10% show no significant peaks in either process.

Tab. 3-4-2-1: T_{onset} and T_{peak} of Kollicoat MAE and 3.6 mm F108 in thermal process

Kollicoat MAE in 3.6 mm F108 solution at scan rate of 0.5 °C/min				
	Heating process		Cooling process	
K. MAE/ wt. %	T_{onset}	T_{peak}	T_{onset}	T_{peak}
0	26.6	31.1	39.1	29.6
0.5	27.5	32.4	40.1	30.9
1.0	27.9	33.8	41.1	29.2/33.4
2.0	27.8	33.9	43.6	30.1
5.0	--	--	--	--
10.0	--	--	--	--

Table 3-4-2-1 summarizes the thermal behaviour of T_{onset} and T_{peak} values for the 3.6 mm F108 solution in the presence of Kollicoat MAE. The temperatures of T_{onset} and T_{peak} result in no decreasing values when the amounts of Kollicoat MAE are increasing. It results in both temperatures slightly increasing in the presence of Kollicoat MAE. The absence of Kollicoat MAE results in the lowest temperature of onset and peak in this part. It indicates that Kollicoat MAE appears to have no influence on lowering the temperature of dehydration of the F108 solution.

Tab. 3-4-2-2: Integration Q and $\Delta H_{(\text{PO})}$ of Kollicoat MAE and 3.6 mm F108 solution in thermal process

Integration Q and $\Delta H_{(\text{PO})}$ of 3.6 mm F108 with the variation of Kollicoat MAE/ % at 0.5 oC/ min				
	Integration Q/mJ		$\Delta H_{(\text{PO})}/ \text{kJmol}^{-1}$	
K. MAE/ wt. %	Heating	Cooling	Heating	Cooling
0	194.2	189.1	3.8	3.7
0.5	140.2	133.1	2.7	2.6
1.0	102.7	95.2	2.0	1.9
2.0	59.2	52.1	1.2	1.0
5.0	--	--	--	--
10.0	--	--	--	--

Tab. 3-4-2-2 organizes the results of integration area and enthalpy pro PO block for the samples of increasing Kollicoat MAE in the 3.6 mm F108 solution, respectively. Fig. 3-4-2-1 shows the decrease of peak intensity, so the results of integration area are reduced in the presence of Kollicoat MAE. The enthalpy of $\Delta H_{(\text{PO})}$ is also decreased with increasing amounts of Kollicoat MAE. In the presence of Kollicoat MAE results in no effect on increasing the energy of phase transition of F108, like polar oils and PPO, but results in decreased enthalpy. However, Kollicoat MAE acts as a water-structure –breaker that prevents self-hydration of water to increase the solubility of copolymer [78].

Viscosity

The viscosity of the 3.6 mm F108 solution in the presence of Kollicoat MAE was measured by means of capillary viscosimeter, which the type of I_c and O_a were selected in this experiment.

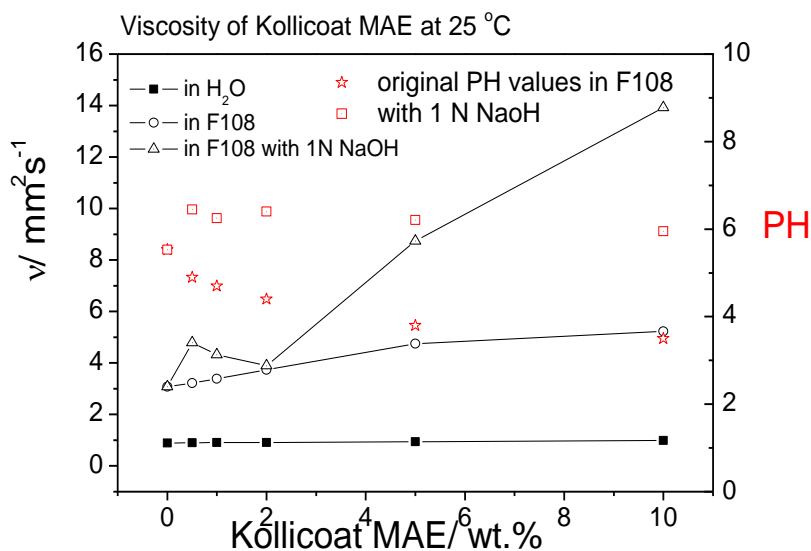


Fig. 3-4-2-2: Results of viscosity and PH values as a function of Kollicoat MAE in wt. %

Fig. 3-4-2-2 presents results of viscosity as function of Kollicoat MAE. Each of them is soluble in solution under the different condition and was measured at 25 °C. When Kollicoat MAE is soluble in water, induces not much. Because the viscosity of water is $0.890 \text{ mm}^2\text{s}^{-1}$, in the presence of Kollicoat MAE increases to $0.903 \text{ mm}^2\text{s}^{-1}$. By adding Kollicoat MAE increases the viscosity of F108 solution, meanwhile the PH of F108 solution decreases. When the samples are deprotonated with 1 N NaOH and control the PH around 6, the adhesive property becomes amplified more apparently especially by adding high amounts of Kollicoat MAE.

4. Effect of copolymer addition to the stability and permeability of Phospholipid and Diesterquat (CR3099) vesicles

In this chapter we discuss the effect of different copolymers on the properties of phospholipic and diesterquat vesicles, with a particular emphasis on their stability and the permeability of their bilayers. Phospholipids, which are the major components of the cell membrane, form the bilayer structure in solution. They contain a phosphate head group as the hydrophilic part and two hydrophobic tails and normally form multilamellar vesicles in aqueous solutions. The other chemical compound CR 3099 (chemical formula given in Tab. 5) is a diesterquat based on oleic acid, which forms a relatively big vesicle (ca. 400 nm in diameter) in aqueous solutions at a concentration of 0.5%. These vesicle dispersions with different amounts of different copolymers were added in order to see how they affect the bilayer properties.

4-1 Phospholipids solution

In this part DMPC at concentrations of 0.1 and 0.2 wt.% is used mostly to analyze the phase behaviour, stability of unilamellar vesicles, permeability and conductivity.

4-1-1. Phase behaviour

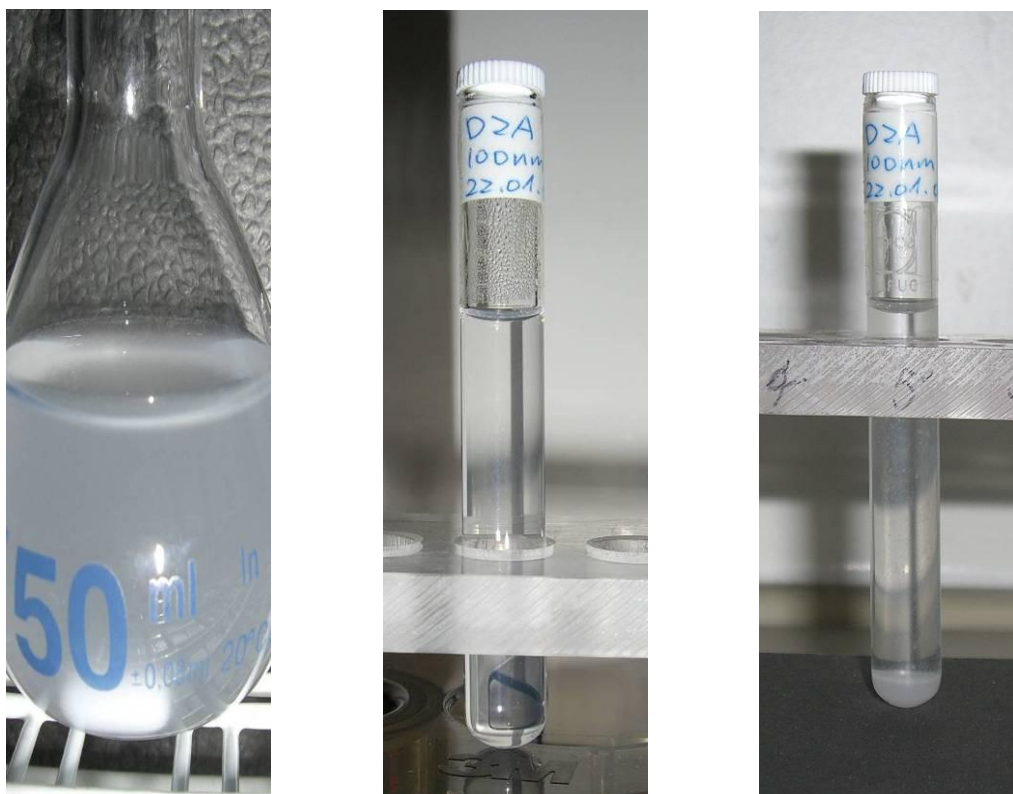


Fig. 4-1-1-1: 0.1 wt.% DMPC solution, no extrusion (left), after just extrusion with 100 nm polycarbonate filter, extruded for a long time

The phase behaviour of 0.1 wt. % DMPC presents turbid and heterogeneous aqueous solution. Staying quietly for one day, sediment appears at the bottom of the bottle. This could be due to collapsed multilamellar or unilamellar vesicles of different sizes. Multilamellar vesicles are rather large and their diameter is several μm . The advantage of these vesicles is that they consist of a more or less large number of bilayers arranged in subsequent shells and are characterized by a high degree of cooperativity in comparison with unilamellar liposomes. They are therefore not suitable in experimental arrangements that do not allow the stirring of the solution. In contrast, unilamellar phospholipic vesicles can be prepared by extrusion methods at the size of 100 nm to be suitably analysed by the scattering method. After just extrusion, the sample is homogenous and almost transparent, waiting for a period of time; sediments of lipids can be observed and sometimes suspended as well. Other DMPC solutions in the presence of additives, like copolymer or DHPC, appear with the same phase behaviour.

4-1-2 Phase transition [36]

Gel-to-liquid crystal phase transitions characteristic of lipid bilayer structures can be observed by thermal techniques. At a given temperature, phospholipids go from a less ordered liquid crystalline phase to a more ordered gel phase when the temperature decreases. The peak values T_m and T_c for the heating and cooling process, respectively, were determined by the Nano DSC.

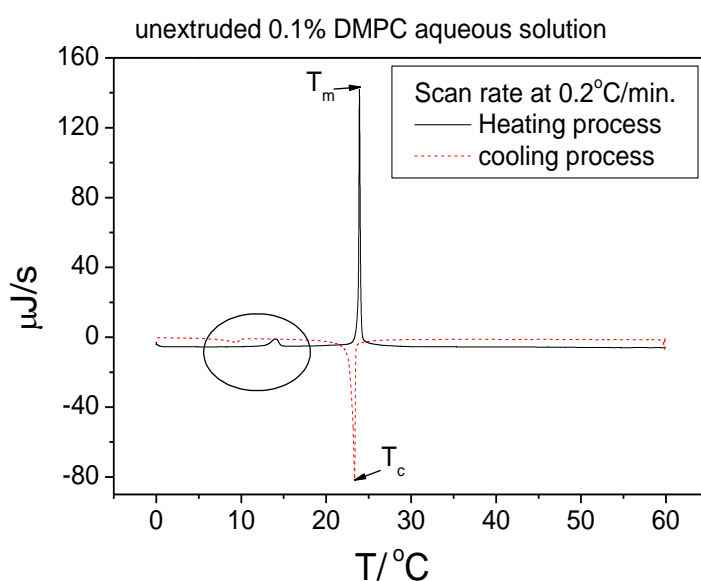


Fig. 4-1-2-1: Calorimetric measurements of unextruded DMPC at concentration of 0.1 wt.%

The phase transition of the sample of 0.1 wt% DMPC solutions, which was not extruded, was measured by means of the Nano DSC. The phase transition is reversible and the transition temperatures T_m and T_c are at 24.3°C and 23.3°C in the heating and cooling process, respectively, which is connected with the main transition from gel to fluid lamellar phase or fluid lamellar back to gel phase. In Fig. 4-1-2-1, the enthalpy ΔH of the main phase transition is 23.4 and 28.4 kJmol⁻¹ in both processes. Other additional unapparent peaks appear around 14°C in the heating process and 9.4°C in the cooling process. It is called the pretransition effect and the enthalpy of the peak is 2.84 and 2.24 kJmol⁻¹. For other kinds of phospholipids this effect has been found by DSC method [89]. The phenomenon could be explained as Trans-Gauche Isomerization (see Ch.1-6). Each kind of phospholipid has a different transition temperature T_m , such as DMPC at approximately 24.3 °C, that is determined by our Nano DSC (see Fig. 4-1-2-1) and DPPC is approx. 42°C and its pretransition temperature is around 35 °C [90].

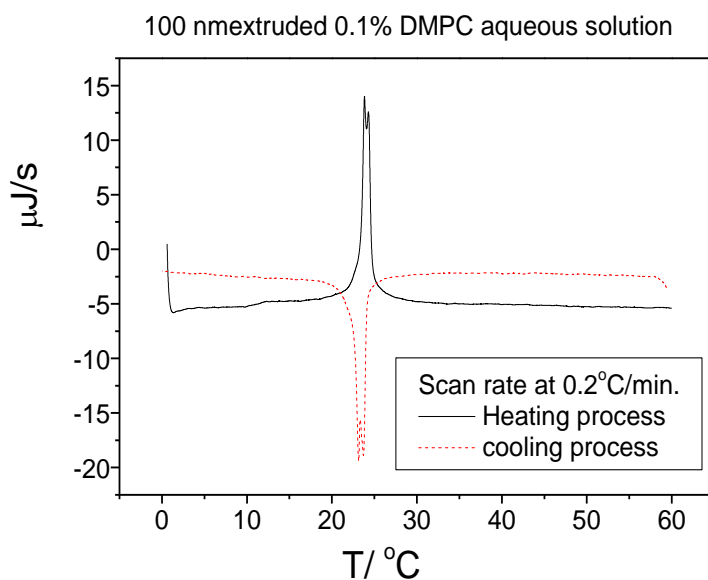


Fig. 4-1-2-2: Calorimetric measurements of extruded (100 nm) DMPC at concentration of 0.1 wt.%

The 0.1 wt. % DMPC solution after extrusion does not influence the peak values T_m and T_c much. Both are at 23.9 and 23.2 °C, respectively. The pretransition peaks disappeared. The main transition gets broader when the vesicle radius of DMPC decreases. The enthalpies are 16.4 and 14.3 kJmol⁻¹ in the heating and cooling processes. The density of the DMPC solution decreases and a two-step process is clearly observed by the Nano DSC, especially for the vesicles smaller than 200 nm [91]. Other phospholipids, such as DPPC vesicles, in any aggregate dimension do not appear to have similar effects. DSC

measurements show evidence to corroborate density results, showing a splitting of the main peak that becomes more evident as the chain length decreases and as the curvature of the aggregate increases [91].

4-1-3 Membrane thickness of unilamellar vesicles [51, 92, 93]

The experimental SANS data of DMPC is shown in Fig. 4-1-3-1. In order to determine the membrane thickness of DMPC, the model of Kratky-Porod is selected. Making the plots of $\ln((I(q)-I_{inf}(q))*q^2)$ vs q^2 should give the linear portion of gradient. The equation is given by

$$m = -\frac{d^2}{12} \quad (4-1-3-1)$$

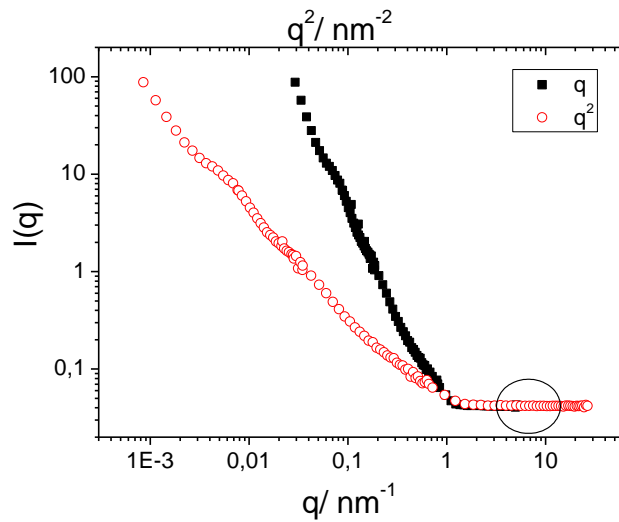


Fig. 4-1-3-1: Experimental SANS data for 0.1 % DMPC in D₂O (100 nm extruded)

$I_{inf}(q)$ is the intensity at the background and $I_{inf}(q)$ is read at the red circle position.

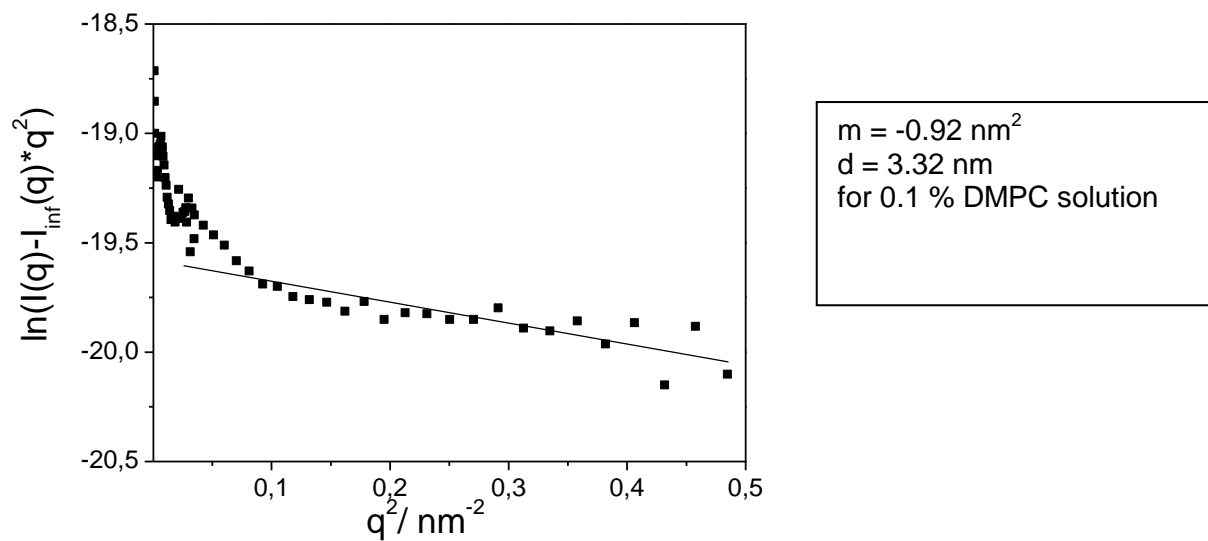


Fig. 4-1-3-2: Kratky–Porod plot of experimental SANS data

The membrane thickness of DMPC is determined by plot of Kratky – Porod. It is 3.32 nm. Generally the thickness of phospholipids is around 3 to 5 nm. The thickness of lipid bilayer is dependent on chainlength of lipids [94]. The result in this experiment corresponds with the publication, although the data presents not an optimal linear function against q^2 between 0.001 nm^2 to 0.1 nm^2 .

4-1-4 Stability of the unilamellar vesicles

DLS measurements

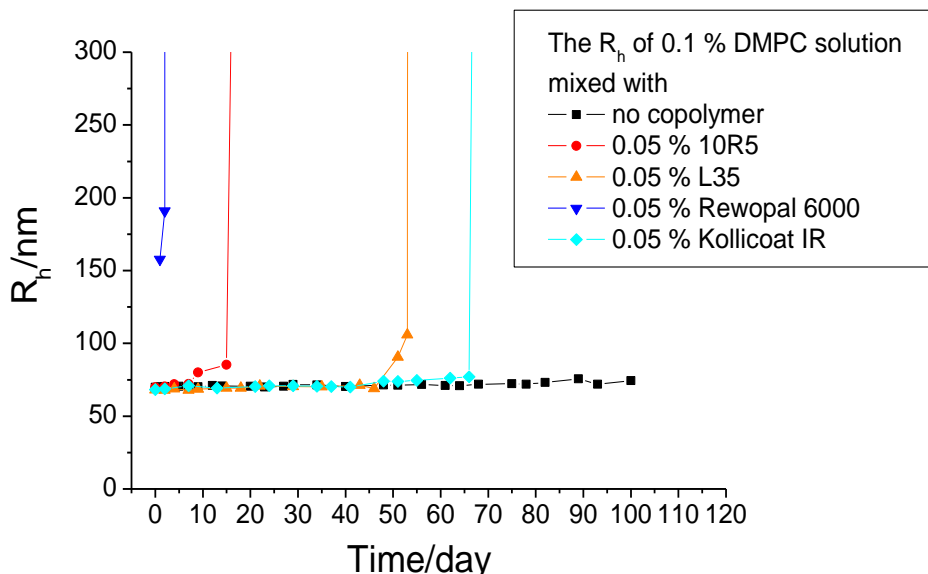


Fig. 4-1-4-1: R_h of the mixtures in 0.1 % DMPC solution were measured as a function of time

In our experiments we employed the copolymers 10R5, L35, Rewopal 6000 and Kollicoat IR in a 0.1% DMPC solution at a concentration of 0.05 wt%. After preparation they were extruded with a polycarbonate filter of diameter 100 nm for 10 times at room temperature. This large number of extrusions is necessary in order to form long-time stable unilamellar vesicles. Reducing the number of extrusions shortens the stability time of the unilamellar vesicles in the solution. Fig. 4-1-4-2 shows R_h of 0.1% DMPC for a different number of extrusion times as a function of time. The 5 times extrusion which presents a much shorter stability is observed compared to the case extruding 10 times. One observes here that the slightly turbid solutions without sediment become much more turbid and sediments occur in solution. It can be explained that unilamellar vesicles, due to the presence of bilayer material not yet in the form of unilamellar vesicles, are transformed to a state of multilamellar vesicles or become condensed together.

The results of the hydrodynamic radius R_h of without and with addition of copolymers at 0.05 wt.% into 0.1 wt.% DMPC solution, respectively, are presented in Fig. 4-1-4-1. The samples were measured day by day after extrusion until the results were not appropriate because of time-dependent fusion processes. The sample that contains only DMPC keeps the vesicle size for the longest time. The presence of the different copolymers reduces the time of stability of the unilamellar vesicles in the solution. Four copolymer mixtures are

together with the same characteristics: that they contain ethylene oxide blocks and connect with other hydrophobic molecules. The individual unilamellar vesicle distributes homogenously in the solution. It is not easy to approach each other because of hydration repulsion. When vesicles are closed to each other, a strong repulsion occurs, which can be measured by means of surface force apparatus (S.F.A) [31, 32]. It can be explained that unilamellar vesicles after the extrusion method can hold the controlled size in the solution for a period of time. The times of extrusion and size of controlled particles can influence the time length of stabilizing unilamellar vesicles.

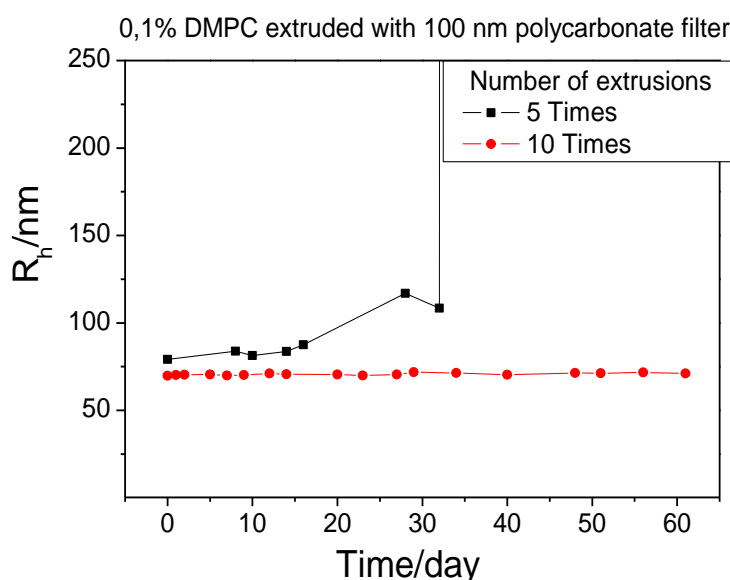


Fig. 4-1-4-2: 5 and 10 extrusion times measured by DLS as a function of time for 0.1 % DMPC solution

The presence of Rewopal 6000 and 10R5 leads to rather short stability times. Both are telechelic polymers with two hydrophobic end groups on a water-soluble polymer, which enables them to bridge bilayers. The Rewopal 6000 contains 150 central EO units and stearyl groups on both ends. Due to its structure, it has the capacity EO to connect two individual unilamellar vesicles and thereby induce their fusion or formation of multi-lamellar structures. A similar argument holds for 10R5, with the difference that it contains only 23 EO units. For Kollicoat IR, the longest time of stability of the unilamellar vesicles is observed. It contains no hydrophobic units and thereby lacks the ability to bridge vesicle bilayers. After extrusion, Kollicoat IR could exist in water or attached to the unilamellar DMPC vesicles. The pure DMPC solution without copolymer additions is the most stable one in solution.

0.1 % DHPC and DMPC solution

In order to produce bicelles vesicles in a solution mixing the variation of DHPC lipids with DMPC and keeping the concentration is always at 0.1 wt.% in total. Due to the differing lengths of hydrophilic tails from both, they are highly probable to form the long cylindrical bilayer vesicles in aqueous solutions, for which the scheme is presented in Fig. 4-1-4-4. Investigating the stability of bicelles vesicles are with time analysed by the DSL instrument.

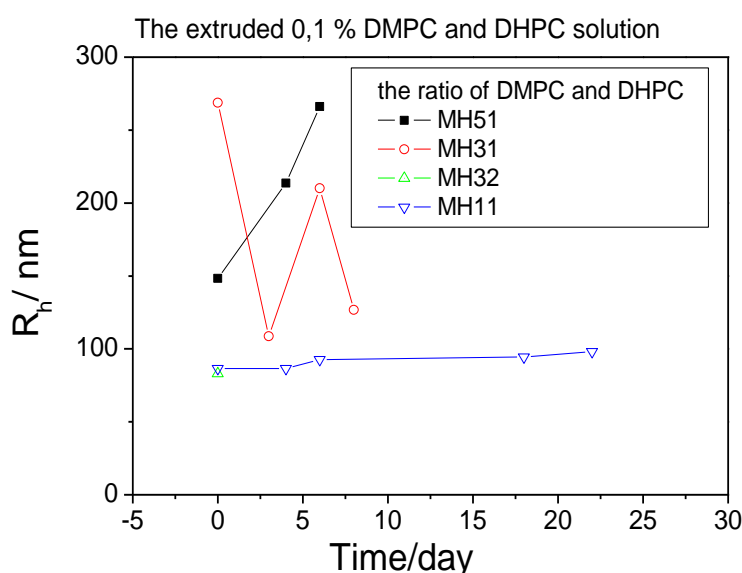
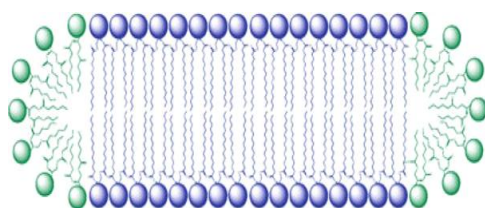


Fig. 4-1-4-3: Different ratio of 0.1 % DMPC and DHPC solutions (MH51 is the mass ratio of DMPC and DHPC 5:1, MH31 is 3:1, MH32 is 3:2 and MH11 is 1:1)

Fig. 4-1-4-3 summarizes the R_h and stability investigation of the DMPC and DHPC solution. The samples are at different mixing of mass ratios but a total concentration are controlled at 0.1 wt. %. They are all one phase and homogenous after extrusion. Compared with the pure 0.1% DMPC solution, they result in a short stable time after extrusion with 100 nm. Different mass ratios of DMPC and DHPC take different lengths of stable time. The sample MH32 keeps the shortest time of the others. After just the beginning of the fresh extrusion time, the R_h of MH 32 is around 100 nm. Three days later the R_h increased to 1000 nm, it is not presented in this curve. Keeping the longest stable time is the sample of MH11. It keeps over 20 days at the constant R_h , around 90 nm. The R_h of MH 51 keeps increasing ten days after extrusion. The MH31 shows the unstable R_h during the ten days. Other publications show that the R_h is around 25 nm to 40 nm for 0.1% lipid concentration, but it contains mostly salts or acids in the solution [95-97].





 DMPC	<chem>CCCCCCCCCCCCCCCC(=O)OCC(=O)OCCOP(=O)([O-])OCCN(C)C</chem>
 DHPC	<chem>CCCCCCCC(=O)OCC(=O)OCCOP(=O)([O-])OCCN(C)C</chem>

Fig.: 4-1-4-4: Two-dimensional projection of bicelle vesicle and chemical structures of DMPC and DHPC [98]

4-1-5 Permeability [37]

A way to determine the permeability of unilamellar vesicles is to measure the transport of probe molecules/ions through the bilayer and detect them by means of UV-VIS spectroscopy and employing a Stopped Flow instrument for high time-resolution. In the case of our vesicles, this was done by means of using a coloured iron complex and mixing it with F^- ions.

UV-VIS

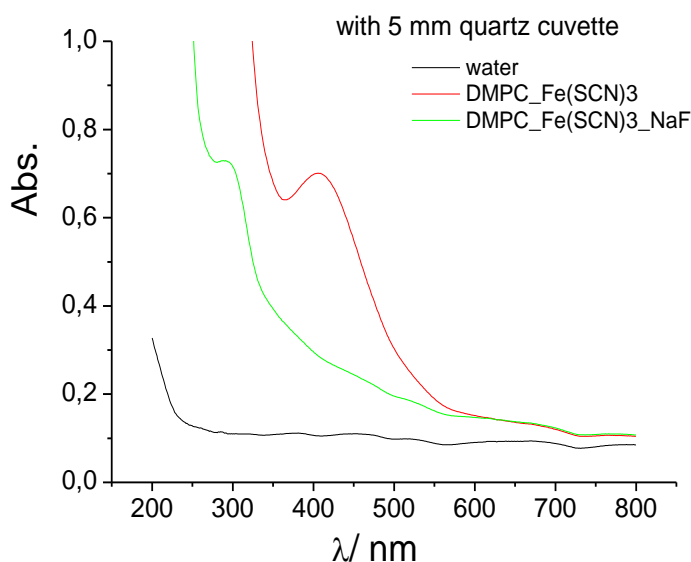


Fig. 4-1-5-1: UV-VIS absorbance spectra at 25°C with thickness of cuvette at 5 mm

The 0.2 wt. % DMPC with iron (III) thiocyanate complex inside presents red colour in the solution. A strong binding of the iron (III) thiocyanate complex to DMPC phospholipids can be observed by UV-VIS spectroscopy. The spectra of 0.2% DMPC and 2 mM $Fe(SCN)_3$, including 200 mM $NaNO_3$ in the solution, have a maximum absorbance at a wave length of 450 nm. After mixing with 200 mM NaF solution at a volumen ratio of 1 to 1 the red colour disappears because $Fe(SCN)_3$ with F^- solution turns to $(FeF_6)^{3-}$ and SCN^- ions in the solution. This results in the spectra for sample $DMPC_Fe(SCN)_3_NaF$ not expecting a peak at the 450 nm position. After mixing with the NaF solution shows a white, the sample is a turbid, non-homogenous solution.

Stopped Flow

It is assumed that the reaction between the FeSCN^{2+} complex and F^- ions outside of the vesicles is faster than the deadtime of the Stopped Flow experiments. For the reaction between FeSCN^{2+} inside the vesicles and F^- outside the vesicles, one type of ion must permeate through the vesicle membrane.

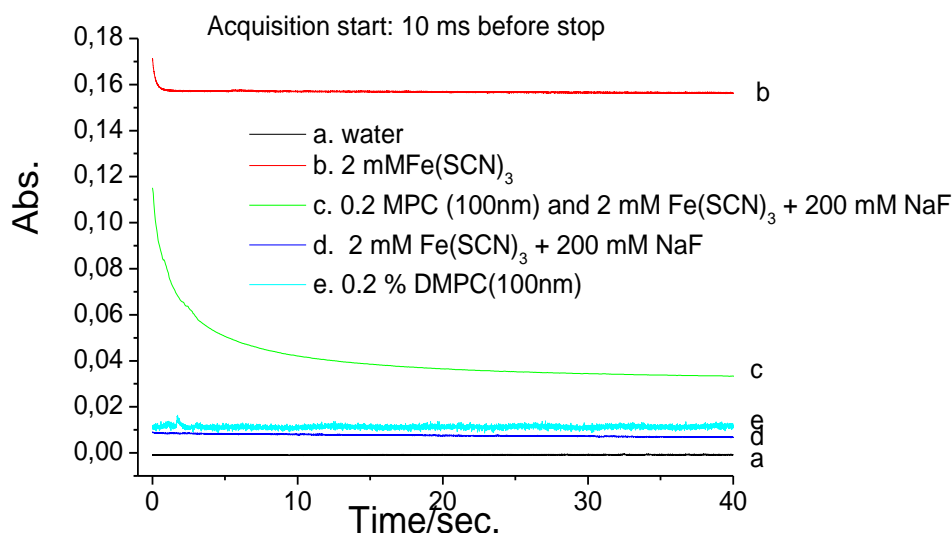


Fig. 4-1-5-2: Absorbance of stopped-flow signals at 25°C and at a wave length of 450 nm. (deadtime: 10 ms)

The solution in Stopped Flow measurements contains 0.2 wt. % DMPC unilamellar vesicles, which has been extruded with an 100 nm filter, 2 mM FeCl_3 , 6 mM NH_4SCN , 200 mM NaNO_3 and was mixed with a solution containing NaF. The amount of NaNO_3 was equal to that of the NaF solution in order to prevent osmotic pressure differences. Fig. 4-1-5-2 shows water used as the baseline; curve b is the iron (III) thiocyanate complex solution without phospholipid vesicles and has a high absorbance at 450 nm. Curve d is the iron (III) thiocyanate complex solution mixed with 200 mM of NaF solution in the volumen ratio of 1 to 1 that contains no phospholipids vesicles, either, which show a low absorbance. Curve e is the DMPC solution at 0.2 wt.% and this sample has been already extruded ten times with a 100 nm polycarbonate filter. Curve c is the 0.2% DMPC vesicles containing 2 mM $\text{Fe}(\text{SCN})_3$ and 200 mM NaNO_3 after mixing with 200 mM NaF and showing a decreasing exponential curve as a function of time. The DMPC solution with ions is more turbid than the pure DMPC solution, because the absorbance intensity is higher than pure DMPC (curve e). From the relaxing curve it can be concluded that the movements of ions for FeSCN^{2+} diffuse outside of membrane and/or F^- diffuse inside of membrane. The vesicles are detected by passing through the DMPC bilayer here. The signal for curve c can be analysed by a stretched exponential fit and the equation is given

by

$$\Delta A \propto \exp \cdot \left[- \left(t / \tau \right)^\alpha \right], \quad (4-1-4-1)$$

where ΔA is the absorbance change of the signal, τ is the relaxation time, and α is the stretching factor, typically between 0.4 and 0.7. In this dissertation, the sample for Stopped Flow was measured only at fixed concentration of 0.2% DMPC, ions and complex for the 200 mM NaF and 2 mM FeSCN^{2+} solution to observe the kinetic movements of irons penetrating into the vesicle of DMPC. If the complex and FeSCN^{2+} is increased as a function of concentration for fixed phospholipids, the relaxation time τ is decreased. However, increasing the concentration of NaF solution did not modify the τ not much [37].

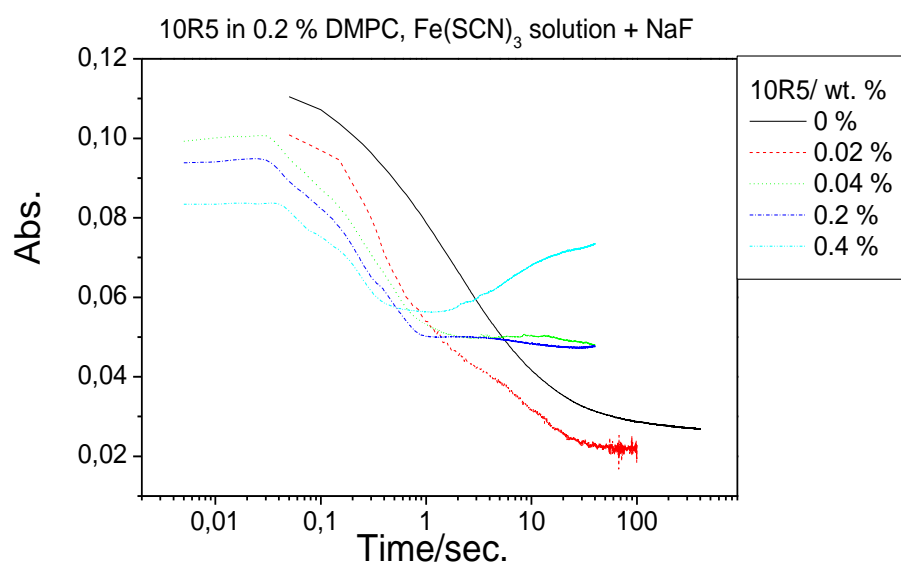


Fig. 4-1-5-3: Abs. of Stopped Flow in the presence of 10R5 at a wavelength of 450 nm

Fig. 4-1-5-3 shows the results of 0.2% DMPC, 2 mM $\text{Fe}(\text{SCN})_3$ with 200 mM NaF after mixing at a volumen ratio of 1 to 1. In the presence of 10R5, the kinetic rate of the FeSCN^{2+} and F^- ion reaction increases. At the concentration of 0.02% 10R5 the relaxation time is reduced to 5.86 seconds and for 0.04% 10R5 it decreases sharply to 0.36 seconds, (summarized in Tab. 4-1-5-1). The sample of 0.4% 10R5 appears increasing baseline after absorbance intensity decreases to 0.055. It is caused by the redundant sediments of molecules from DMPC, $\text{Fe}(\text{SCN})_3$, NaF and NaNO_3 .

Tab. 4-1-5-1: Relaxion time τ of 0.2 % DMPC solution in the presence of 10R5 and L35

10R5/wt. %	τ / sec	L35/wt. %	τ / sec
0	6.62	0	6.62
0.02	5.86	0.02	8.36
0.04	0.36	0.04	32.85
0.2	0.32	0.1	48.60
0.4	--	0.2	--

Tab. 4-1-5-1 summarizes the relaxion time τ of the 0.2% DMPC vesicle solution in the presence of 10R5 and L35, respectively.

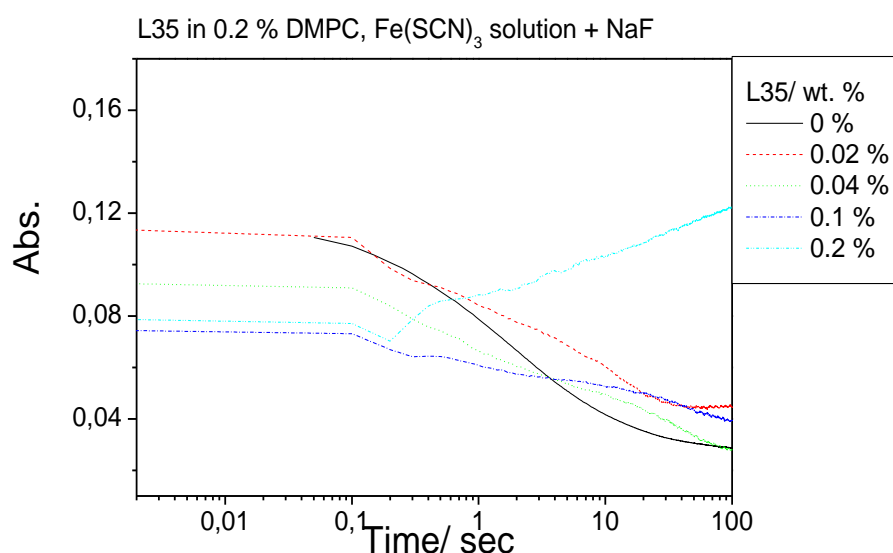
**Fig. 4-1-5-4: Abs. of Stopped Flow in the presence of L35 at a wave length of 450 nm**

Fig. 4-1-5-4 shows the absorbance of Stopped Flow at 450 nm for the sample of 0.2% DMPC small vesicles and ions solution in the presence of L35. The relaxion time τ is increased in the presence of L35. The intensity of absorbance decreased because the F^- ions react with $\text{Fe}(\text{SCN})_2^+$. When L35 is increased to 0.2 wt.% in the solution, no optimal curve appears as a function of time. The baseline increases as a function of time after mixing with a volumen of NaF and it is because of sediments caused by copolymer L35.

Equations (1-7-12) and (1-7-13) give a relation between the relaxation time of the Stopped Flow signals and the calculated permeability coefficients. In this situation the relaxation time should be independent of the concentration of F^- and $FeSCN^{2+}$ under the experimental conditions.

In this experiment, the relaxation time of the DMPC solution is analysed by the Stopped Flow. The first-order rate constant of k_{exp} can be calculated with eq. 1-7-15 and the value results in 0.151 s^{-1} . The permeability coefficient P is calculated by eq. 1-7-14 and the value is $3.52 \times 10^{-7}\text{ cm/s}$. For the vesicles of egg phosphatidyl choline the permeability P is the range of $2 \times 10^{-4}\text{ cm/s}$ [37]. The vesicles of DMPC results in that the permeability is slower than the vesicles of egg phosphatidyl choline. The presence of 10R5 and L35 in 0.2% DMPC, respectively, is summarized in Tab. 4-1-5-2. The radius of DMPC vesicles, including additives, takes 70 nm.

Tab. 4-1-5-2: Results of K_{exp} and P of 0.2 % DMPC in the presence of 10R5 and L35

Additives and 0.2 % DMPC unilammellar vesicle solution					
10R5			L35		
Con/wt. %	K_{exp}/s^{-1}	$P/cm \cdot s^{-1}$	Con./ wt. %	K_{exp}/s^{-1}	$P/cm \cdot s^{-1}$
0	0.151	3.52×10^{-7}	0	0.151	3.52×10^{-7}
0.02	0.171	3.99×10^{-7}	0.02	0.120	2.80×10^{-7}
0.04	2.78	6.49×10^{-6}	0.04	0.030	7.0×10^{-8}
0.2	3.13	7.30×10^{-6}	0.1	0.021	4.9×10^{-8}

The presence of 10R5 decreases the relaxation times of DMPC vesicles solutions and the presence of L35 increases. Rate constant of K_{exp} is inversely proportional to relaxation time τ . By adding the 10R5 into DMPC vesicles solution, it lets the K_{exp} increase but the K_{exp} of DMPC is decreased by adding L35. The permeability of DMPC solution is increased in the presence of 10R5, but is decreased in the presence of L35.

4-1-6 Conductivity

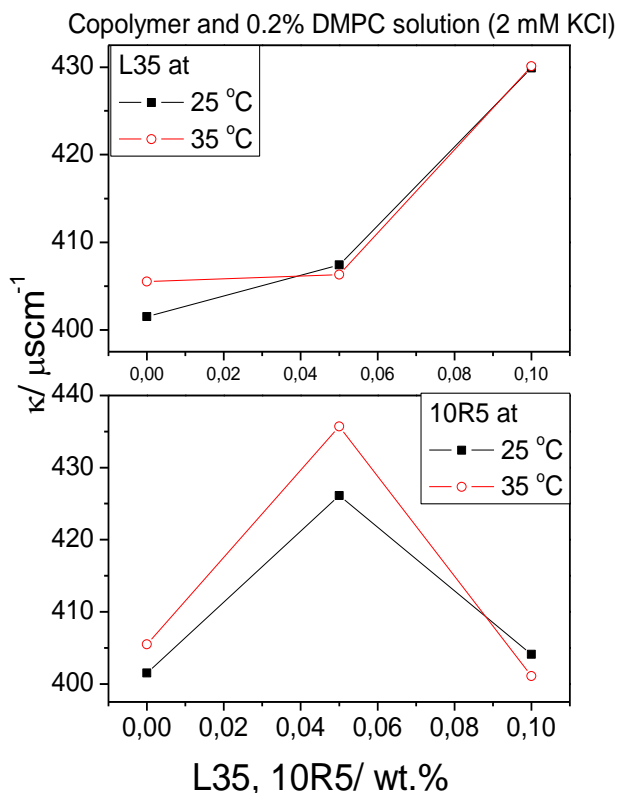


Fig. 4-1-6-1: Conductivity of L35 and 10R5 in 0.2 % DMPC (2 mM) respectively

The respective results of conductivity of 0.2% DMPC solution in the presence of L35 and 10R5 are shown in Fig. 4-1-6-1. Both have been already extruded 10 times by a 100 nm filter before measuring. The samples contain 2 mM KCl to achieve a reasonable value of conductivity, because the conductivity of DMPC is extremely low. The presence of L35 and 10R5 only influence the conductivity of 0.2% DMPC solution a little. They are prepared with the concentration of 0.05% and 0.1% in the 0.2% DMPC solution. At 25°C the maximal conductivity for L35 is at 0.1% but for 10R5 is at 0.05%. When the concentration of 10R5 increases to 0.1% in 0.2% DMPC solution, the conductivity reduced. If the samples are measured at 35°C, the pure 0.2% DMPC solution results in a higher conductivity value than at 25°C. The presence of L35 leads to no influence on the conductivity when the temperature increases to 35°C. However for 10R5 the highest conductivity is at 0.05%. When the temperature is increased to 35 oC, the conductivity is increased. This sample was measured at two different temperatures.

4-2 Diesterquat CR3099 solution

The surfactant CR3099 is of the diesterquat type, and based on oleic acid. Due to some advantages like fast water film displacement, its ability to impart shine and optimal hydrophobic properties it is widely used in commercial applications [99-102]. Typically it forms vesicles in aqueous solution [103]. The CR3099 surfactant is compatible with non compatible with non-ionic and amphoteric surfactants and is no problem in a pH range between acidic and slightly alkaline [104]. However it is incompatible with anionic surfactants due to the formation of insoluble surfactant complexes.

4-2-1 Phases Behaviour



Fig. 4-2-1-1: Pictures of 0.5% CR3099 solution before extrusion (left) and after extrusion with 100 nm (middle and right)

CR3099 dissolved in water at a concentration of 0.5% is a cloudy and homogeneous solution (Fig. 4-2-1-1). After extrusion with a 100 nm filter, the turbidity of the sample becomes weaker as the size of particles is reduced in the solution. The extruded sample is very stable and only observed under macroscopic conditions. Over six months, the phase behaviour of the extruded sample (see Fig. 4-2-1-1) remains unchanged, which is clearly different to the ageing behaviour typically seen for phospholipids.

4-2-2 Stability of small vesicles for the CR3099 solution

DLS Measurements

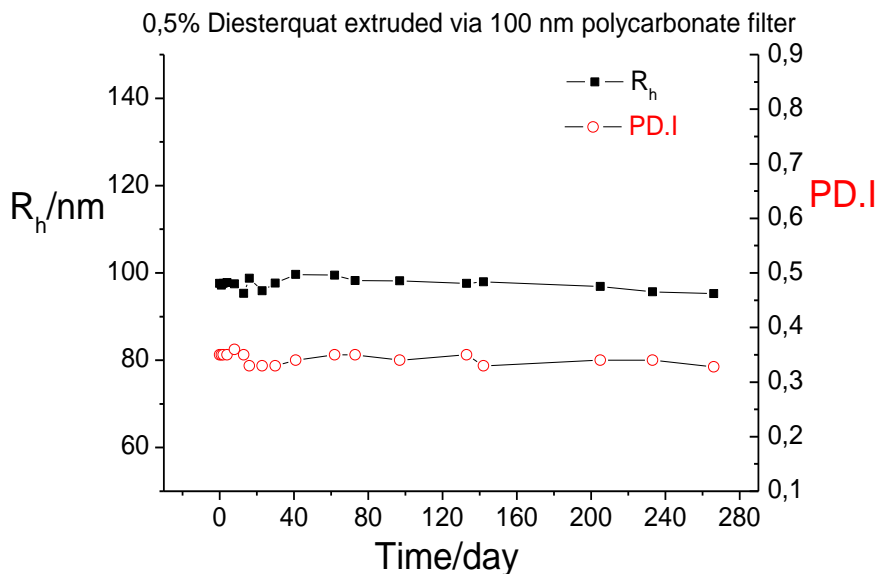


Fig. 4-2-2-1: Results of R_h and PD.I with the function of time

Fig. 4-2-2-1 gives the hydrodynamic radius as a function of time for a 0.5% CR3099 solution, which has been extruded with 100 nm poly carbonate filters, and investigated over the course of six months. Before extrusion, the R_h of 0.5 % CR3099 solution is 202.9 nm and the PD.I is 0.31. The radius can be induced depending on the concentration. After extrusion with a 100 nm filter, the R_h decreases to around 100 nm and the values of the PD.I are around 0.33. They remain constant during this period of time. The PD.I of the 0.5% CR3099 solution is not influenced strongly by the method of extrusion. The molecules of diesterquat can be biogradegated by bacteria, especially with a CO_2 -monitor [105]. However, all CR3099 samples, even without any protection agents, like NaN_3 , show no signs of biogradegation.

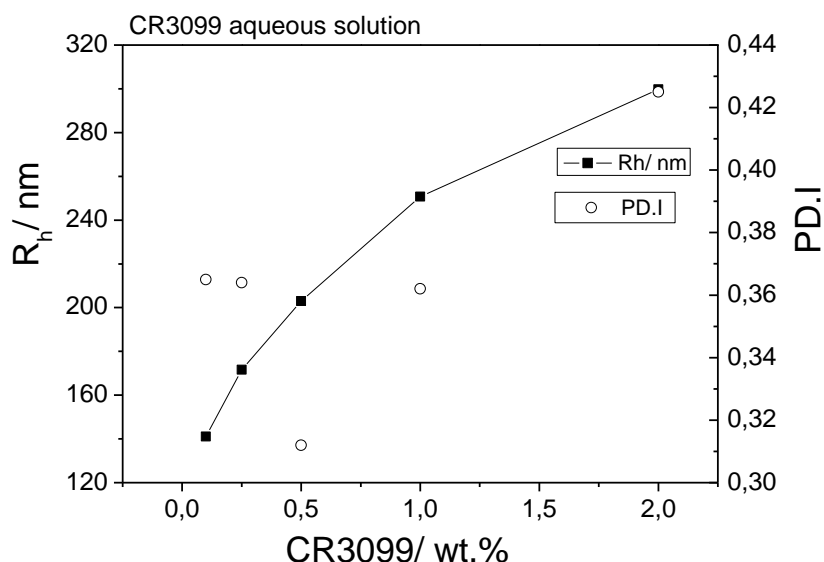


Fig. 4-2-2-2: DLS measurements of CR3099 solution as function of concentration

Diesterquat CR3099 forms vesicles in solution. The R_h of CR3099 is dependent on the concentration. The sample of 2.0 % results the largest R_h of CR 3099 solution. Fig. 4-2-2-2 presents the R_h and PDI of CR3099 as function of concentration. They are measured without extrusion. The sample of 0.5 % results the lowest PDI values of CR3099 solution.

4-2-3 Membrane thickness of the unilamellar vesicles

SANS measurements

The samples were dissolved in D_2O directly and without any extrusion. They were measured by Dr. Sylvain Prévost at ILL in Grenoble, France.

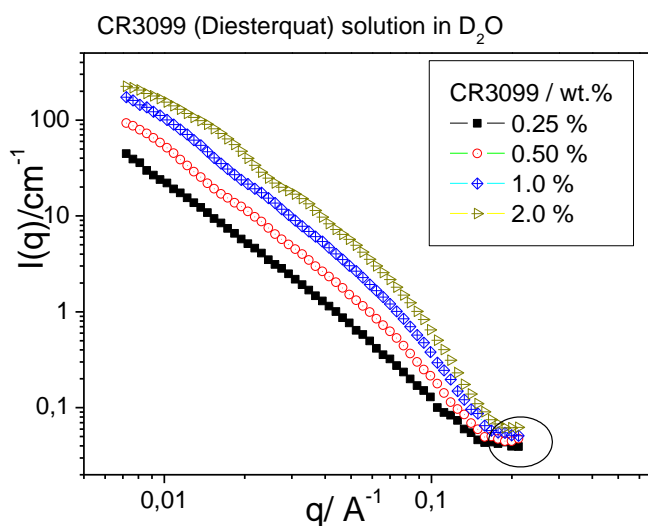
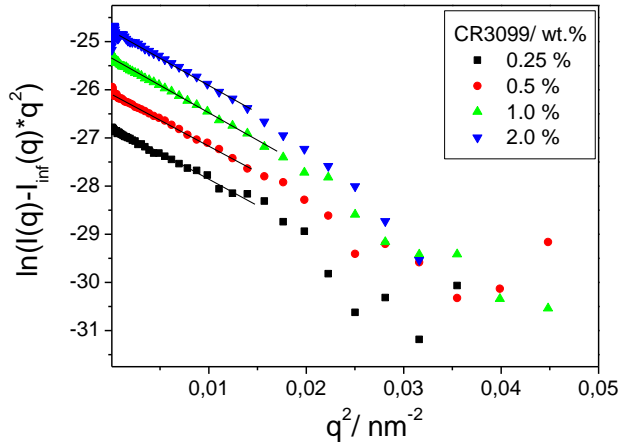


Fig. 4-2-3-1: Experimental SANS data for CR3099 in D_2O

Fig. 4-2-3-1 presents the SANS data of the CR3099 solution from 0.25 % to 2.0 %. Making a plot of $\ln(I(q)-I_{inf}(q)q^2)$ vs q^2 gives a straight line portion of gradient $-d^2/12$ where d is the second moment of the vesicle lamella thickness [92, 93]. $I_{inf}(q)$ is the intensity at the background and $I_{inf}(q)$ is read at red circle position. The curve is shown as follows:



Tab. 4-2-3-1: slop and thickness of CR3099

CR3900/ wt. %	Slop/ nm ²	d/ nm
0.25	-92.29	33.28
0.5	-110.94	36.49
1.0	-115.24	37.19
2.0	-112.10	36.68

Fig. 4-2-3-1: Kratky-Porod plots of the SANS data obtained from CR3099 in D₂O

Tab. 4-2-3-1 summarizes the slope of CR3099 and the thickness of the vesicles. The vesicle thickness of CR3099 is slightly dependent on the concentration.

4-2-4 Additive and CR3099 solution

In the following, our focus was then on the effect of adding amphiphilic polymers to these vesicle solutions in order to see how their presence affects the structure and stability of the CR3099 vesicles.

10R5 and 0.5 % CR3099 solution

We then studied the effect of the copolymer 10R5 on the vesicle structure of CR3099. To that end, 10R5 was added in fixed amounts directly to a 0.5% CR3099 solution. For the preparation, one day of homogenisation was done and homogenous solutions were always obtained.

DLS measurements

Investigating the effect on the vesicles of CR3099 is analysed by the DLS in the presence of 10R5. The samples were traced for at least one month.

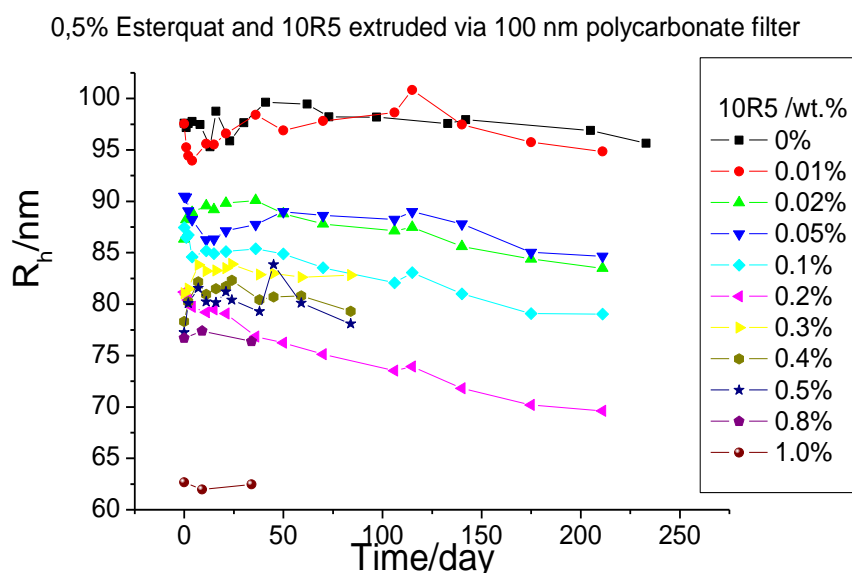


Fig. 4-2-4-1: R_h of increasing 10R5 in a fixed 0.5 % CR3099 solution respectively as a function of time

The R_h of a 0.5 % CR3099 solution containing the various amounts of 10R5 remains stable for over a half a year after extrusion. The additional mixture of a telechelic polymer, like 10R5, has an influence on the hydrodynamic radius of a CR3099 solution after extrusion. The R_h of 0.5% CR3099 decreases upon the addition of 10R5 (Fig. 4-2-4-1).

The reduced R_h is proportional to the amounts of 10R5 in a fixed CR3099 solution. Only for the smallest amount of 10R5 (0.01%) does the R_h for the 0.5% CR3099 solution remain unchanged. Upon increasing the concentration to above 0.02%, R_h becomes reduced. For these 10R5-containing samples, a slow decrease of particle size over the course of weeks is observed. For the higher concentrations of 10R5 (0.3%, 0.5%, 0.8%, 1.0%) they were prepared later and therefore measured only for a shorter period of time.

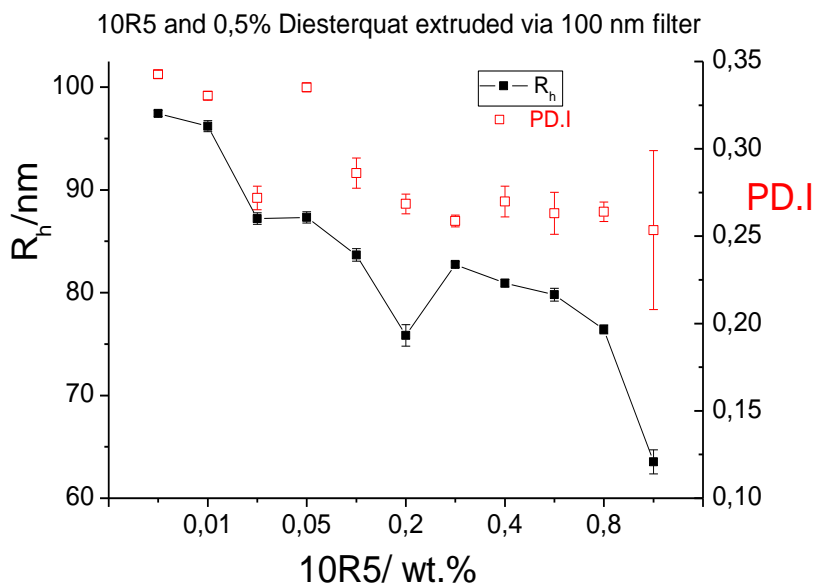


Fig. 4-2-4-2: Results of R_h and PD.I present as a function of 10R5 in a 0.5 % CR3099 solution. Both values are calculated based on the average of their own total measuring day.

Fig. 4-2-4-2 summarizes the results of the hydrodynamic radius R_h and polydispersity index PD.I as a function of 10R5 in 0.5% CR3099 solutions. By adding 10R5 into the 0.5% CR3099 solution, the PD.I and R_h are influenced. Both values are decreased proportionally as a function of concentration. The decreasing values of R_h and PD.I do not appear as an optimal linear function. The R_h of the sample 0.3% is higher than 0.2% and the PD.I of the sample 0.02% is lower than 0.05%.

Results of Viscosity

Measuring the viscosity of a 0.5% CR3099 solution was done by means of an ubbelohde viscosimeter.

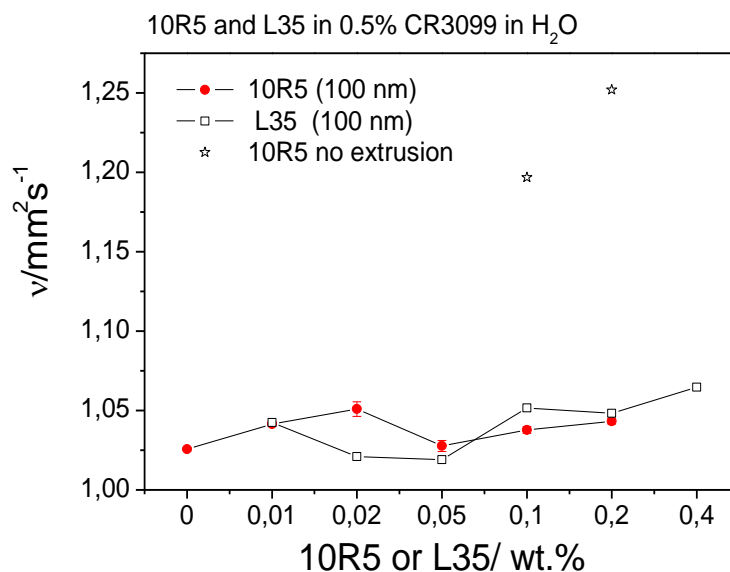


Fig. 4-2-4-3: Results of viscosity for 10R5 (extruded and unextruded) and L35 (extruded) in 0.5% CR3099 solutions, respectively, as a function of concentration

Fig. 4-2-4-3 shows the respective viscosity results of 10R5 and L35 in a 0.5% CR3099 solution as a function of concentration. Basically constant values are seen. Apparently, the 10R5, with its hydrophobic end groups, is not able to lead to a cross-linking of the vesicles that should lead to an increased viscosity. The samples prepared without extrusion at the concentrations of 0.1% and 0.2% show somewhat higher viscosity values. This can be correlated to the larger particle size and the corresponding larger effective volume fraction.

Kollicoat IR and 0.5 % CR3099 solution

In the following we then studied the effect of the polymer Kollicoat IR on the vesicle structure of CR3099. To that end, Kollicoat IR was added directly, in fixed amounts, to a 0.5% CR3099 solution. For the preparation, one day of homogenisation was done and homogenous solutions were always obtained.

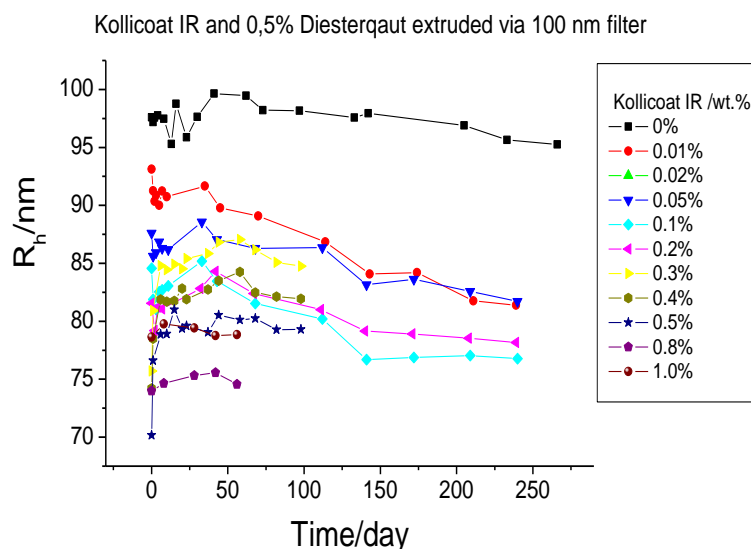


Fig. 4-2-4-4: R_h of increasing Kollicoat IR in fixed 0.5% CR3099 solutions, respectively, as a function of time

Fig. 4-2-4-4 presents the results for the hydrodynamic radius of 0.5% CR3099 solutions with increasing concentrations of Kollicoat IR, varying from 0% to 1.0%, that were regularly measured by means of the DLS over the course of six months. The addition of Kollicoat IR leads to reduced R_h values where the reduction is proportional to the concentration of Kollicoat IR. A substantial decrease of R_h was already observed for the lowest concentration of Kollicoat IR of 0.01%. With time, the particle size tends to somewhat decrease.

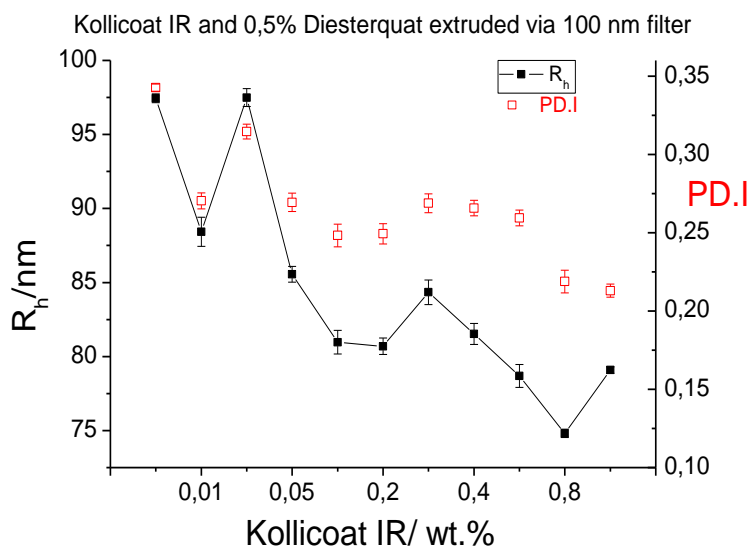


Fig. 4-2-4-5 : Results of R_h and PD.I present as a function of Kollicoat IR in 0.5 % CR3099 solutions. Both values are calculated based on the average of their own total measuring day.

Fig. 4-2-4-5 shows the results of R_h and PD.I values as functions of Kollicoat IR in a 0.5% CR3099 solution. The presence of Kollicoat IR leads to decreasing R_h and PD.I values. At low concentrations of Kollicoat IR, like the samples of 0.01% and 0.02%, it presents unexpected results. The R_h and PD.I of sample 0.02% are higher than sample 0.01%. This could be due to the uncertainty of small amounts and the experimental inaccuracy.

5. Addition of polymers to gel phases of multilamellar vesicles (MLV) (TDMAO, TTABr and 1-Hexanol)

In this part we investigated the effect of the addition of polymers on the properties of a gel phase densely packed with multilamellar vesicles (MLV). This viscoelastic phase contains densely packed MLV, composed of alkyldimethylaminoxides (C_x DMAO), n-alcohols (C_6 - C_9) and the ionic surfactant tetradecyltrimethylammonium bromide (C_{14} -TMABr) or sodium dodecyl sulphate (SDS) [106]. For our experiments, we selected TDMAO, TTABr and 1-Hexanol as amphiphilic components in aqueous solutions.

5-1 Phases behaviour

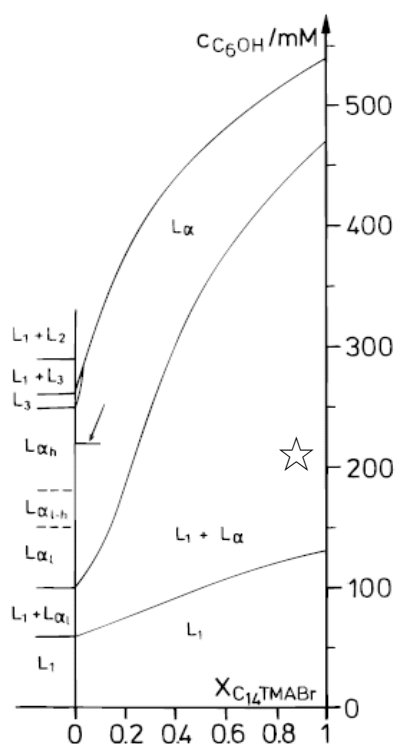


Fig. 5-1-1 : Schematic quaternary phases diagram of TDMAO, TTABr, 1-Hexanol and water at 25°C and a total surfactant concentration of 100 mM and for varying concentrations of 1-Hexanol [106]

Fig. 5-1-1 summarizes the phase behaviour of zwitterionic tetradecyldimethylamineoxide (TDMAO), cationic tetradecyltrimethylammonium bromide (TTABr), 1-Hexanol and water at 25°C. The phase behaviour depends strongly on the ratios of TDMAO, TTABr and 1-Hexanol. In this system, vesicles are formed easily in the presence of the cationic surfactant TTABr in the ternary system of TDMAO/1-Hexanol/ H_2O [57, 107-109]. The Phase L_1 is the isotropic micellar solution, $L_{\alpha 1}$ the vesicle phase, and $L_{\alpha h}$ the classical

lamellar phase of planar bilayers. In our experiment, the concentrations of TDMAO, TTABr and 1-Hexanol are 90 mM, 10 mM and 220 mM, respectively. They fall into the phase diagram regime indicated by the single star. The other solution contains the same ratio of TDMAO and TTABr, but the 1-Hexanol increases to 350 mM. It is close to L_α phase but still at the range of $L_1 + L_\alpha$ phase.

90 mM TDMAO, 10 mM TTABr and 220 mM 1-Hexanol solution with 220 mM and 350 mM respectively



Fig. 5-1-2 : Gel solution of 90 mM TDMAO, 10 mM TTABr with 220 mM and 350 mM 1-Hexanol (right and left)

Fig. 5-1-2 shows the phase behaviour of a gel solution of 90 mM TDMAO and 10 mM TTABr with different concentrations of 220 mM and 350 mM 1-Hexanol respectively. The sample of 90 mM TDMAO, 10 mM TTABr and 220 mM 1-Hexanol is in the gel phase, which is homogeneous, transparent and highly viscous. When the concentration of 1-Hexanol is increased to 350 mM, the sample is more turbid and the viscosity is lower.

10R5 and 90 mM TDMAO, 10 mM TTABr and 220 mM 1-Hexanol solution

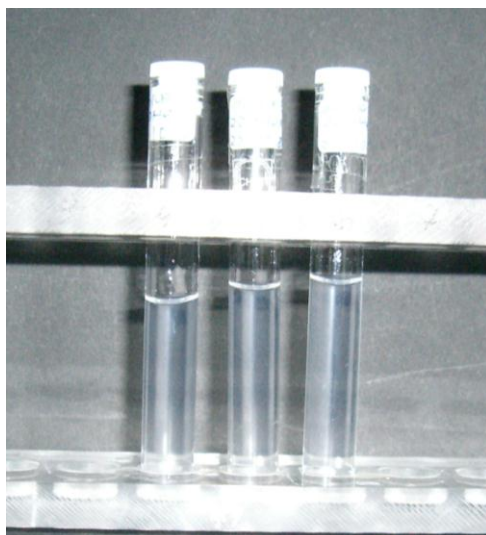


Fig. 5-1-3 : (From left to right) 0 %, 1.0 % and 2.0 % of 10R5 in gel solution of 90 mM TDMAO, 10 mM TTABr and 220 mM 1-Hexanol

The addition of 10R5 does not lead to larger differences in the gel phase of 90 mM TDMAO, 10 mM TTABr and 220 mM 1-Hexanol. The amounts of added 10R5 are 1.0% and 2.0%, respectively, and the solutions remain homogeneous and clear.

10R5 and 90 mM TDMAO, 10 mM TTABr and 350 mM 1-Hexanol solution



Fig. 5-1-4 : (From left to right) 0 %, 1.0 % and 2.0 % of 10R5 in gel solution of 90 mM TDMAO, 10 mM TTABr and 350 mM 1-Hexanol

The mixture of 90 mM TDMAO, 10 mM TTABr and 350 mM 1-Hexanol presents turbid but homogeneous gel phases. The presence of 10R5 clarifies the turbid gel phase. If the amounts of 10R5 increases to 2%, the sample at the right side, becomes more transparent compared to the sample of 0% at left side.

Rewopal 6000 and 180 mM TDMAO, 20 mM TTABr and 400 mM 1-Hexanol solution

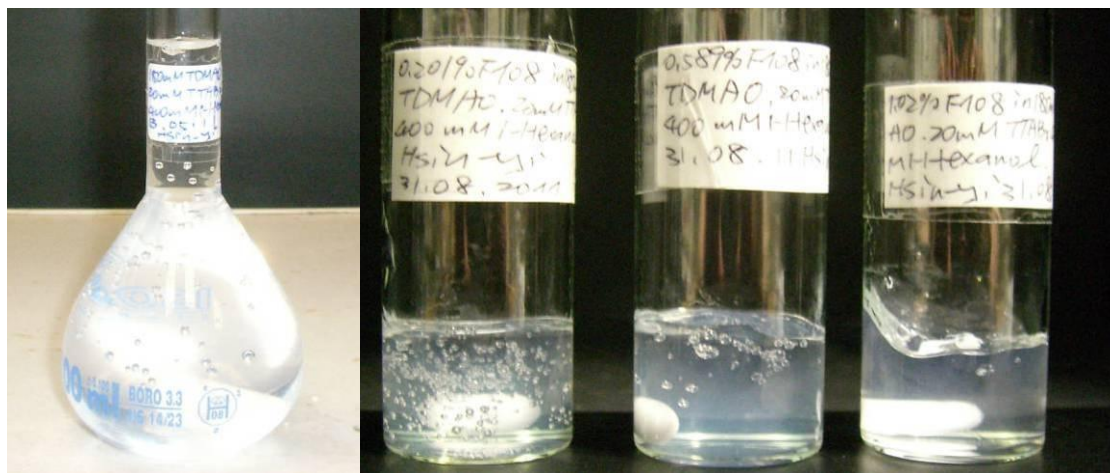


Fig. 5-1-5: Samples of Rewopal 6000 at 0, 0.2, 0.6 and 1.0% (from left to right) in the gel solution of 180 mM TDMAO, 20 mM TTABr and 400 mM 1-Hexanol

Fig. 5-1-5 shows the gel solutions of a mixture of 180 mM TDMAO, 20 mM TTABr and 400 mM 1-Hexanol. The concentrations of TDMAO and TTABr were doubled and 1-Hexanol increased to 400 mM. It remains homogenous, transparent and turns into a strongly viscous, gel-like solution. The appearance of the gel solution becomes less turbid in the presence of Rewopal 6000. However the viscosity is hard to tell if it is affected by Rewopal 6000.

5-2 Properties of gel phases

Amplitude sweep

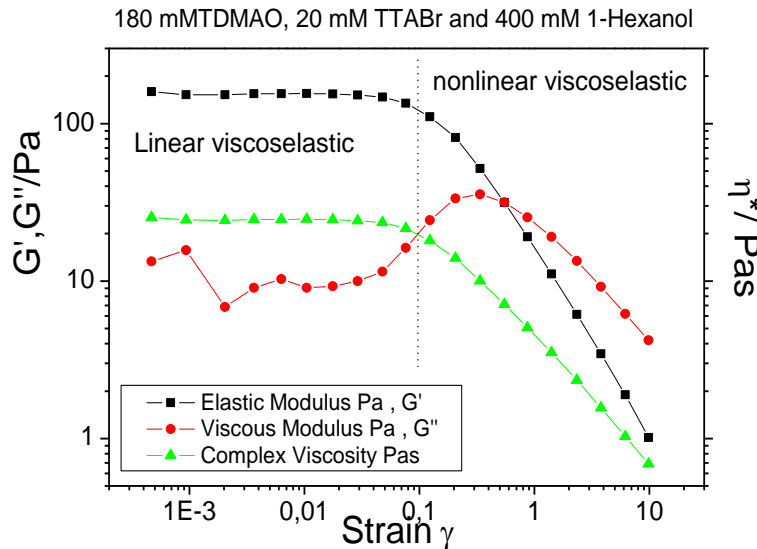


Fig. 5-2-1: Amplitude rheogram of a solution 180 mM TDMAO, 20 mM TTABr and 400 mM 1-Hexanol

The modulus for the sample of 180 mM TDMAO, 20 mM TTABr and 400 mM 1-Hexanol results in two parts of viscoelastic characteristics as functions of strain. In the first part, the elastic modulus and the complex viscosity are independent of the strain. They obey the linear viscoelastic rule when the strain increases to 0.1 Pa. If the strain force continues to increase to 10 Pa, the appearance of nonlinear viscoelastic phases are observed. In the second part, the elastic modulus and complex viscosity decrease after the strain forces grow from 0.1 Pa to 10 Pa. The viscous modulus G'' of the sample does not behave totally independently of the strain force in the first part. It results in the same phenomenon as other parameters in the second part of strain range. The decreasing plateau begins around 0.5 Pa, which is higher than the elastic modulus and complex viscosity.

Frequency sweep

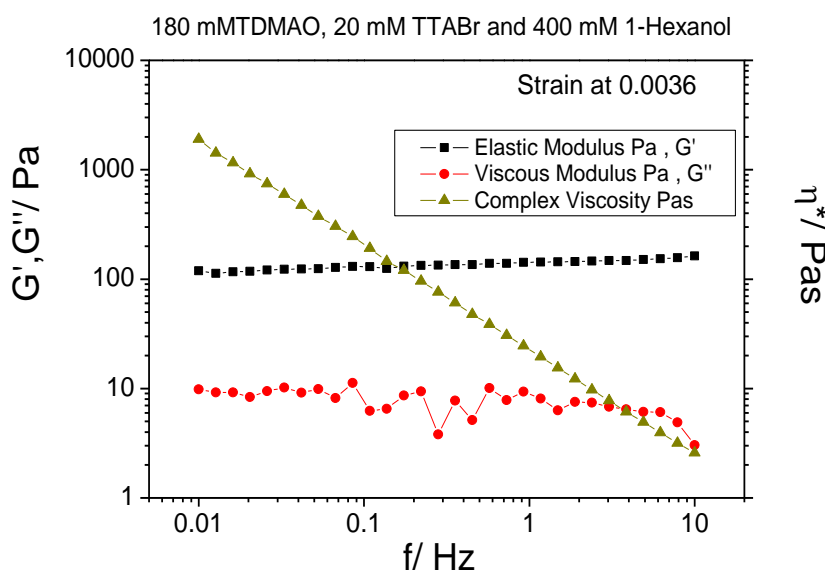


Fig. 5-2-2 : Oscillatory rheogram of a solution 180 mM TDMAO, 20 mM TTABr and 400 mM 1-Hexanol

The frequency sweep curve gives us good rheological information on the materials how they behave during storage and application. It is a useful test to determine the viscoelastic properties of samples as a function of timescale. Several parameters would be obtained, such as Storage (Elastic) Modulus G' , the Viscous (Loss) Modulus G'' , and the Complex Viscosity η^* . The figure is the typical for a well-structured gel system. The elastic modulus G' is greater than the viscous modulus G'' and both are almost independent of frequency. In this case, it is impossible for sedimentation to occur. There are other typical cases like non-associated particulate dispersion and weakly-structured systems. The frequency of a sweep curve of non-associated particulate dispersion appears in the viscous modulus, which is dominant over the elastic modulus. Both of these are highly dependent on frequency. Besides, the complex viscosity is almost independent of frequency. The other system results in that the viscous modulus is greater than the elastic modulus. However, the difference between these is less great than in the non-associated system. The complex viscosity is also now dependent on the frequency.

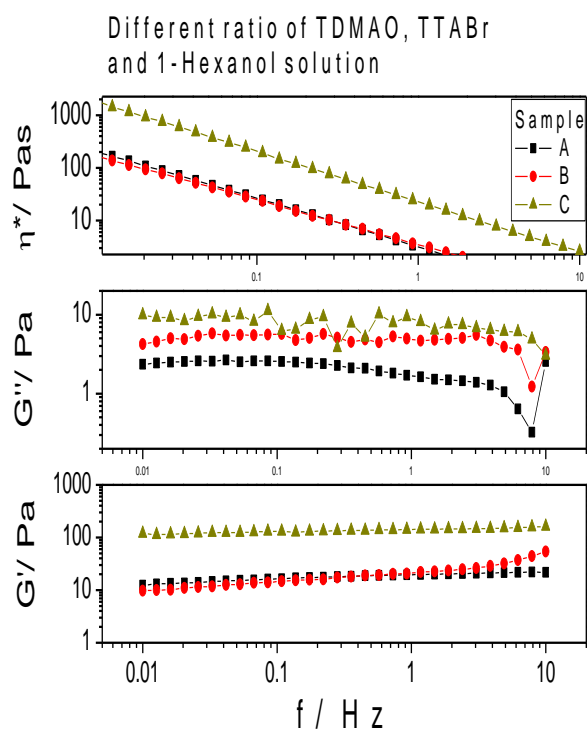


Fig. 5-2-3: Oscillatory result of different ratios of TDMAO, TTABr and 1-Hexanol in solutions

In this part, three solutions composed of various concentrations of TDAMO, TTABr and 1-Hexanol, as shown in Tab. 5-2-1, were measured by Rheology.

Tab. 5-2-1: Ratio of TDMAO, TTABr and 1-Hexanol

Sample	TDMAO/ mM	TTABr/ mM	1-Hexanol/ mM
A	90	10	220
B	90	10	350
C	180	20	400

Three parameters – G' , G'' and η^* – are measured as a function of frequency from 0.01 Hz to 10 Hz. At the given constant strain sample A and B result in optimal stability and little dependency on frequency in the elastic modulus. Sample C results in higher elastic characters than do samples A and B. This is due to the doubling of the concentration compared to sample A. Sample B leads to an increase of the elastic property when the frequency increases to 10 Hz. In the viscous modulus, all three samples result in lower values than in the elastic modulus. Below 5 Hz the viscosity is independent of frequency. The complex viscosity is linearly dependent on frequency when the frequency is close to 10 Hz.

10R5 in a 90 mM TDMAO 10 mM TTABr and 220 mM 1-Hexanol solution

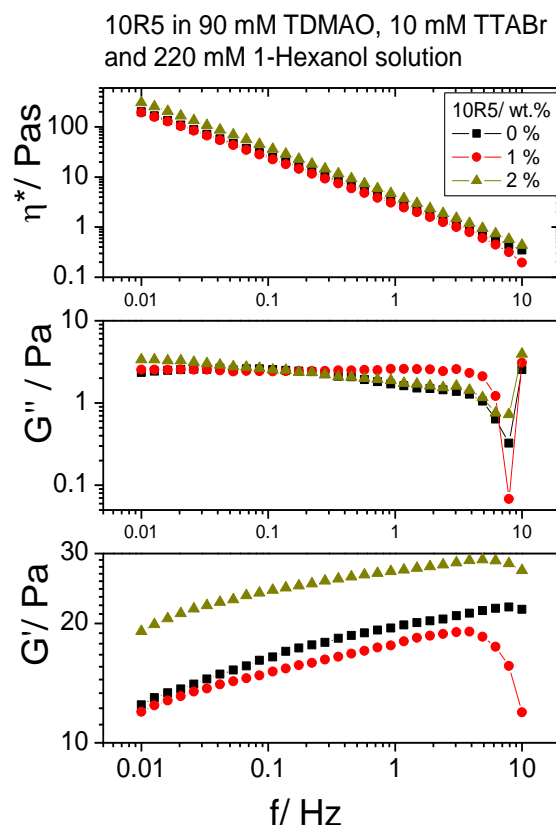


Fig. 5-2-4: Oscillatory result of 10R5 in a 90 mM TDMAO, 10 mM TTABr and 220 mM 1-Hexanol solution

In the elastic modulus, the three samples show little dependency on frequency; in addition, the presence of 10R5 in 90 mM TDMAO, 10 mM TTABr and 220 mM 1-Hexanol induces the values of elastic modulus. The sample of 1.0% 10R5 shows the lowest elastic appearance in comparison to the other two samples; moreover, it decreases dramatically at high frequencies. The elastic property increases when the concentration of 10R5 increases by 2% in the same parent gel solution. In the viscous modulus, the samples of 0 and 2% 10R5 tend to decrease with respect to frequency. On the other hand, the sample of 1% keeps constant viscose value independent of frequency. However they decrease sharply between 7 and 9 Hz. At 10 Hz, the viscous modulus becomes slightly higher than the original value. The sample of 1% 10R5 contains the lowest elastic properties and leads to lowest G'' value at a high frequency range. The values of complex viscosity are decreased in the presence of 1% 10R5 and increased slightly when the 10R5 increased to 2%.

10R5 in a 90 mM TDMAO 10 mM TTABr and 350 mM 1-Hexanol solution

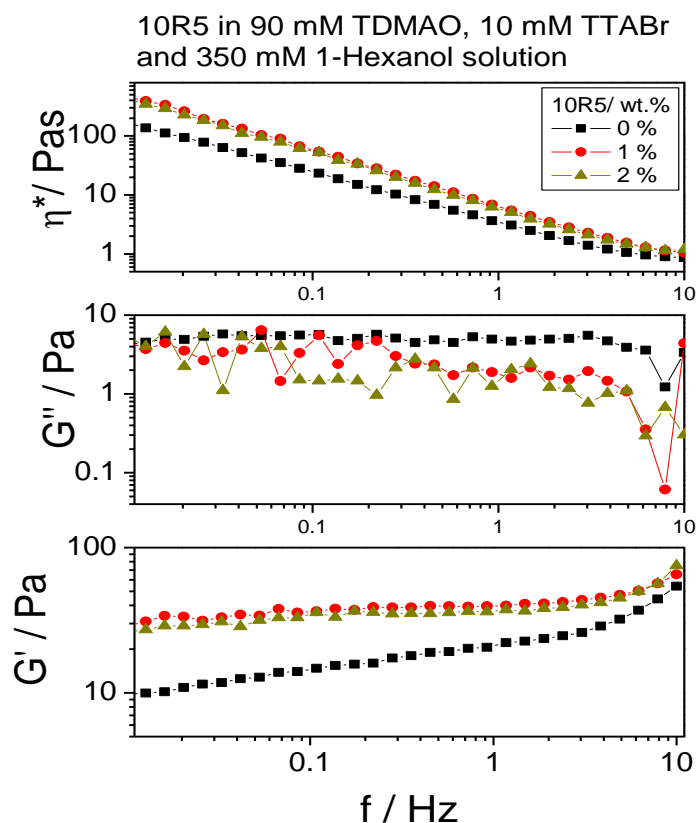


Fig. 5-2-5: Oscillatory result of 10R5 in a 90 mM TDMAO, 10 mM TTABr and 350 mM 1-Hexanol solution

With the same concentrations of TDMAO and TTABr, that of 1-Hexanol increases to 350 mM and the phase becomes turbid. The rheological parameters G' and η^* do not change much; however, when 10R5 is added to this solution, elasticity and complex viscosity are enhanced, especially at the low frequency range. When the frequency is close to 10 Hz, the values of 1% and 2% 10R5 are closer to each other. It indicates that three samples share similar properties of both moduli at high frequencies. In a viscous modulus, regular and limited variation appears when the samples contain 10R5 in the solution. This indicates that the presence of 10R5 disturbs the constant stability value of pure gel turbid solution. The sample of 0% has lower values at high frequency. The lowest value of G'' appears when the sample contains 1% 10R5.

Rewopal 6000 in a 180 mM TDMAO, 20 mM TTABr and 400 mM 1-Hexanol solution

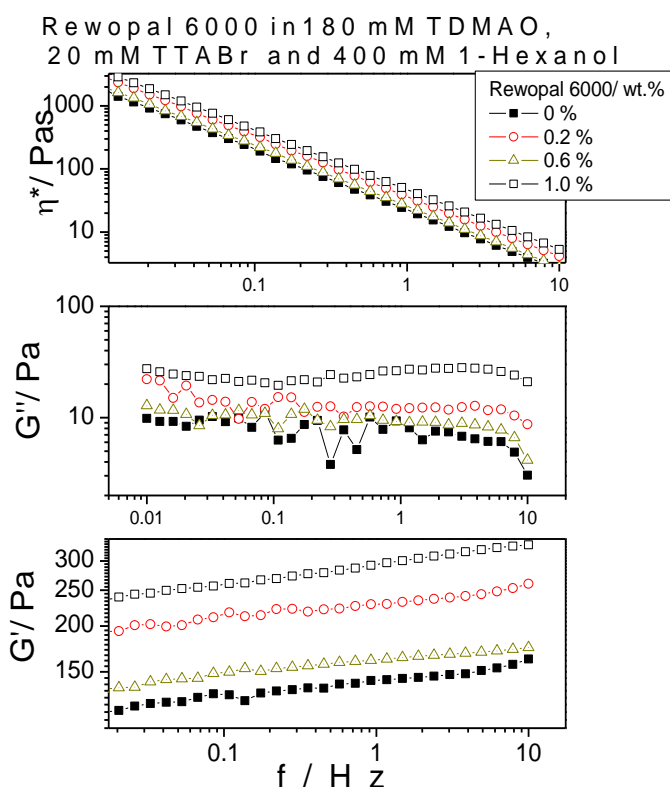


Fig. 5-2-6: Oscillatory result of Rewopal 6000 in a 180 mM TDMAO, 20 mM TTABr and 400 mM 1-Hexanol solution

The gel solution of 180 mM TDMAO, 20 mM TTABr and 400 mM 1-Hexanol results in higher G' , G'' and η^* values in comparison to the other two gel solutions. The presence of Rewopal 6000 are influenced the values of G' , G'' and η^* . The results show that they increase non-linearly with respect to the amounts of Rewopal 6000. In all three parameters, the sample of 0.2% has greater values than the sample of 0.6%; meanwhile, the value of both samples falls behind the 1.0% sample. The elastic and viscous moduli are almost independent of frequency. In every sample, the elastic modulus shows higher pascal than the viscous modulus; in addition, the complex viscosity decreases with respect to the frequency after the addition of Rewopal 6000. It indicates that Rewopal 6000 does not influence the good structure of the gel solution; however, it promotes all G' , G'' and η^* .

F108 in a 180 mM TDMAO, 20 mM TTABr and 400 mM 1-Hexanol solution

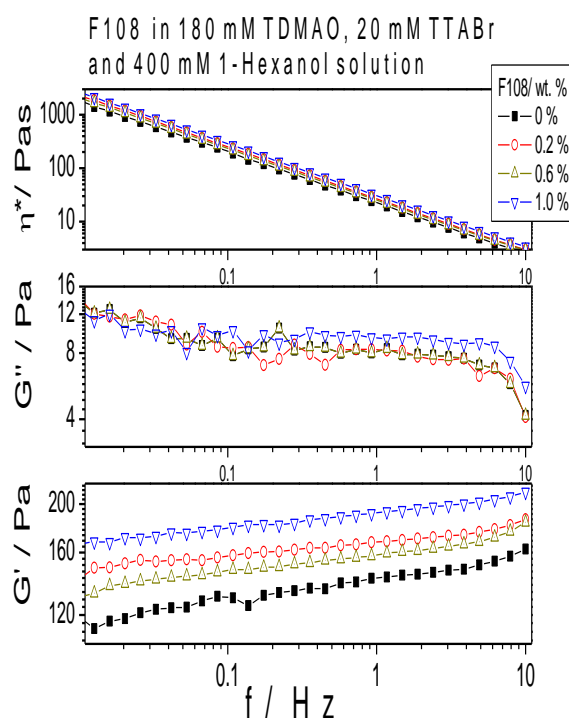


Fig. 5-2- 7: Oscillatory behaviour of F108 in a 180 mM TDMAO, 20 mM TTABr and 400 mM 1-Hexanol solution

In this part, the triblock copolymer F108 is selected to mix with the gel solution of 180 mM, 20 mM TTABr and 400 mM 1-Hexanol at weight concentrations from 0 to 1.0 %. The presence of F108 influences the elastic modulus mostly visibly. The value of G' increases substantially upon the addition of F108. However the other parameters, like viscous modulus and complex viscosity, are not much affected by the presence of the F108. One explanation for these increased elastic properties could be that a bridging of the MLVs by the presence of the telechelic polymer occurs here.

MLVs with additive

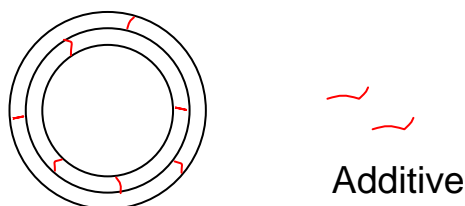


Fig. 5-2-8: Schematic MLVs and additives.

6. Conclusions and outlooks

The first part puts the solubilisation of differently polar oils in solutions of amphiphilic triblock copolymer F108 as a function of temperature is studied. In general, in the presence of F108, the solubility of the selected oils in aqueous solution is enhanced. At the same time the presence of the oils enhances the propensity of the Pluronics to micellise. In this process, the originally present unimers get together to form micellar aggregates. In general, for these copolymers, micellisation is related to the dehydration process of the PO blocks, which takes place upon increasing the concentration and/or the temperature. However, the addition of the polar oils also facilitates this dehydration process and thereby can largely reduce the critical micellisation temperature (cmt), where this effect depends strongly on the molecular architecture of the oil and in general is proportional to the amount of it present. Here medium chain alcohols, such as hexanol or geraniol, are very effective. These changes were followed by a DSC, which can easily detect the enthalpy connected with the dehydration of PPO. From the peak position one can define the value of the critical micelle temperature (cmt). At the same time the homopolymer PPO and the copolymer Kollicoat MAE do not influence the temperature of the phase transition peaks. In the presence of PPO a shoulder peak combine with thermal peak is observed and it shifts to lower temperatures with increasing concentrations. Observing the phase behaviour of PPO in 3.6 mm F108, the turbid solution appears at the given temperature that the shoulder peak appears. This phenomenon is explained as the cloud point. There is a very high probability that it is caused by homo compolymer PPO. The triblock copolymer F108 has its own cloud point as well. It appears when the PO and EO blocks are dehydrated. The dehydration process of EO blocks needs more energy than PO blocks, so it takes two steps to reach the cloud point. This thesis presents not futher evidence that the shouder peak caused by PPO because of cloud point. The enthalpy $\Delta H_{(PO)}$ of F108 in the presence of PPO is much higher than 1-Hexanol. The enthalpy is enhanced by it, but it has no influence on lowering the cmt. The presence of Kollicaot MAE decreases the thermal peak of F108 and so does the enthalpy. Limited to the time, there is more information to find out what their behaviour is like in the thermal property. The viscosity of Kollicoat MAE increases in the presence of F108. Deprotonating the samples and controlling the PH value around 6 results in higher values of viscosity.

The R_h of F108 solution, in the presence of polar oil for unimer and micelle phases, was determined by means of DLS because it were measured as a function of temperature. The R_h of the unimer phase was found at low tempweratures when F108 was not in the dehydration process. If the temperature is controlled over its cmt, the determined Rh belongs to size of micelle phases. However, the dehydration process is still not over, and

the temperature keeps on increasing to 35 and 40°C and the R_h of micelle decreases but not by much. The shape of the micelle has formed, but inside the micelle still contains the remaining water, which continues to discharge from PO blocks when the temperature is already increased above the cmt. The presence of polar oil seems not to induce the size of micelle phases but to let the R_h of micelle form in advance. In other words, it has been once again confirmed by the DLS the presence of polar oil affects the lowering of the cmt of the fixed F108 solution.

In the SANS measurements it has been proved that the presence of 1-Hexanol is soluble certainly in F108 solution. The results of parameters, which are analysed with SASfit programmes, are not conclusive in interpreting the appearance of the F108 solution in the presence of 1-Hexanol. However, the best fit curve is obtained with measurements. The scattering intensity increases with increasing amounts of 1-Hexanol, especially at the middle q position. It proves indirectly that the existence of 1-Hexanol dissolved in F108 D_2O solution at the certain range of fixed environments.

In the second part, the interaction of phospholipids and diesterquats with amphiphilic copolymers was investigated with respect to the structure and stability of the unilamellar vesicles formed in these solutions. By means of increasing the number of times of extrusion, the stability of the formed unilamellar vesicles was substantially enhanced beyond a certain number of extrusions. The presence of amphiphilic copolymers, like 10R5, L35, Rewopal 6000 and Kollicoat IR, reduces the stability time of the vesicles in the solution. Because the mixtures have hydrophilic and hydrophobic characteristics, they play an important role in connecting the vesicles, causing the distance of the vesicle to decrease, thereby enhancing the probability for vesicle fusion. The hydration repulsion of each vesicle becomes powerless with their help and, meanwhile, the hydrophobic attraction and the attraction of van der Waals forces is enhanced as well.

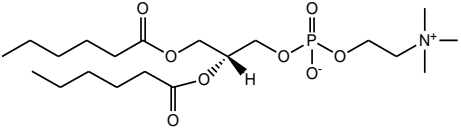
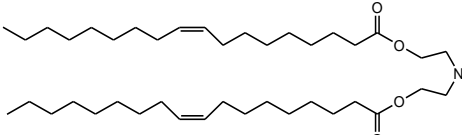
The permeability of DMPC bilayers of the small vesicles has been analysed by means of the Stopped Flow method, which was followed by the exchange reaction of F^- and SCN^{2+} . The presence of 10R5 in the vesicles shortens the reaction time of F^- and SCN^{2+} , and apparently the transport of ions through the vesicle bilayers is facilitated by the presence of 10R5. However, it results conversely in the presence of L35. Both triblock copolymers contain the same values of EO and PO blocks, but lay with converse position order. The forces of vesicle bilayers of phospholipids are an interesting topic to investigate in the future.

The mixtures of 0.1% DMPC and DHPC were prepared at different mass ratio behaviours to form the bicell vesicles in the solution. Furthermore, the stability of the vesicles was investigated by a DLS as a function of time. The sample MH11 keeps the most stable time than other samples. The small vesicles of M11 keep around 20 days after extrusion. In the presence of DHPC reduces the stable time of small unilamellar vesicles of DMPC solution. Bicellar vesicles are composed of long and short alkyl chain phospholipids. It is not conclusive to prove that the bicellar viscles have been already formed by DMPC and DHPC in the solution especially analysed by one method of DLS. The shape and structure of Bicellar vesicles can be further investigated by other techniques, such as DSC, because the phospholipids have characteristics of thermotropic transitions. Microscopy methods are like Cryo-transmission electron microscopy (Cryo-TEM): the direct image can be seen. The X-ray experiment, like SAXS, provides the information for the phases behaviour and organization of lipids [110].

The phase transition from the lamellar gel phase L_β to the fluid L_α phase of DMPC solutions, which exist as large unilamellar vesicles in solutions, was determined by DSC where T_m is at 24.3°C and the pretransition temperature is at 14.0°C in the heating process. The transition state is that the trans-conformation of the hydrocarbon chain of DMPC turns to gauche-trans-gauche conformation (see Fig. 1-6-2). The T_m of DMPC solution does not have much influence when the large unilamellar vesicles become small. However, the entropy decreases when they become small vesicles. The curvature of the increasing vesicles is caused by the extrusion, and the small pore size of polycarbonate filter leads to the production of a large curvature effect [91].

The diesterquat CR3099 forms stable vesicles in solutions spontaneously. However, its size can be reduced by extrusion and these smaller unilamellar vesicles are then stable for a long time. In the presence of polymers, like 10R5 and Kollicoat IR, the vesicle size is reduced and this reduction is proportional to the concentration. The presence of copolymers results in no influence on stable time of reduced small vesicles. They can still keep this size for a period of time. It is very stable and independent of temperature. The small vesicles of CR3099, which have been extruded, result in lower viscosity than larger vesicles. The addition of 10R5 has no influence on the viscosity. This experiment takes 0.5 wt.% CR3099 solution and 0.1 % DMPC as the parent solutions to analyse kinetic stability thermal property, permeability, viscosity and conductivity. The thickness of both is determined by a Kratky-Porod model. Tab. 6-1 summarizes the physical and chemical properties of both small vesicle solutions.

Tab. 6-1: Characters of DMPC and CR3099 solution

	Phospholipids DMPC	Diesterquat CR3099
Name	1,2Dimyristoyl-sn-Glycero-3-Phosphocholine	Di-Oleic Acidyl Isopropylester Dimethylammonium Methosulfate
Structure		
Phases transition	Yes	No
Vesicle size after extrusion	70 nm	100 nm
thickness	2.15 nm	2.72 nm
Stability after extrusion	Yes, one month	Yes, six months
Permeability	Yes	No
Sediments	Yes	No
Fusion effect	Yes	No

Finally, vesicle gels composed of uncharged surfactant TDMAO, ionic surfactant TTABr and apolar oil 1-Hexanol have been studied with respect to their interaction with amphiphilic copolymers, with a particular emphasis on the effects on the rheological behaviour. For these gels the elastic modulus G' is higher than the viscous modulus G'' . The increasing amounts of TDMAO, TTABr and 1-Hexanol lead to high elastic properties, such as the sample of 180 mM TDMAO, 20 mM TTABr and 400 mM 1-Hexanol. The presence of copolymers, like 10R5, Rewopal 6000 and F108, changes the elastic properties of each gel solution respectively. Fig. 5-2-8 presents a simple schema of multilammellar vesicle (MLV) with additives. In this experiment, these are 10R5, Rewopal 6000 and F108. The additives could exist between layers of vesicles. The steadfast MLVs are improved especially with the addition of Rewopal 6000. Under macroscopic conditions, the birefringence property can be observed by the tool of cross polarizers. No signals of birefringence are observed in this experiment for these gel samples. (Some rheology measurements are not discussed since it is not within the scope of this dissertation.) The yield stress σ is the point when the gel solution begins to deform as function of shear rate. They can be further investigated by properties of conductivity, for the composition of the gel solution composed of ionic surfactant. The shape and size of the vesicle gels can be analysed by scattering methods, such as DLS, SAXS and SANS, by microscopy, such as TEM, the method of microscopy provides the real space image of the vesicle gel phases [106, 111].

7. Appendix

Polar oils and F108 solution measured by Fluorescence spectroscopy

1-Hexanol and 3.6 mm F108

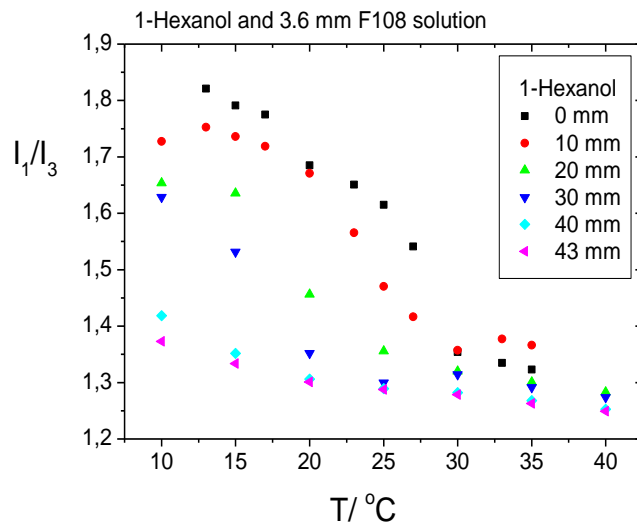


Fig. 7-1: Ratio of I_1 and I_3 for 1-Hexanol in 3.6 mm F108 as function temperature

1-Hexanol and 7.0 mm F108 solution

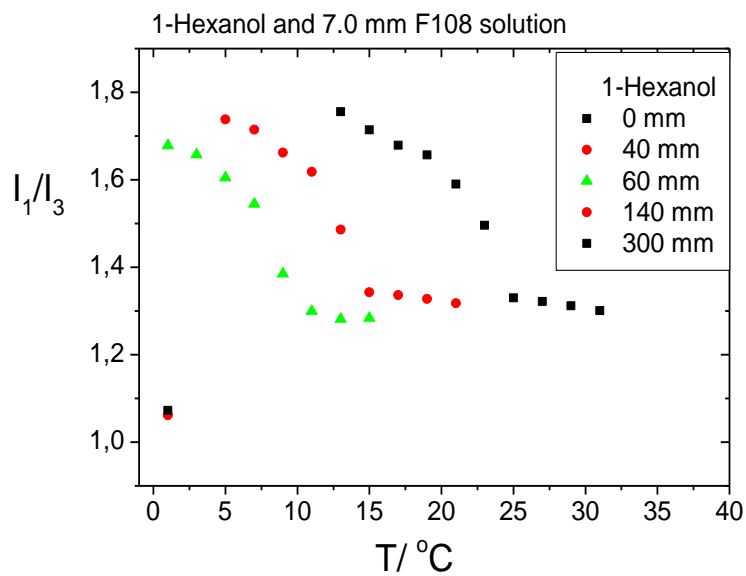


Fig. 7-2: Ratio of I_1 and I_3 for 1-Hexanol in 7.0 mm F108 as function temperature

Geraniol and 3.6 mm F108

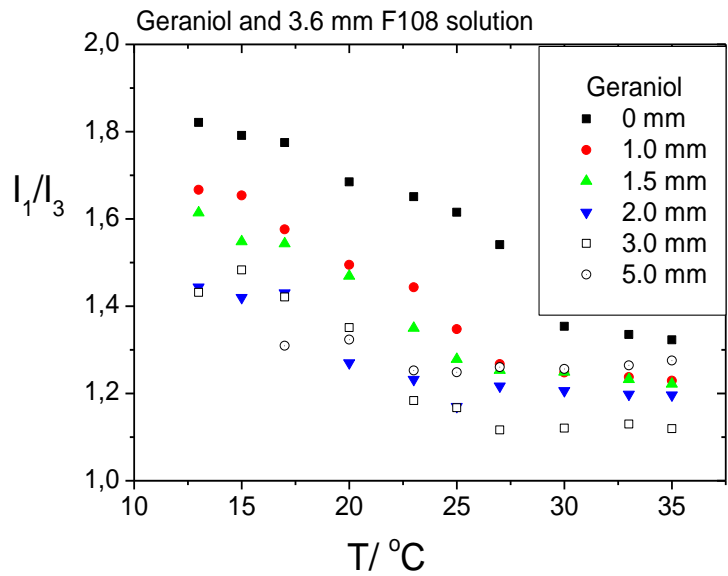


Fig. 7-3: Ratio of I_1 and I_3 for Geraniol in 3.6 mm F108 as function temperature

Toluene and 3.6 mm F108

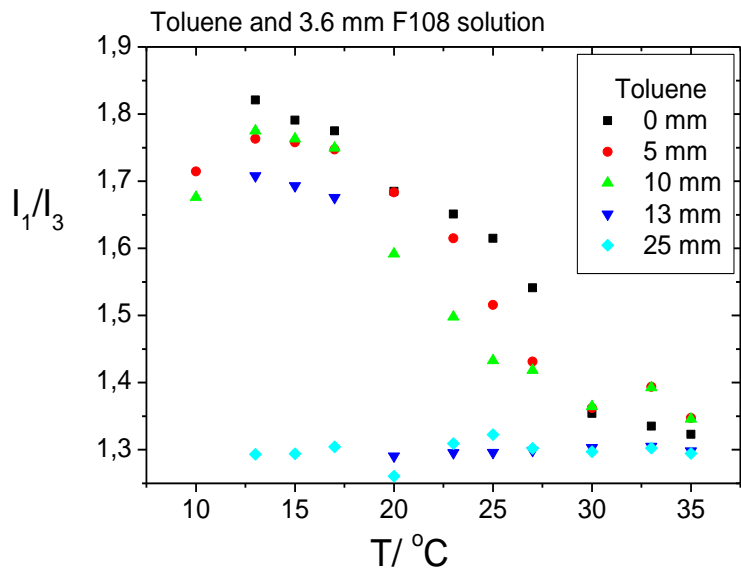


Fig. 7-4: Ratio of I_1 and I_3 for Toluene in 3.6 mm F108 as function temperature

Homo copolymer PPO and 3.6 mm F108

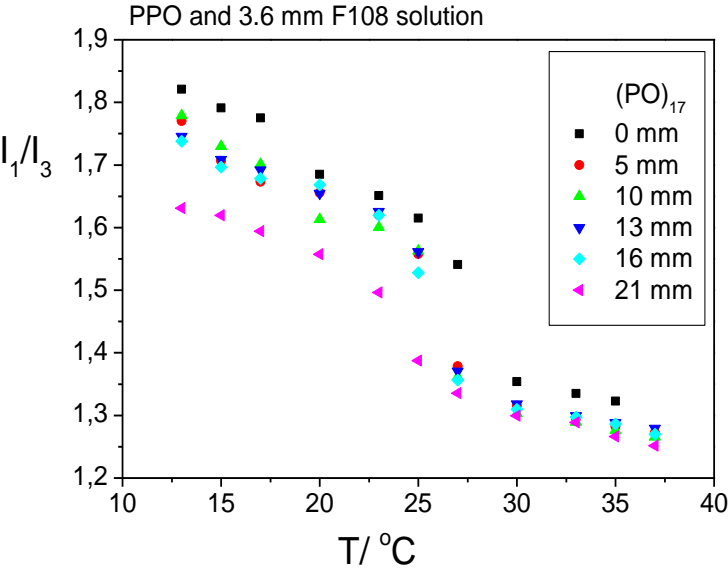


Fig. 7-5: Ratio of I_1 and I_3 for PPO in 3.6 mm F108 as function temperature

8. Acknowledgement

I would like to express my gratitude to all those who gave me the possibility to complete this thesis. I am deeply thankful to my supervisor Prof. Dr. Michael Gradzielski from the Technical University Berlin whose encouragement, stimulating suggestions and supports helped me in all the time of research for and writing of this thesis.

My colleagues from Stranski laboratorium supported me in my research work. I want to thank them for all their help, support, interest and beamtime. My friend he looked the last part of the thesis for English style and grammar, correcting both and offering suggestions for improvement.

Lastly, I offer my regards and blessings to all of those who supported me in any respect during the completion of the doctorthesis.

Hsin-yi Liu

9. Literature

1. Gradzielski, M., *Vesicles and vesicle gels - structure and dynamics of formation* J. Phys.: Condens. Matter, 2003. **15**: p. 655.
2. R. Borsali, R.P., *Soft matter characterization*. 2008: springer.
3. Ekwall P, M.L., Fontell K, Mol. Cryst. Liq. Cryst., 1969. **8**: p. 157.
4. Wennerstoerm H, L.B., Phys. Rep., 1979. **52**: p. 1.
5. Tiddy G J T, Phys. Rep., 1980. **57**: p. 1.
6. Chevalier Y, Z.T., Rep. Prog. Phys., 1990. **53**: p. 279.
7. Laughlin R G, *The Aqueous Phase Behavior of Surfactants*. 1994, London: Academic.
8. Tanford C, *The Hydrophobic Effect: Formation of Micelles and Biological Membranes* 1980, New York: Wiley.
9. Israelachvili J N, M.D.J., Ninham B W, , J Chem Soc Faraday Trans II, 1976. **72**: p. 1525.
10. Hung-Wei Tsui , J.-H.W., Ya-Hui Hsu , Li-Jen Chen, *Study of heat of micellization and phase separation for Pluronic aqueous solutions by using a high sensitivity differential scanning calorimetry*. Colloid Polym Sci, 2010.
11. Ga-Er Yu, Y.D., Stephen Dalton, Qing-Guo Wang, David Attwood, Colin Price and Colin Booth *Micellisation and gelation of triblock copoly(oxyethylene/oxypropylene/oxyethylene), F127* J Chem Soc Faraday Trans, 1992. **88**: p. 2537.
12. West R C, L.D.R., *Handbook of Chemistry and Physics*. 1989: CRC.
13. Neeraj Rai, A.J., Wagner,, J. Chem. Theory Comput, 2008. **4**: p. 136.
14. Hildebrand, J.H., Scott, R. L., , *The Solubility of Nonelectrolytes*. 1950, New York: Reinhold.
15. Mutelet F., E.G., Solimando R., Rogalski M., , Energy Fuels, 2004. **18**: p. 667.
16. Hancock B. C., Y.P., Rowe R. C.,, Int. J. Pharm., 1997. **148**: p. 1.
17. Gu C. H., L.H., Gandhi, R. B., Raghavan K.,, Int. J. Pharm., 2004. **283**: p. 117.
18. Squillante E., N.T., zia H., , Int. J. Pharm., 1997. **159**: p. 171.
19. Minghetti P., C.F., Casiraghi A., Montanary L.,, Int. J. Pharm., 1999. **190**: p. 91.
20. Ray S. K., S.S.B., Joshi J. B., Pangarker V. G.,, Ind. Eng. Chem. Res., 1997. **36**: p. 5265.
21. Hirst A. R., S.D.K., Langmuir, 2004. **20**: p. 10851.
22. Lin Y., A.P., Langmuir, 2002. **18**: p. 4220.
23. Jang B. N., W.D., Wilkie C. A.,, macromolecules, 2005. **38**: p. 6533.
24. Bicerano J., *Prediction of Polymer Properties*. 1996, New York: Marcel Dekker.
25. Ilhem F. Hakem, J.L., Michael R. Bockstaller,, Macromolecules, 2004. **37**: p. 8431.
26. Robeson, L.M., *Polymer blends: a comprehensive review*. 2007: Hanser.
27. Hamley, I., *Block Copolymers in Solution: Fundamentals and Applications* 2005: John Wiley.
28. Anna Angela Barba, M.d.A., Mario Grassi, Serafina Chirico, Gaetano Lamberti, Giuseppe Titomanlio, *Investigation of Pluronic F127–Water Solutions Phase Transitions by DSC and Dielectric Spectroscopy*. Wiley Interscience, 2009.
29. A. F. Kostko, J.L.H.a.M.A.M., *Dynamic Light Scattering Study of Concentrated Triblock Copolymer Micellar Solutions under Pressure*. Macromolecules, 2009. **42**: p. 5328.
30. K. Patela, P.B., C. Guob, J.H. Mab, H.Z. Liub, *Salt induced micellization of very hydrophilic PEO–PPO–PEO block copolymers in aqueous solutions*. European Polymer Journal, 2007. **43**: p. 1699.
31. Travers H. Anderson, J.N.I., *Formation of Supported Bilayers on Silica Substrates*. Langmuir, 2009. **25**: p. 6997.
32. Joyce Y. Wong, J.I., *Polymer-Cushioned Bilayers. II. An Investigation of Interaction Forces and Fusion Using the Surface Forces Apparatus*. Biophysical Journal, 1999. **77**: p. 1458.

33. R.P R, A., Reviews of Biophysics and Bioengineering, 1981. **10**: p. 277.
34. Leckband D, I.J., *Intermolecular forces in biology* Quarterly reviews of biophysics, 2001. **34**: p. 105.
35. Horia I. Petrache, N.G., *Interbilayer interactions from high-resolution x-ray scattering*. 1998. **57**: p. 7014.
36. Bartlett, P.N., *Bioelectrochemistry: Fundamentals, Experimental Techniques and Applications*: WILEY.
37. Hoffmann, S.K.a.H., *Transport of Ions through Vesicle Bilayers*. Journal of Colloid and Interface Science, 1996. **184**: p. 1-10.
38. Below, J.F., Connick, R. E., and Coppel, C. P., Am. Chem. Soc., 1958. **80**: p. 2961.
39. Caldin, E.F., *Fast Reactions in Solution*, ed. **Blackwell**. 1964: Oxford.
40. Sillen, L.G.a.M., A. F., *Stability Constants of Metal-Ion Complexes*. Chemical Society London, 1964. **17**.
41. Clas, S.D., *Differential scanning calorimetry : applications in drug development*. Pharm. Sci. & Tec. To, 1999. **2**: p. 311.
42. Turi, E.A., *Thermal Characterization of Polymeric Material*. 1997, CA, USA: Academic Press.
43. Bruce J. Berne and R. Pecora, *Dynamic light scattering*. 2000, New York: Dover.
44. P. Lindner and Th. Zemb. 2002: North Holland.
45. Kohlbrecher, J., *SASfit: A program for fitting simple structural models to small angle scattering data*. 2011.
46. Grillo, I., *Small-angle neutron scattering and applications in soft condensed matter*. 2008, Springer.
47. Narayanan, T., *Synchrotron Small-Angle X-Ray Scattering*. 2008, Springer.
48. R. Das, S.D., *Structural Studies of Proteins and Nucleic Acids in Solution Using Small-Angle X-Ray Scattering* 2008, Springer.
49. Harada, S., Nakajima, T., Komatsu, T., and Nakagawa, T., J. Solution Chem, 1978. **7**: p. 463.
50. Vass, S., Torok, T., Jakli, G., and Berecz, E., J. Phys. Chem. B, 1989. **93**: p. 6559.
51. Maccarini, M.a.B., G., J. Phys. Chem. B, 2000. **104**: p. 11451.
52. Cantu, L., Corti, M., Del Favore, E., Dubois, M., and Zemb, T., Biophysical Journal, 1998. **74**: p. 1600.
53. J. B. Hayter and J. Penfold, Colloid Polym. Sci., 1983. **261**: p. 1022.
54. Flory, P.J., *Statistical Mechanics of Chain Molecules*. 1969, New York: Interscience.
55. Hammouda, B., ed. *the SANS toolbox. pdf*.
56. Mezger, T.G., *The rheology handbook: for users of rotational and oscillatory rheometers* 2006.
57. Hoffmann, H.T., C.; Schmiedel, P.; Munkert, U., Langmuir, 1994. **10**: p. 3972.
58. Jang, J., Ha, H, Langmuir, 2002. **18**: p. 5613.
59. Jeong B, B.Y., Lee DS, nature, 1997. **388**: p. 860.
60. Q. Chen, H.S.a.G.J.V., small, 2009. **5**.
61. T. Kojarunchitt, S.H., T. Rades and etc, Inte. Jou. of Pha. , 2011. **408**.
62. S. Alexander, T.C., S. Prescott, Langmuir, 2011. **27**.
63. Y-I Su, X.-F.W., H-Z Liu, Langmuir, 2003. **19**(7): p. 2995-3000.
64. M. Nilsson, B.H., Macromolecules, 2007. **40**(23).
65. J-h Ma, C.G.a.Y.-I.T., J.Phys. Chem. B, 2007. **111**(19).
66. K. Bouchemal , F.A.a.e., Journal of Colloid and Interface Science 2009. **338**.
67. S. Zhang, N.L., L. Zheng, X. Li and etc, J.Phys. Chem. B, 2008. **112**.
68. BOON KIAK LAU, Q.W., WEI SUN, LIN LI, *Micellization to Gelation of a Triblock Copolymer in Water: Thermoreversibility and Scaling*. J Polym Sci Part B: Polym Phys, 2004. **42**: p. 2014 - 2025.
69. Walther Batsberg, S.N., Christa Trandum, and Søren Hvidt, *Effects of Poloxamer Inhomogeneities on Micellization in Water*. Macromolecules, 2004. **37**.
70. Hvidt S, B.W., *Characterization and Micellization of a Poloxamer Block Copolymer*. Int J Polym Anal Charact, 2007. **12**.
71. Kell Mortensen, W.B., and Søren Hvidt, *Effects of PEO-PPO Diblock Impurities on the Cubic Structure of Aqueous PEO-PPO-PEO Pluronics Micelles: fcc and bcc*

- Ordered Structures in F127*. Macromolecules, 2008. **41**(5).
72. Hecht E, H.H., *Kinetic and calorimetric investigations on micelle formation of block copolymers of the poloxamer type*. Colloid Surf A, 1995. **96**: p. 181.
 73. G. Lazzara, S.M.a.M.G., *The solubilisation behaviour of some dichloroalkanes in aqueous solutions of PEO–PPO–PEO triblock copolymers: a dynamic light scattering, fluorescence spectroscopy, and SANS study*. Phys. Chem. Chem. Phys., 2006. **8**: p. 2299.
 74. Debye, P., J. Phys. Colloid Chem., 1947. **51**: p. 18.
 75. Liu, H.Y., Prevost, S., Gradzielski, M, Z. Phys. Chem., 2012. **226**: p. 675.
 76. Hsin-yi Liu, S.P., M. Gradzielski, Z. Phys. Chem., 2012. **226**: p. 675.
 77. IFA, *GESTIS Substance Database*.
 78. J.P. Mataa, P.R.M., O. Kubotac, A. Khanal, K. Nakashima, P. Bahadur, *Effect of phenol on the aggregation characteristics of an ethylene oxide–propylene oxide triblock copolymer P65 in aqueous solution*. Journal of Colloid and Interface Science, 2008. **320**(1): p. 275 - 282.
 79. Alexandridis, P.N., T.; Hatton, T. A, Langmuir 1995. **11**: p. 1468.
 80. J.P. Mataa, P.R.M., C. Guoc, H.Z. Liuc, P. Bahadur, *Concentration, temperature, and salt-induced micellization of a triblock copolymer Pluronic L64 in aqueous media*. Journal of Colloid and Interface Science, 2005. **292**(2): p. 548 - 556.
 81. Winnik, E.F.a.F.M., *Interaction between Pluronic F127 and Dioctadecyldimethylammonium Bromide (DODAB) Vesicles Studied by Differential Scanning Calorimetry*. Langmuir, 2010. **26**(23): p. 17852 -17857.
 82. Xiang Yuan Xiong, K.C.T., Leong Huat Gan, *Synthesis and thermally responsive properties of novel Pluronic F87/polycaprolactone (PCL) block copolymers with short PCL blocks*. Journal of Applied Polymer Science, 2006. **100**(5): p. 4163 - 4172.
 83. K. W. Kwon, M.J.P.a.K.C., Polymer Journal, 2001. **33**: p. 404.
 84. J. Armstrong, B.C., J. Mitchell, A. Beezer and S. Leharne, J. Chem. Phys, 1996. **100**: p. 1738.
 85. <http://www.inchem.org/documents/icsc/icsc/eics1030.htm>. 2008.
 86. Bahadur, B.B.a.P., Journal of Colloid and Interface Science, 2008. **320**: p. 452.
 87. Schömer, M.F., H. , Macromolecules, 2012. **45** (7): p. 3039.
 88. Mortensen, K.S., D.; Janssen, S. , Phys. Rev. Lett., 1993. **71**(11): p. 1728.
 89. Rui-Guang Wu, Y.-R.W., *A DSC study of paeonol-encapsulated liposomes, comparison the effect of cholesterol and stigmasterol on the thermotropic phase behavior of liposomes* JOURNAL OF THERMAL ANALYSIS AND CALORIMETRY 2012. **109**: p. 311.
 90. C. DEMETZOS, Journal of Liposome Research, 2008. **18**: p. 159.
 91. M., B.P.C.L.C., *Curved single-bilayers in the region of the anomalous swelling: Effect of curvature and chain length* COLLOIDS AND SURFACES A-PHYSICOCHEMICAL AND ENGINEERING ASPECTS 2006. **291**: p. 63.
 92. Kratky, O., PROGRESS IN BIOPHYSICS & MOLECULAR BIOLOGY 1963. **13**: p. 105.
 93. G. Ma, D.J.B.a.M.J.L., J. Phys. Chem. B 2000. **104**: p. 9081.
 94. Kucerka, N.U., D. , Balgavye, P., *LIPID BILAYER THICKNESS IN EXTRUDED LIPOSOMES PREPARED FROM 1,2-DIACYLPHOSPHATIDYLCHOLINES WITH MONOUNSATURATED ACYL CHAINS: A SMALL-ANGLE NEUTRON SCATTERING STUDY*. Aata Fac. Phar. Uni. com., 2003: p. 78.
 95. L. Rubio, C.A., *Structural effects of flufenamic acid in DPPC/DHPC bicellar systems*. Soft Matter, 2011. **7**: p. 8488.
 96. B. Yue, C.Y.H., *Highly Stable Phospholipid Unilamellar Vesicles from Spontaneous Vesiculation: A DLS and SANS Study*. J. Phys. Chem. B, 2005. **109**: p. 609.
 97. B. Yue, C.Y.H., *Spontaneously Forming Unilamellar Phospholipid Vesicles*. Macromolecular Symposia, 2005. **219**: p. 123.
 98. P. Mohanty, K.L., *Discoic Bicelles as Efficient Templates for Pillared Lamellar Periodic Mesoporous Silicas at pH 7 and Ultrafast Reaction Times*. Nano express, 2010. **6**: p. 61.

99. J. Wang, Y.Z., *Handbook of Detergents. Part D: Formulation*, ed. M.S. Showell. 2006: CRC Press.
100. Smulders, E., *Laundry Detergents*. 2002, New York: J. Wiley & Sons.
101. S. Mishara, V.K.T., *Journal of Oleo Science*, 2007. **56**: p. 269.
102. Farm, R., *Chemistry and technology of surfactants*. 2006, Oxford: Blackwell Publishing Ltd.
103. N. Calero, M.A., *Rheological Behavior and Structure of a Commercial Esterquat Surfactant Aqueous System*. *Chem. Eng. Technol.* , 2010. **33**: p. 481.
104. *REWOQUAT CR3099*. 2003, degussa: essen.
105. Floyd E. Friedli, R.K., C. Joe Toney , *Journal of Surfactants and Detergents*, 2001. **4**: p. 401.
106. M. Bergmeier, M.G., H. Hoffmann, and K. Mortensen, *J. Phys. Chem. B*, 1999. **103**: p. 1605.
107. Hoffmann, H.M., U.; Thunig, C.; Valiente, M, *J. Colloid Interface Sci.*, 1994. **163**: p. 217.
108. Hoffmann, H.T., C.; Schmiedel, P.; Munkert, U., *Faraday Discuss*, 1995. **101**: p. 319.
109. Hoffmann, H.T., C.; Schmiedel, P.; Munkert, U., 1994. **16D**: p. 1373.
110. J. Pereira-Lachataignerais, R.P., H. Amenitsch, M. Rappolt,, *Langmuir*, 2006. **22**: p. 5256.
111. C. Wolf, K.B., M. Drechsler, and M. Gradzielski,, *Langmuir*, 2009. **25**: p. 11358.

10. List of Publication

1. Solubilisation of Oils of Different Polarity in Aqueous Solution of Pluronic Triblock Copolymers, Hsin-yi Liu, Sylvain Prévost, and Michael Gradzielski Z. Phys. Chem. 226 (2012) 675-694